NONLINEAR ANALYSIS OF CONNECTED AND DISCONNECTED SOIL-PILE-RAFT SYSTEM UNDER EARTHQUAKE LOADING

A DISSERTATION

Submitted in partial fulfillment of the

requirement for the award of the degree

of

MASTER OF TECHNOLOGY

in

EARTHQUAKE ENGINEERING

(With specialization in Soil Dynamics)

by

AMAN GARG

DEPARTMENT OF EARTHQUAKE ENGINEERING
INDIAN INSTITUTE OF TECHNOLOGY ROORKEE
ROORKEE – 247667, UTTARAKHAND, INDIA
MAY, 2016

CANDIDATE'S DECLARATION

I, hereby, declare that the work being presented in this dissertation entitled "**Nonlinear Analysis of Connected and Disconnected Soil-Pile-Raft System under Earthquake Loading**", prepared in partial fulfillment for the award of the degree of **Master of Technology** in **Earthquake Engineering** with specialization in **Soil Dynamics**, submitted in the Department of Earthquake Engineering, IIT Roorkee is an authentic record of my own work carried out from July 2015 to May 2016, under the guidance of **Dr. D. K. Paul**, Emeritus Professor, Department of Earthquake Engineering, IIT Roorkee and **Prof. Dr.-Ing. habil. Christian Moormann**, Director, Institute for Geotechnical Engineering, University of Stuttgart, Germany.

The matter embodied in this report has not been submitted by me for the award of any other degree or diploma of this institute or any other University/Institute.

Date: Aman Garg

Place: Roorkee M.Tech (II Year) – Soil Dynamics

CERTIFICATE OF APPROVAL

This is to certify that the above statement made by the candidate is true to best of my knowledge.

Prof. Dr.-Ing. habil. Christian Moormann
Head of Institute
Institute for Geotechnical Enngineering
University of Stuttgart
Germany

Dr. D. K. Paul
Emeritus Professor
Department of Earthquake Engineering
IIT Roorkee
India

ACKNOWLEDGEMENT

The research work presented in this dissertation is the result of the work carried out during the year July 2015 to May 2016 at Indian Institute of Technology Roorkee and University of Stuttgart in Germany. Behind this work there are important contributions and the significant support of number of persons, whom I would like to thank sincerely.
First and foremost, I would like to thank my family for their endless support. Knowing that they are proud of my accomplishments is one of my biggest inspirations.
I would like to express my deep gratitude to **Dr. D. K. Paul**, Emeritus Professor, Department of Earthquake Engineering, IIT Roorkee, for his extensive, invaluable and steadfast guidance, for his support and patience, sharing his knowledge and experience, throughout my master dissertation work.
Likewise, I would like to express a thankful note to **Prof. Dr.-Ing. habil. Christian Moormann**, Director, Institute for Geotechnical Engineering, University of Stuttgart, Germany for providing me the opportunity to carry out my dissertation work at University of Stuttgart in Germany and his careful guidance. I am also grateful to **Mr. Julian Lehn**, Institute for Geotechnical Engineering, University of Stuttgart, Germany for providing his timely suggestions and helping me out at every stage of this work during the period of stay in Germany.
I am also grateful to the German Academic Exchange Service (DAAD) for providing me opportunity to carry out my research work in Germany.
I would like to thank all the other respected faculty members of Department of Earthquake Engineering, IIT Roorkee and dear colleagues for their guidance and assistance whenever required.

Date: Aman Garg

Place: Roorkee M.Tech (II Year) – Soil Dynamics

ABSTRACT

In design of High-rise buildings, the main issue is to transfer the subjected loads to the ground safely. So to prevent probable damages and to reduce the deformation, a proper design of foundation is required. In theses cases a combined piled raft foundation is being preferred from two to three decades. However, when the piles are connected to the raft, high stresses are generated in the piles. To overcome this problem a new approach, to disconnect the piles from raft forming a new type of foundation called disconnected piled raft foundation (DPRF), has been suggested. The work done in this field is very less specially under dynamic loads.

The objective of this work to perform numerical analysis on connected and disconnected Soil-Pile Systems under different soil conditions and loading taking into account the nonlinear soil-pile-raft interaction modeling the interfaces appropriately using Finite element software PLAXIS 3D. Furthermore, the influence of geosynthetic reinforcements in the granular layer of disconnected systems should be investigated.

In detail, the following subjects should be dealt with:

- Literature review on existing design approaches and guidelines combined pile raft foundations (connected and disconnected with and without geosynthetic reinforcement).
- Description of the load transfer mechanism of different system under vertical and horizontal loading.
- Representation of different modeling techniques of elements used in the system.
- Numerical simulation of connected and disconnected (with and without geosynthetic reinforcement) Soil-Pile-Raft Systems under dynamic loads.
- Comparison of the calculation results of the different systems with regard to the determination of the influence of various parameters on the load-bearing and deformation behavior.
- Evaluation of the achievements and identification of further research needs

Contents

List of Figures

List of Tables

Chapter 1

Introduction

1.1 Motivation

Infrastructure development is a vital component in stimulating a country's economic growth. Infrastructure is one of the main issues in its development of the country. Infrastructure includes several technical structures such as roads, bridges, buildings, tunnels, water supply, sewers, electrical grids, telecommunications, and so forth.

The stability and serviceability are the main design requirements that are associated with these structure. The loads subjected to them should be resisted safely for stability and no large deformations should be there for serviceability. The loads and deformations are controlled by its *Foundation*. It transfers the loads from superstructure to the ground safely and keeps the deformations (i.e settlement) within the permissible limit. Several types of foundations such as spread footing, raft foundation, pile foundation, combined piled raft foundation (CPRF), etc., are available but selection of them is based on the type and amount of loads, soil condition, area available for foundation and so forth.

But if the situations of heavy vertical loading, high lateral forces and/or poor soil conditions are available, piled raft foundation is being preferred from two decades because it is an economic and sustainable foundation system. Many high rise buildings (towers)

e.g. Burj Khalifa (Dubai), many towers in Frankfurt (Germany), etc., and many others structures have been constructed with CPRF and several are being constructed. Figure 1.1 shows some of the towers constructed on CPRF in Frankfurt (Germany).

First *Burland et al. (1977)* introduced the use of CPRF where settlement was more than the permissible limit in which the piles below raft foundation acted as "settlement reducers". After that lot of research has been conducted regarding the behavior of CPRF. Many issues has been measured regarding CPRF and resolved. One of the main issue is that in areas subjected to high lateral loads due to wind or seismic events, high shear forces and bending moments may be generated at pile's heads when the piles are connected to raft. In these cases, the carrying capacity of piles may be governed by its structural rather than geotechnical capacity *Fioravante and Giretti (2010)*. Due to this high stresses generate in the piles and it leads to an uneconomical design. To overcome this problem *Wong et al. (2000)* suggested to disconnect the piles from raft with an interposed layer between piles and raft.

Some recent projects e.g. foundation system of the Rion Antirion Bridge (Greece) and Golden Ears Bridge (Canada) have employed piled raft foundation with an interposed layer. Both of the bridges are constructed in seismically active region. Because this type of foundation is more convenient in the region where high lateral loads generate and also there are few studies regarding this field so there is a strong requirement to investigate the seismic behavior of disconnected piled raft system.

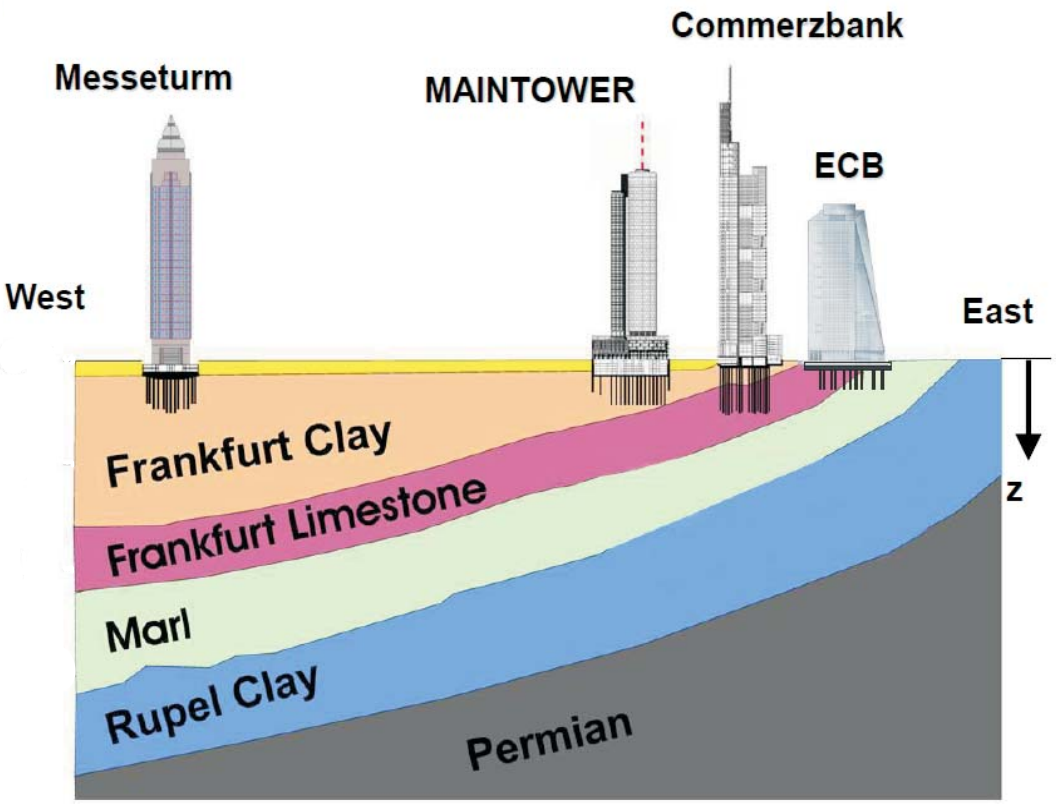

Figure 1.1: Towers with combined piled raft foundation in Frankfurt *Matthias Vogler et al. (2015)*

1.2 Objective of work

The main aim of this work is to investigate response of the disconnected piled raft system under earthquake loading and make comparison with the connected piled raft system. A dense granular layer will be provided between piles and raft in disconnected system and the influence of its thickness and stiffness will be investigated. The effect of geogrid in granular layer, introduced to improve the lateral stability of DPRF, will be examined.

The different interactions such as pile-soil, pile-raft, raft-soil interaction, etc, will be considered in numerical analysis. The Piled raft system will be modeled using the Finite element modeling software PLAXIS 3D 2013.01 and PLAXIS 3D AE.01 2015 with the essential material properties and conditions. The advance constitutive model (e.g. Hard-

ening soil model) will be used to simulate the real dynamic behavior of soil. The piles will be modeled by embedded pile approach and a literature study regarding this new approach will be conducted. The existing literature on experimental studies will be used to validate the finite element model.

Finally results from the different analyses will be summarized and further scope of research will also be identified.

1.3 Outline of thesis

The thesis is arranged in the following chapters:

Chapter 1 presents the motivation regarding this work, objective and organization of this thesis.

The detailed existing literature review on combined piled raft foundations (connected and disconnected with and without geosynthetic reinforcement) has been carried out in *Chapter 2*. And also load transfer mechanism for different system has been discussed.

Chapter 3 contains the basic formulations of finite element method and different aspects of modeling of components such as soil, pile, raft, geogrid and dynamic loading have been discussed. Brief discussion on embedded pile approach has been presented.

The numerical model has been calibrated using existing experimental study in *Chapter 4* under both static and dynamic loading. It also verifies the value of the properties of elements used in modeling and parameters of the soil constitutive model.

The calibrated model has been used for investigation of the load-bearing and deformation behavior of piled raft foundation under dynamic loading in *Chapter 5*. The comparison has been made between the results of both the systems. In addition, a parametric

study has also been carried out to investigate the performance of DPRF under seismic loading.

Chapter 6 gives the conclusions of the thesis and provides recommendations for further research. References have been provided at the end of thesis.

Chapter 2

Literature Review:- Piled Raft Foundation

Foundation is the interface between superstructure and ground. Its task is to transfer the building loads safely to the ground and to keep the deformation within the permissible limit. It supports superstructure weight, resists horizontal forces, due to wind and earthquake, by base friction and side passive forces. Based on the properties of soil and loads, the foundation can be broadly grouped into two categories:-

1. Shallow Foundations
2. Deep Foundations

2.1 Shallow foundation-Raft foundation

Shallow foundations are normally used at shallow depth. So this type of foundation transmits structural loads to the soil strata at relatively small depth. The Raft or Mat

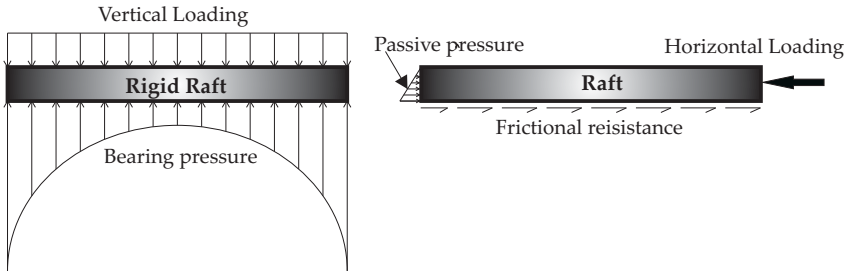

Figure 2.1: Schematic representation of load transfer mechanism only in raft foundation, *Quick (2005)*

foundation is a shallow foundation which covers the entire area of a structure and spreads

the entire structural load over a large area. In raft foundation total vertical load is resisted by the bearing pressure generated below the raft and horizontal load by side pressure and interface frictional resistance between raft and soil as illustrated in Figure 2.1. Mostly high rigid raft is considered to reduce the differential settlement of foundation system, so in Figure 2.1 contact pressure distribution below rigid raft over soft soil has been shown.

2.2 Deep foundation-Pile foundation

The superstructure load has to be transferred to deeper firm strata, where the soil at shallow depth is either loose or soft or of a swelling type. This foundation transfers the structural loads to earth far below the surface. Usually pile foundation is used as deep foundation in the shape of long slender columns. The piles may be of different types such as driven, bored or cast-in-situ. The loads on piles may be vertical or lateral or combination of both loads.

Load transfer mechanism of pile foundation

- **Vertical load :-** The vertical load on piles is resisted by the side friction developed along the shaft i.e. skin friction and remaining part by the soil below the tip of the pile i.e. end bearing. Generally piles are used in group. It is observed that center pile carries the highest end bearing and skin resistance followed in order by mid-edge piles then corner piles as shown in Figure 2.2.

- **Horizontal load :-** When a pile is subjected to lateral loads, a part or whole of the pile tries to move horizontally in direction of subjected load. Due to this bending, rotation or translation of the pile is occurred. The pile pushes the front soil (i.e., the soil mass lying in the direction of the applied load), causing shear and compressive stresses and strains in the soil that provides resistance to the pile movement. The total soil reaction along the pile shaft resists the external lateral force. Right portion of the Figure 2.2 illustrates the horizontal load transfer mechanism of pile

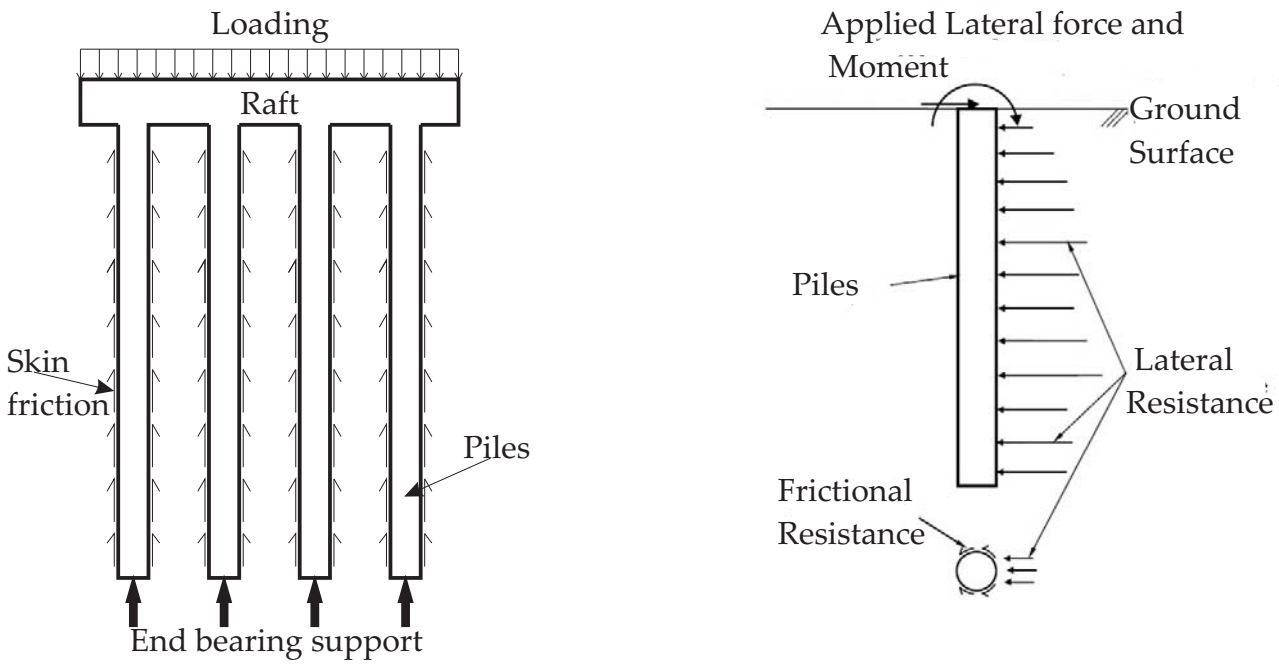

Figure 2.2: Representation of load transfer mechanism of Pile foundation

foundation.

2.3 Piled raft foundation

Most of the time piles are provided in group with a solid slab (called Pile Cap) on the top of them for uniform loading. In conventional design, the load bearing capacity of this cap is not considered but if the pile cap is designed properly, to take a shear, and the response behavior coming from the soil, because of the soil pressure below cap, then this combined action of the pile cap and piles is known as the piled raft foundation (PRF) as shown in Figure 2.3. By using this combined design approach, the reduced number of piles or diameter of pile or more spacing between piles can be provided for a particular loading in comparison of pile foundation. So, this approach leads to considerable economic savings without compromising the safety and performance of the foundation system (*Poulos (2001)*).

From last two decades, the use of PRF has become more popular. The piled raft foundation is one of the most effective types of foundation which has both advantages of shallow and deep foundation. The PRF can behave in two manners, in first manner piles are called upon only to take a small percentage of loads and rest is designed to be carried out by raft and here piles act as settlement reducers. Secondly, in case of high raised buildings or when subsoil conditions such as thick clay deposits even with a high water table and the clay shear strength is very low, long load-bearing piles are introduced to transfer the entire load to deeper and stiffer soil layers and here the majority of load is carried by piles. First *Burland et al. (1977)* introduced piles as settlement reducers below the raft.

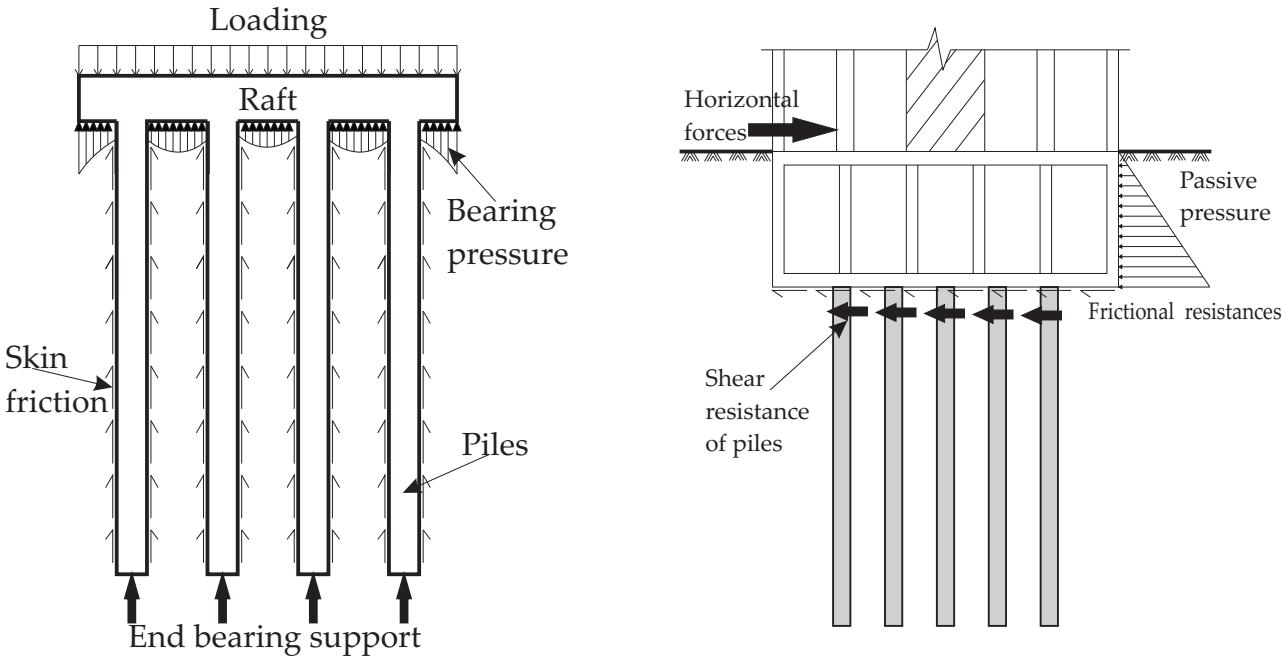

Figure 2.3: Schematic representation of load transfer mechanism in Connected piled raft system, *Quick (2005)*

Load transfer mechanism of CPRF

In comparison to a pile foundation, in the combined pile-raft-foundation both the piles and the raft transfer the loads to the ground. The vertical loads are resisted by skin friction and end bearing as well as contact pressures of the raft foundation (bearing pressure) as shown in Figure 2.3. The lateral loads are restrained by the shear resistance of

piles, base frictional resistance along the raft-soil interface and passive pressure along side walls.

2.4 Disconnected piled raft foundation

When the raft has sufficient bearing capacity to support super structure but the total and differential settlements of raft are more than the permissible limit, the small numbers of piles can be provided to control these settlements *Burland et al. (1977)*. Commonly these pile heads are structurally connected with the raft to form a rigid connection. These piles should provide not only an adequate bearing capacity but also have sufficient factor of safety against structural failure. Because high axial stress may be developed in piles and horizontal forces due to wind and earthquake may damaged the connections as shown in Figure 2.4. Even though this structural failure can be avoided by providing high strength materials and high factor of safety but it may be an uneconomical approach.

Figure 2.4: Damage at pile to pile cap connection due to strong earthquake, *Teguh et al. (2006)*

To overcome this problem, an alternative approach has been purposed by *Wong et al. (2000)* that piles should be used as purely an enhancing the stiffness of the base soil by disconnecting them from raft as illustrated in Figure 2.5. A gap can also be introduced between the piles and raft such that the loads from the superstructure would not be directly transferred to the piles and this gap can be filled with an appropriate material that can be chosen according to different conditions. Since the piles are not structurally connected to the raft so less factor of safety (as low as 1.3 according to *Wong et al. (2000)*) can be used as against structural failure of the pile materials. Thus, these disconnected piles may be carried much higher loads in comparison of structurally connected piles with resulting economical benefits.

Load transfer mechanism of DPRF

- **Vertical load :-** Figure 2.5 illustrates the vertical load distribution along the piles in disconnected piled raft system and distribution of settlements of the raft (w_r), the piles(w_p) and the soil (w_s) along the pile-soil interface. Some portion of the load is transfered to the piles by way of the piles head through the arching effect that is allowed by the load distribution layer (*Mattsson et al. (2013)*).

  The compressibility of this layer also permits relative settlement between the raft and the piles; as the raft loads the piles and the surrounding soil; in the upper region of piles, the soil settles more than the piles ($w_r \geq w_s > w_p$); that causes the soil applies a downward drag (i.e negative skin friction) on the upper pile shaft perimeter. Other portion of load is transmitted by this negative skin friction. Conversely, $w_s < w_p$ along the lower portion, so that positive skin friction develops up to the pile base. As shown in Figure 2.5 when negative skin friction transferred to positive, a neutral plane exists at which $w_s = w_p$ and maximum axial force is attained (*Tradigo et al. (2015)*). The vertical load on the piles is supported by this positive skin friction and the end bearing at the base.

- **Horizontal load :-** The horizontal loads can be effectively transmitted through the

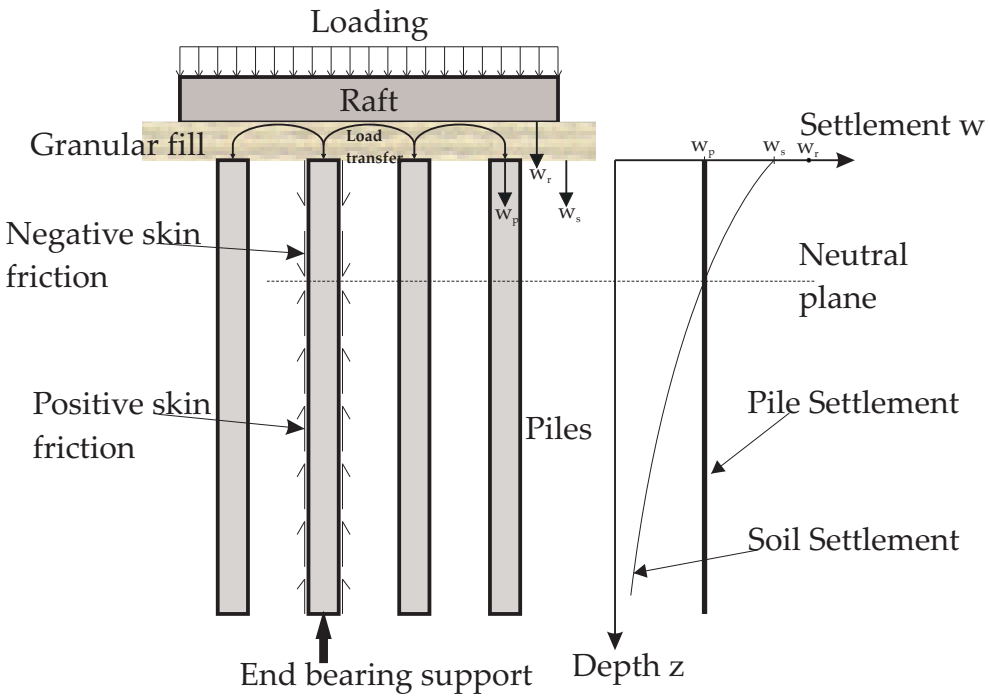

Figure 2.5: Schematic diagram of vertical load transfer mechanism of Disconnected piled raft system

mobilized friction force along the soil-raft interface as illustrated in Figure 2.6. Besides, as the construction of raft foundation for high-rise buildings usually consists of a basement, the lateral loads may also be resisted by passive pressures acting on the basement walls (*Wong et al. (2000)*)

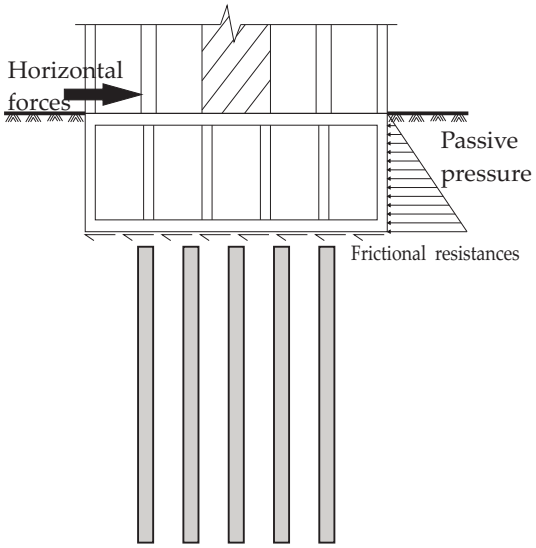

Figure 2.6: Transfer mechanism of horizontal forces, *Wong et al. (2000)*

2.5 Reinforcement of load distribution layer

Although construction of disconnected piled raft system with interposed layer under seismic loading produces less stresses in the piles however large lateral deformation in comparison of CPRF may occur. So to reduce the lateral deformation, interposed layer can be reinforced with geosynthetic. This technique i.e. soil reinforcement with geosynthetic is an old and ancient idea. Soil reinforcement provides several benefits such as enhancement in the stability of foundation and shear strength of soil, reduction in settlement and lateral deformations, etc,. These geosynthetics are usually classified into: Geotextiles, Geogrids, Geomembrane, Geonets, Geofoams, Geocells and Geocomposites.

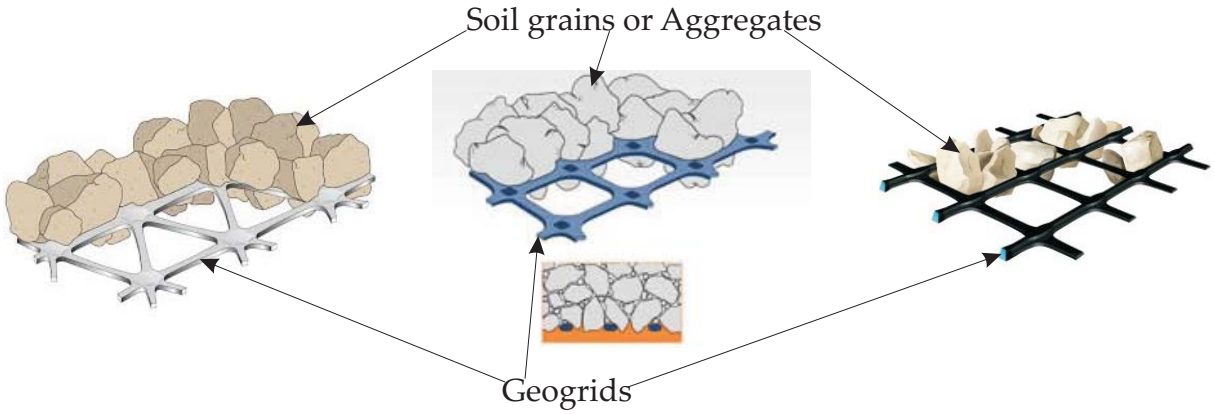

Figure 2.7: Geogrid-soil interlocking

Among them geogrid is the most useful geosynthetic to reduce the lateral deformation due to its interlocking mechanism as shown in Figure 2.7. Geogrid is a high-modulus polymeric material, such as polypropylene and polyethylene, containing tensile ribs with opening, called aperture, of adequate size to permit interlock with surrounding soil. This geogrid-soil interlocking mechanism, named "Static interlock", enables the geogrid to act as reinforcement element, through which it provides lateral confinement and enhances the soil shear strength. In geogrids stresses are dominantly transfered through the development of bearing stress on the cross bars of geogrids rather than the mobilization of surface friction at soil-geogrid interface.

McGown et al. (1995) presented that "static interlock does not make full use of the deformability and resilience of these pre-stretched polymer geogrids during compaction or dynamic loading. In this situation, author introduced a new interlock mechanism, known as 'Dynamic interlock', in which after application of load, deformation in the soil and geogrid occurs and stresses are set up in the ribs, cross-bars and junctions of the geogrid. As the applied forces are removed, the geogrid tries to return to its original configuration; however, the soil particles filling the apertures in the structure may wholly or partially prevent it from doing so. This results in locked-in stresses in the geogrid which will be transmitted into the trapped soil as compressive (confining) stresses".

Geogrids generally are of two types (a) Biaxial geogrids and (b) Uniaxial geogrids as illustrated in Figure 2.8. Both Uniaxial and Biaxial geogrids are manufactured by stretching a punched sheet of polymer in one direction and two orthogonal directions respectively under carefully controlled conditions. The resulting grid apertures are either square or rectangular. Uniaxial geogrids have high tensile strength in one direction while Biaxial have equal tensile strength in both perpendicular directions. Geogrids are manufactured so that the open areas of the grids should be greater than 50% of the total area. They develop reinforcing strength at low strain levels, such as 2% (Carroll (1988)).

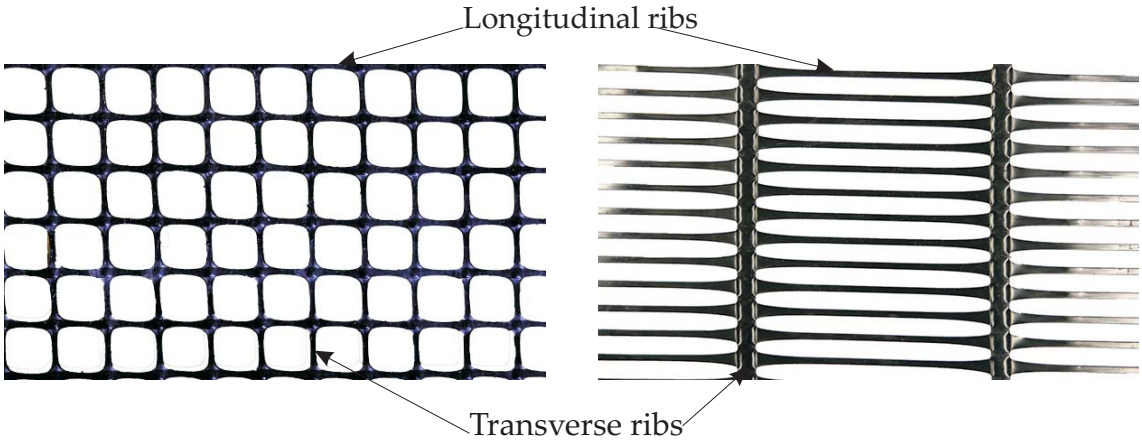

Figure 2.8: Biaxial geogrid (left) and Uniaxial geogrid (right)
(www.technicalcivils.co.uk)

2.6 Soil-structure interaction

A free-field seismic motion is that motion in which displacement of soil deposit occurs without any influence of structural motion. If the structure is supported on the soil deposit, response of both structure and soil depends on each other. So the process in which the response of soil influences motion of the structure or motion of structure influences response of the soil, is referred as Soil-structure interaction (SSI) as illustrated in Figure 2.9. However, the foundation embedded into the soil will not follow the free field motion. This inability of the foundation to match the free field motion causes the "kinematic interaction". On the other hand, the mass of the super-structure transmits the inertial force to the soil causing further deformation in the soil, which is termed as "inertial interaction". At low level ground shaking kinematic interaction is predominant. On the contrary, inertial interaction prevails in strong ground shaking.

The interactions are more significant for stiff and/or heavy structures supported on relatively soft soils. It is also significant for closely spaced structure that may subject to pounding, when the relative displacement is large.

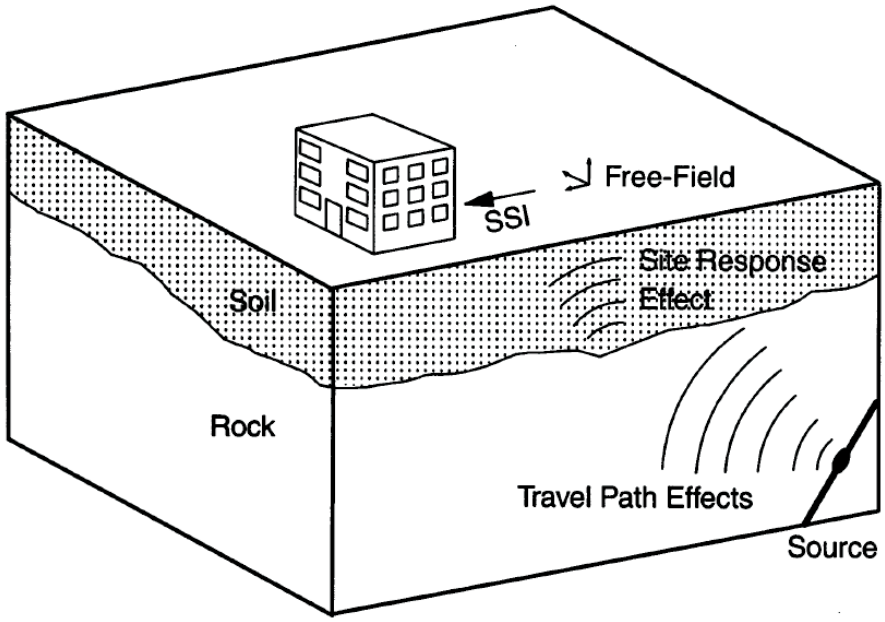

Figure 2.9: Schematic representation of soil-structure interaction (www.civil.ist.utl.pt)

In case of piled raft foundation complex interactions occur between different elements such as: Pile-pile; Raft-Pile; Raft-soil and Pile-soil interactions as shown in Figure 2.10. These interactions should be considered during numerical analysis.

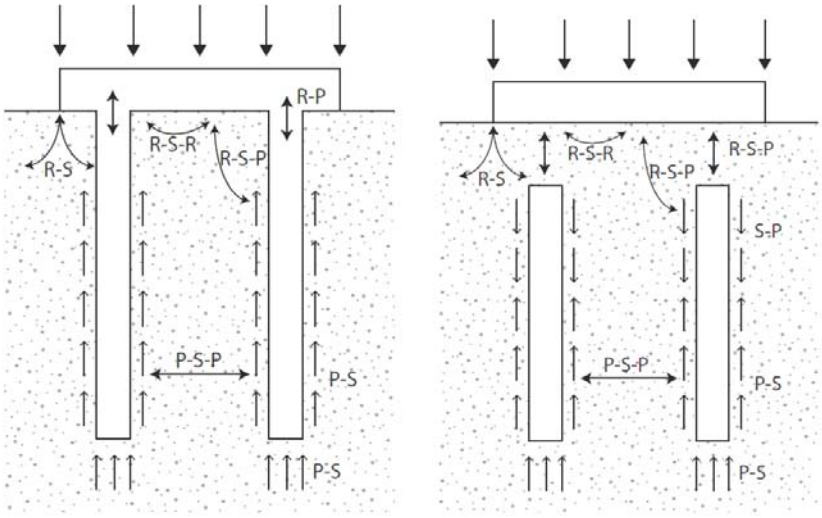

Figure 2.10: Different soil-structure interactions in CPRF (left) and DPRF (right), *Tradigo et al. (2016)* (R = raft; P = pile; S = soil)

2.7 Experimental studies on Piled Raft system

Horikoshi et al. (2003b) conducted several model tests on piled raft foundation in Toyoura dry sand under static horizontal loads. The load-displacement response and load sharing by piles and raft in piled raft system have been checked. The results shows that the single pile in piled raft system provides more resistance than the isolated single pile of same size. Initially piled raft system has less horizontal stiffness than raft foundation. Also, pile to raft connection behavior has been checked and it is concluded that rigidly connected pile head to raft has more horizontal stiffness than hinged connected pile head. During initial stage, the piles carry more proportion of vertical load than raft under vertical loading but in horizontal loading it is opposite. And it also seemed that the proportion of vertical load shared by piles does not change under horizontal loading while the proportion of horizontal load shared by piles increase with increase in horizontal loading.

Horikoshi et al. (2003a) performed a series of shaking table tests on piled raft foundation in Toyoura dry sand under dynamic loading and compared the results with the static horizontal tests (*Kenichi Horikoshi et al. 2003a*). All the results have similar pattern as in static horizontal loading. It is also concluded that the contact of raft with the soil surface has great influence in reducing horizontal acceleration, inclination and bending moments of piles.

Nakai et al. (2004) performed both experimental and numerical analysis to study the behavior of piled raft foundation under seismic loading. They studied the different types of foundation i.e. pile foundation, unpiled raft foundation, connected piled raft foundation, disconnected piled raft foundation and piled raft foundation with supplementary short piles using centrifuge model test and FEM in a computer code ACS SASSI. They found that the dynamic response of structure was reduced on using piled raft foundation. In disconnected piled raft foundation, piles had significant contribution in dynamic soil structure interaction. They made a comparison between computed values and measured values and found that computed values were significant smaller than measured values. Also, if the connection between pile and raft is either fixed or hinge, there will be little difference in response of both piled foundation and piled raft foundation. But, the result showed that the response of disconnected piled raft foundation was slightly larger than that of connected piled raft foundation. By introducing short piles, there was greater influence on shear forces and bending moments acting on piles.

Another attempt had been made by **Cao et al. (2004)** to study experimentally the behavior of rafts resting on pile reinforced sand and subjected to discrete concentrated loads. They tested effect of different parameters on the unpiled raft and disconnected pile raft. The foundation stiffness increased with using disconnected piles as reinforcement. Also, negative skin friction affected the load transfer in the upper part of the piles and helped in transmission of load from the raft to the piles. The differential settlement and bending moment were found to decrease in case of disconnected pile raft system.

With increase in the applied load, the fraction of loads carried by the piles increased rapidly and then decreased gradually to a stable value. The concentration of piles under the central portion of the raft led to a significant reduction in the differential settlement and the bending moment of the raft.

Sawwaf (2010) performed lots of laboratory tests to assess the effectiveness of using vertical short piles under an eccentrically loaded raft with connected piles (as structural members) and disconnected piles (as soil reinforcement) on sandy soil. He observed the effect of different parameters, e.g. pile length, pile number, pile arrangement, load eccentricity, relative density of sand. He introduced an index called Bearing Pressure Index (i.e. the ratio of the bearing pressure of a piled raft either connected or disconnected to piles, to the bearing pressure of an unpiled raft. He concluded that the using short piles adjacent to the raft edges not only significantly improves the raft bearing pressures but also reduces settlements and tilts in raft. This leads to an economical design of the raft. Also, connecting short piles to the raft gives greater improvement in the raft behavior than unconnected piles. It was also observed that after conducting tests on dense sand, the connected piles structurally deformed but no deformation was observed in the disconnected piles.

Fioravante and Giretti (2010) performed a series of centrifuge model tests on connected and disconnected piled raft foundation to investigate the load transfer mechanism between raft and a group of piles embedded in dry dense sand subjected to uniform vertical loading ranging from 25 to 700 kpa. In connected piled raft foundation, the piles are directly loaded by the raft through their heads. However, in disconnected piled raft foundation, load is transferred partially through piles heads and partially through negative skin friction acting on the upper part of piles. This load is balanced by positive skin friction acting on lower part of piles and the base resistance. They found that initial foundation stiffness depends mainly on the pile stiffness and interposed layer stiffness for on connected and disconnected piled raft foundation respectively. Also, in connected piled raft foundation, pressure transmitted by raft to the sub-soil increases the vertical

and horizontal effective stresses. By this, pile capacity is enhanced compared to isolated pile for both before and after yielding. Also they expressed disconnected piled raft stiffness as function of the isolated pile stiffness, number of piles, and unpiled raft stiffness by a rough procedure. A coefficient β was used to encounter the effect of interposed layer and interactions.

Richter et al. (2011) used visco-hypoplastic model for soft soil and hypoplastic model for gravel layer in the FE software Abaqus (version 6.8-3) for the numerical analysis of the spread footing over reinforced ground with gravel interface during a strong earthquake. Their analysis was done for the foundation of the Golden Ears Bridge spanned the Fraser River in the metropolitan area of Vancouver i.e. a seismically active area. They validated the estimated constitutive parameters by a back analysis of a large-scale in situ test. Also, the layer was wrapped in a geosynthetic to provide lateral support and to minimize vertical deformation. They concluded that by disconnecting piles from footing by gravel layer there is neither guarantee of decoupling of ground and foundation nor reduction in inertial forces on the superstructure. Nevertheless, disconnecting piles from footing by gravel layer leads to a drastic decrease in bending moments and shear forces induced in the piles during the earthquake. The pile spacing was found to have a minor effect on the internal pile forces but in the range investigated, the layer thickness have no effect on those.

Fioravante (2011) performed the small scale physical model test to compare the load transfer mechanism from a raft to a pile with and without an interposed granular layer. He used siliceous sand as soil and performed on centrifuge test on unpiled raft, unpiled raft with an interposed granular layer, connected piled raft and disconnected pled raft with an interposed granular layer. He observed that in disconnected piled raft foundations the load transfer from raft to the pile takes place partially through the pile head and partially through the negative skin friction around the upper pile shaft perimeter. Within the serviceability range for raft settlement (i.e. approximately settlement/width of raft < 0.5%), the efficiency of connected piled raft foundation as a settlement reducer is

higher than that of disconnected pled raft foundation. When the raft settlement is small in connected piled raft foundation, a connected pile acts as settlement reducer otherwise it acts by reducing raft stress on the soil. However, a disconnected pile acts mainly as a reinforcement of the soil, enhancing the unpiled raft stiffness.

A series of full-scale load tests has been conducted by **Mattsson et al. (2013)** to design a piled raft foundation with an interposed granular layer for a nuclear storage facility that was being constructed on the site of existing nuclear power plant at Burgey, east of Lyon, France. The foundation was rested mainly on clay soil. The load was transferred partially from raft to piles head through arching effect and partially from surrounding soil to pile surface through negative skin friction on upper part of piles. From the numerical analysis, predicted results were found different from measured values. This difference was happened due to difference between in situ parameters and parameters considered for numerical model. But, after parameter adjustments, the results were satisfactory. Both construction details and soil parameters namely soil compressibility, OCR, Poisson's ratio, all affecting the SSI and permeability were adjusted.

Taha et al. (2014) performed an experimental studies to check the behavior of piled raft system founded on geosynthetic reinforced soil under static lateral load also compared with numerical analysis conducted PLAXIS 3D. Mohr-Coulomb model, Embedded pile and plate element were used to model soil, piles and raft respectively. Both experimental and numerical results showed that by providing geosynthetic layer, lateral resistance of the foundation was increased by 15% and reduces the structural forces in that foundation. It was also observed that with increase in loads, benefits of reinforcement increases.

A series of physical model test had been conducted by **Taha et al. (2015b)** on a shaking table in 1g environment to study the geosynthetic reinforced piled raft foundation system under seismic loading. The model supported a single degree of freedom (SDOF) structure was installed in a uni-directional laminar box containing a 3-layer soil stratigraphy, which included a layer of artificial clay (Glyben) sandwiched between two gran-

ular layers. The dynamic loading was used in form of strong sine sweep, harmonic and scaled earthquake. It founded that the dynamic responses of low frequency SDOF structure and raft were reduced under strong motion due to reinforcing the soil with geogrid but in other hand high frequency SDOF structure under weak motion did not reveal significant effect of reinforcing the soil.

Table 2.1: Summary of experimental studies on Connected and Disconnected piled raft foundations describing the type of study

Serial No.	Authors	Test type	Numerical software	Soil model
1	Horikoshi et al. (2003b)	Model test	-	-
2	Horikoshi et al. (2003a)	Shake table model test	-	-
3	Nakai et al. (2004)	Centrifuge model test and numerical simulation	Computer code ACS SASSI	Elastic half space
4	Cao et al. (2004)	Model test	-	-
5	Sawwaf (2010)	Model test	-	-
6	Fioravante and Giretti (2010)	Centrifuge model test	-	-
7	Richter et al. (2011)	Large scale field test and numerical analysis	Abaqus	Hypoplastic
8	Fioravante (2011)	Centrifuge model test	-	-
9	Mattsson et al. (2013)	Full-scale load test (Field test) and numerical study	Z_soil	MCC model and M-C model
10	Taha et al. (2014)	Model test	PLAXIS 3D	M-C model
11	Taha et al. (2015b)	Shake table model test	-	-

Table 2.2: Summary of experimental studies on Connected and Disconnected piled raft foundations describing the soil and loading type

Serial No.	Authors	Soil type	System	Loading type
1	Horikoshi et al. (2003b)	Dry Toyoura sand	Raft with four piles	Static horizontal loading
2	Horikoshi et al. (2003a)	Dry Toyoura sand	Raft with four piles	Dynamic loading
3	Nakai et al. (2004)	Sand	Raft over nine piles with disconnection	Artificial Earthquake loading
4	Cao et al. (2004)	Dry Sand	Different arrangements with imposed layer	UDL at center and two symmetrically located line loads
5	Sawwaf (2010)	Dry sand	Different arrangements with cushion	Eccentrically vertical load
6	Fioravante and Giretti (2010)	Dry Siliceous Sand	Different arrangements with cushion	Uniform vertical loading
7	Richter et al. (2011)	Composite soil(Field geometry)	Spread footing over two piles with gravel interface	Vertical, horizontal and earthquake loading
8	Fioravante (2011)	Dry Siliceous Sand	Single pile with cushion	Uniform vertical loading
9	Mattsson et al. (2013)	Field geometry	Embankment on nine piles with cushion	Vertical load with consolidation effect
10	Taha et al. (2014)	Composite soil	Raft with four piles founded on geogrid strengthened soil	Static horizontal load
11	Taha et al. (2015b)	Composite soil	Raft with four piles founded on geogrid strengthened soil	Earthquake loading

2.8 Numerical studies on Piled Raft system

Naesgaard et al. (2008) studied geotechnical seismic design aspect of Golden Ears Bridge for different events. In this they did determination of site-specific response spectra, ground motion time histories, assessment of liquefaction triggering and its consequences using dynamic numerical analysis with the program FLAC and UBCHYST and UBC-SAND constitutive models, assessment of foundation stiffness by push-over analysis using program FLAC with UBCSAND model, by using P-Y/T-Z method and the programs LPILE Plus 5.0 or GROUP and soil structure interaction analysis. There are three parts of bridge i.e. South approach, main river piers and north approach. The north approach of bridge is founded on two different types of piles i.e. the short shear piles are fixed to the cap, whereas the precast piles are not connected to the pile cap. From the analysis they founded that disconnecting the precast piles from pile cap reduced the earthquake induced moments and shears in the piles.

Wong et al. (2000) presented a chapter on raft foundation with disconnected settlement-reducing piles in a book editing by J. A. Hemsley. They discussed about the behavior of unpiled raft foundation, piled raft foundation and the problem associated with both. They gave an alternative economic design approach in which piles are not connected with raft. Because whenever the piled raft foundation is designed in areas susceptible to earthquake or high wind loads, the structural capacity of piles can be critical due to relatively high axial stress that may develop in piles. Also, the horizontal forces may damage the structural connections between the piles and the raft. They compared the behavior of rafts with structurally connected and disconnected piles based on the plane strain finite element method. They found that for disconnected piled raft foundation, lower factor of safety against structural failure of the piles can be used since piles behave as soil-reinforcing members. In case connected piled raft foundation, more loads are directly transferred to the piles heads while in disconnected piled raft foundation load is transferred from the raft to the piles mainly due to down-drag forces.

Liang et al. (2003) presented a paper on numerical analysis of composite piled raft with cushion subjected to vertical load. In this type of foundation, the short piles are used to strengthen the shallow soft soil, the long piles are used to reduce the settlement and the cushion is used to redistribute and adjust the stress ratio of piles to subsoil. Analysis had been done by 3D finite element method proposed by Ottaviani in ANSYS. They used bottom boundary as fixed and lateral surrounding boundary as vertically sliding but horizontally restrained. Results showed that increasing lengths of long piles is much more effective to reduce the settlement of foundation than increasing the elastic modulus of short piles. There exists an optimum value of length and elastic modulus of piles to reduce settlement with the least cost. With the use of cushion, the maximum axial stress shifts lower from the head of piles to certain depth. Decreasing the elastic modulus of cushion can decrease the axial stresses of long piles and mobilize the bearing capacity of short piles and subsoil. With an optimum value of cushion thickness we can make the best use of capacities of short piles and subsoil and reduce the stresses of long piles. Also, they studied a case history. From it they concluded that application of composite piled raft foundation to the subgrade with soft soil in the shallow layers has significant economic benefits.

Eslami et al. (2012) proposed that in pile-raft system the piles are usually provided not for overall stability of the foundation but to act as settlement reducers. If the piles are acting as settlement reducers only, the piles can be disconnected to raft to increase the system stiffness. They performed 2D and 3D finite element analysis of connected and disconnected raft-pile systems on three case studies. In each case piles and raft were modeled as plate elements. Analysis was done in PLAXIS 2D and PLAXIS 3D. They investigated the effect of different parameters, e.g. piles spacing, embedment length, piling configuration and raft thickness to optimize the design. They concluded that optimum design can be achieved by concentrating the piles in the central area of the raft foundation with the minimum total length of piles. Also disconnected piled-raft system can significantly reduce the settlements and raft internal bending moments by increasing the soil stiffness.

Sharma et al. (2011) studied the effect of cushion on composite piled-raft foundation. In composite piled-raft foundation, the short piles made of relatively flexible materials such as sand-gravel columns and the long piles made of relatively rigid materials such as reinforced concrete were used. They investigated the effect of cushion by finite element analysis in MIDAS GTS computer program. The results showed that the axial stress of long piles in composite piled raft foundation with cushion is smaller than that of foundation without cushion, while the axial stress of short piles in composite piled raft foundation with cushion are larger than that of foundation without cushion. Also, the load sharing between the raft and the piles is affected by the cushion.

Faizi et al. (2013) proposed a new technique to improve lateral stability of Non-Connected Piled Raft Foundation (NCPRF). This new technique called Telescopic Non-Connected Piled Raft Foundation (TNCPRF) includes short connected piled to raft with long disconnected piles. For analysis, the Mohr-Coulomb constitutive model was used to simulate the non-linear silty-clay in PLAXIS computer software. The results showed that settlement in TNCPRF was 20% less in comparison with PRF. The stress reduction using TNCPRF was lesser than using NCPRF but is better than using PRF. The horizontal displacement for raft foundation using TNCPRF was improved compared with using NCPRF.

A detailed literature review on rational design of piled raft foundation has been presented by **Mandolinia et al. (2013)**. In recent years, much works have been done to study how piled interact with raft and soils in piled raft foundation. When small piled raft foundations (i.e. width of raft/length of pile < 1) are resting on soft to medium fine grained soils, piles are designed to increase the overall capacity and to reduce the settlement. On the other face, raft is resting on medium to hard fine grained soils or sandy soil; piles are designed to reduce only average settlement for small piled raft foundation; average and differential settlement for large piled raft foundation. When the position of the piles coincides with that of the structural columns, piles are used to reduce bending

moments and shear forces into raft; mainly structural capacity of piles must be checked. If piled raft foundation is subjected to lateral load and piles are not connected to raft, bending moments and shear forces generated in foundation decrease. If foundation is designed in earthquake-prone areas, several new factors have to be considered in design procedure. For example, large diameters piles reduce the structural seismic forces but these are subjected to higher kinematic bending.

Ata et al. (2015) performed numerical analysis of disconnected piled raft with cushion subjected to vertical load. They used ABAQUS finite element analysis software to investigate the effect of different parameters e.g. cushion thickness, cushion elastic modulus, piles number, pile diameter, raft thickness. Raft, cushion and piles were modeled as elastic and layer soil system was used. For all types of soil, Mohr-Coulomb model was used as constitutive model except for soft clay Modified cam-clay model was used. The results showed that the disconnected piled raft system is an economical alternative design approach over connected piled raft system. Since, the axial load along pile length was less in case disconnected piles. Also, the maximum axial load occurred at the pile head in the connected pile raft system and then decreases along length. However, the maximum axial load occurred at certain length below the pile head (approximately three meters) in the disconnected pile raft system and then decreases along the length as in the connected pile raft system. They also found that the maximum settlement of the raft increases slightly with the increase of the cushion thickness, and the axial load decreases slightly along the pile length.

One of the most comprehensive works in the field of non-linear 3D finite element analysis of disconnected piled raft (DPR) foundations has been presented by **Tradigo et al. (2015)**. The effect of different pile figures and raft-pile gap has been investigated on structural response and settlement/stiffness efficiencies of foundation using soil-structure interaction. They used non-associated Mohr-Coulomb elasto-plastic model for soil and kinematic boundary conditions. They found that in DPR foundation, negative and positive skin friction develops on the upper and lower part of pile respectively. The negative

skin friction on the internal side of pile is for greater depth than along the external side. But there exists a neutral plane where the maximum axial force is associated. It is always between the internal and external locations at which skin friction changes from negative to positive. DPR shows significantly different soil-structure interaction. In case connected piled raft (CPR) foundation, severe plastic strains develop along the pile length from raft corners to the pile tip. In case of DPR foundation, it occurs under the tips and heads of the external piles and minimum values develop at neutral plane. Also, lower bending moments in piles due to disconnection generate and with increase in the gap, bending moments decrease.

Tradigo et al. (2014) performed 3D finite element analysis to study suitability of disconnected piled raft foundation. As there has been done less work in this field, they studied the influence of space/time discretization and used an optimum value of time-steps number and mesh element number to get more accurate results. A non-associated Mohr-Coulomb constitutive relationship was used for soil, while linear variation of soil young modulus with depth was assumed. The result showed that structural response of the piles has been improved in case of disconnected piled raft foundation. But, the settlement efficiency is more in case of connected piled raft foundation and decreases with increasing in granular layer thickness. So, the optimum value of thickness has a proper balance between structural and geotechnical requirements. Also, in disconnected piled raft foundation, there exists a neutral plane at which maximum axial load and minimum plastic strain develops.

Mansour et al. (2014) conducted a series of 3D elasto-plastic finite difference analyses to investigate the behavior of a square piled raft in clay soil subjected to vertical loading. To get worst condition, they performed effective drained analyses. They investigated the effect of several parameters e.g. pile numbers, pile length and pile configuration on average settlement, differential settlement and load sharing between raft and piles. From the results, they found that with the increase in numbers of piles, there was no significant effect on piled raft settlements and coefficient. But, pile configuration and pile

length had considerable effect on piled raft settlements and coefficient.

Abdel-Fattah et al. (2014) presented a paper to model the piled raft foundation comprising defective piles. Sub-soil condition consisted of different rock layers and alluvium deposits soil layers. All the elements were modeled in 3D finite element program DIANA VER. 9.4.4 (DIANA, 2012). The results showed that for normal behavior, the maximum settlement of piled raft (PR) and piled group (PG) was identical but for defective behavior the PG settled more than PR. For both behaviors, maximum load per pile is higher in case of PG. Also, percentage of load directly transferred by the raft increases as the percentage of defective piles increases. Finally they concluded that percentages and locations of defective piles have to be considered for worst condition design.

Sharma et al. (2015) conducted FE analysis in Midas GTS 2013 (v2.2) to study the behavior composite piled raft foundation with cushion under earthquake loading. They used the time history of earthquake Sanfer 1971 on Surat city (India) geological conditions. Mohr-Coulomb constitutive model was used to model the nonlinear behavior of stratified soil. The interaction between piles and soil was modeled by using a modified Coulomb theory. The foundation consisted of 4 flexible short pile, 1 rigid long pile, cushion between raft and piles. Aslo, the springs and dampers were applied along all boundaries. For all layers reaction and damping coefficients were calculated by using Eigen value analysis. For long piles, all parameters (i.e. axial stress, tension, shear force and bending moment) at its head reduced to a great extent with inclusion of cushion. With the use of cushion, axial stress, tension and shear force distributed uniformly along the all short piles. However, negligible moments were developed along the short soil-cement piles. Relative displacement between raft and piles is almost negligible after inclusion of cushion.

Taha et al. (2015a) simulated the soil with advanced constitutive model (Hardening soil model with small strain stiffness) in finite element analysis of geosynthetic-reinforced piled raft system under dynamic loading. The model was verified against the results of

reduced scale 1D shaking model test. In that verification, vertical boundaries of model were allowed to free translation in the direction of shaking and vertical direction but fixed in direction normal to shaking (other than vertical) and at bottom, prescribed surface was applied through which harmonic loading was used. The influence of different design parameters have been investigated on foundation system. All results showed that geosynthetic-reinforced soil increases the lateral resistance of foundation and the use of geogrid as reinforcing is more conservative than improving ground along larger depth.

Floroiu and Schweiger (2015) analyzed numerically the influence of soil improvement (by granular soil columns and concrete piles) in ground response during seismic events (Loma Prieta earthquake,1989). All materials were modeled as linear visco-elastic material and rigid bedrock conditions were used. The authors modified the stiffness, damping ratio and unit weight of soil according soil improvement and checked effect this modifications. The results shows that with granular soil improvement, the seismic loads on a structure decrease due to increase in stiffness and damping parameters. In other hand with concrete pile soil improvement, the seismic loads both decrease and increase.

Kumar et al. (2016) carried out numerical analysis with finite element software PLAXIS 3D (version 5.10) to investigate the behavior Combined Pile-Raft Foundation (CPRF) under pseudostatic and dynamic loading. They studied the behavior of CPRF of Messeturm Tower, Frankfurt am Main, Germany under El-Centro 1979, Loma Prieta 1989, Bhuj 2001 and Sikkim 2011 earthquake loading history. They reported that the maximum displacement and bending moment occurred at the head of pile and decreases with depth. And piles provides more resistance in pseudostatic loading as compare to raft but in vertical loading this case is reverse. Under resonance condition, higher responses of foundation occur than other conditions. Also, they suggested that the strong interaction between pile, raft, and soil is presented due to which response spectra of near field is higher than far field.

Table 2.3: Summary of numerical studies on piled raft foundations describing numerical software, soil type and soil model

Serial No.	Authors	Numerical software	Soil type	Soil model
1	Naesgaard et al. (2008)	FLAC	Field geometry	UBCHYST and UBCSAND models
2	Wong et al. (2000)	N/A	Stiff clay	N/A
3	Liang et al. (2003)	ANSYS	Soft soil	Linear elastic model
4	Eslami et al. (2012)	PLAXIS 3D Foundation	Field geometry	M-C model
5	Sharma et al. (2011)	Midas GTS	Soft soil	Linear elastic model
6	Faizi et al. (2013)	PLAXIS 3D Foundation	Silty Clay	M-C model
7	Mandolinia et al. (2013)	-	-	-
8	Ata et al. (2015)	ABAQUS	Composite soil	M-C model
9	Tradigo et al. (2015)	Midas GTS	Sand	M-C model
10	Tradigo et al. (2014)	Midas GTS	Sand	M-C model
11	Mansour et al. (2014)	FLAC 3D	Frankfurt clay	M-C model
12	Abdel-Fattah et al. (2014)	DIANA 2012	Rock and alluvium soil	M-C model
13	Taha et al. (2015a)	PLAXIS 3D	Composite soil	HS SMALL model
14	Sharma et al. (2015)	Midas GTS 2013	Composite soil	M-C model
15	Kumar et al. (2016)	PLAXIS 3D	Toyoura sand and Frankfurt clay	M-C model and HS Model

Table 2.4: Summary of numerical studies on piled raft foundations describing loading type

Serial No.	Authors	System	Loading type
1	Naesgaard et al. (2008)	Foundation of Golden Ears Bridge	Seismic analysis
2	Wong et al. (2000)	Raft over four piles with imposed layer	Vertical loading
3	Liang et al. (2003)	Raft over 1 long and 4 short piles with cushion	Uniform vertical loading
4	Eslami et al. (2012)	Three case histories	Vertical loading
5	Sharma et al. (2011)	Raft over 1 long and 4 short piles with cushion	Vertical loading
6	Faizi et al. (2013)	Raft over 4 piles and 1 center short pile with imposed layer	Horizontal loading
7	Mandolinia et al. (2013)	A Literature review	-
8	Ata et al. (2015)	Different arrangements with cushion	Vertical loading
9	Tradigo et al. (2015)	Raft over 5 piles with imposed layer	Uniform vertical loading
10	Tradigo et al. (2014)	Raft over 5 piles with imposed layer	Uniform vertical loading
11	Mansour et al. (2014)	Piled raft foundation for Torhaus building	Vertical loading
12	Abdel-Fattah et al. (2014)	Piled raft foundation with defective piles	Vetical loading
13	Taha et al. (2015a)	Raft with four piles founded on geogrid strengthened soil	Dynamic loading
14	Sharma et al. (2015)	Composite piled raft foundation with cushion	Seismic loading
15	Kumar et al. (2016)	Combined piled raft system (Messeturm Tower)	Seismic loading

2.9 Literature on embedded pile approach

3D Finite element solution for laterally loaded passive piles was investigated by **Ekici and Huvaj (2014)** in Plaxis 3D software. Comparison of numerical analysis was made with full scale field experimental data using Mohr-Coulomb soil model. They have made a six-edged hexagonal soil elements (having the same diameter and length as the pile and same material properties as surrounding soil) just around the piles to closely observe behavior of soil having immediate contact with the pile by providing finer mesh in that area. The effect of size of the model, boundary fixity conditions and mesh size properties have been investigated. The results show that medium mesh is the optimum mesh size which provide enough numerical accuracy and less time consumption. As we move from coarse to finer meshes, there is decrease in maximum bending moment and shear force in the pile. Also, they suggested that embedded pile option to model the piles is the robust tool.

Septanika et al. (2008) investigated the pile group behavior using Embedded Piles as model of piles. Embedded pile element is slender beam element, which is connected to the soil by embedded skin interfaces and embedded foot interfaces. They checked the effect of piles spacing in raft touching and not touching the soil. With increase in spacing, the capacity foundation increases but above a particular upper limit of spacing, there will be no significant gain in capacity. Full mobilization of the skin tractions and foot resistance illustrates the accuracy of the present interaction models.

A detailed study has been done by **Dao (2011)** to validate the PLAXIS Embedded Piles for lateral loading. It was founded that the embedded pile overestimates the load-displacement behavior. This is because currently it does not take into account the "slide", which is used to model pile-soil interaction, in horizontal direction. Nevertheless, it shows a good performance in modeling the laterally loaded pile.

Tschuchnigg and Schweiger (2015) and Tschuchnigg (2013) verified to model the pile

foundation as the embedded element and gave some improvements. To define the pile-soil interaction, embedded interface elements are used with four stiffnesses i.e. one axial interface stiffness(K_s), two normal interface stiffnesses(K_n and K_t), one base interface stiffness(K_{base}). For it, elastic-plastic model is used. The main parameters i.e. ultimate skin resistance and maximum base resistance should be taken care during assigning. Author have suggested that base interface stiffness should be increased in comparison of the reference embedded pile model and the mean effective stress p' should be used as reference stress for stiffness definition inside the elastic region. To model a realistic mobilization of skin resistance, stress dependent shear interface stiffness should be used. There is no need of modification in default values of K_s, K_n and K_t. Various comparisons have been to show that the embedded pile option is a convenient alternative tool to the standard finite element approach.

Chapter 3

Numerical modeling

In general, to support high-rise building and buildings which are founded on poor soil, deep foundation is required. These buildings cannot be supported by shallow foundation because there will be more deformation and structural forces. Depending upon soil profile and soil properties, piled raft foundation is the solution for most of the cases. Settlement and differential settlement are main design parameters for these types of foundations. But to assess these parameters with considering all interactions within foundation elements, advanced numerical modeling is essential. The finite element method, amongst other numerical technique, is a very power tool for modeling of these elements. Numerical modeling needs the profound knowledge of soil mechanics, constitutive models and numerical methods. And, practical experience is also required for complex modeling. In this chapter, some basic aspects of FEM and modeling the different elements as used in this study are discussed.

3.1 Finite element method

Finite element method is being widely used for modeling of all different interactions of complex structures existing in piled raft foundation. It is a computational procedure which provides approximate results for many engineering problems. Commonly it is applied under static, dynamic and thermal behavior of physical system. In many cases, it is not possible to solve satisfactorily a very complex problem by classical analytical method (due to irregular geometry, non-homogeneous media and arbitrary loading con-

ditions), then FEM is very useful tool in that cases. In this method the model is divided into finite elements and this procedure is called discretization which is the main function FEM. This elements are connected to each other at points (i.e. called nodes or nodal points) common to two or more elements. Firstly the displacements at these nodes are calculated by FE analysis after that this displacement information is used for further calculations.

A continuum body divided into finite elements is called a mesh. In PLAXIS 3D, mesh is generated fully automatically with different element sizes, for finer mesh the element size will be very small. The element size depends on the outer geometry dimensions of model. The mesh should be sufficiently fine to obtain accurate numerical results. On the other hand, very fine meshes should be avoided since this will lead to excessive calculation times. The shapes of these elements can be triangular, quadrilaterals or rectangular in 2D and tetrahedral or cubic in 3D. In PLAXIS 3D 10-node tetrahedral element is used for soil elements as shown in Figure 3.1 and special types of elements are used to model structural elements.

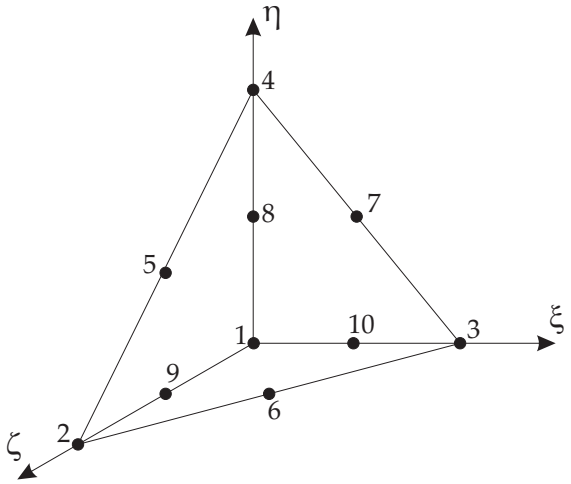

Figure 3.1: 3D soil element (10-node tetrahedral element), *Brinkgreve et al. (2013b) and Brinkgreve et al. (2015b)*

3.1.1 Shape function

The shape function is the interpolation function which is used to interpolate values inside the element based on known values in the nodes. The degree of shape function can be linear, quadratic, cubic, etc. It depends on the number of nodes used in an element e.g. 2-node line element has a linear shape function as illustrated in Figure 3.2. Each node has different shape and the maximum and minimum value of shape function is 1 and 0 respectively.

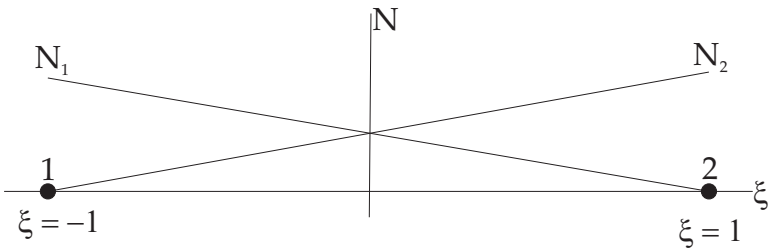

Figure 3.2: Shape function for 2-node line element, *Brinkgreve et al. (2013a) and Brinkgreve et al. (2015a)*

3.1.2 Basic formulation for 4-node tetrahedral element

In PLAXIS 3D 2013.01, 10-node tetrahedral element is used for soil model. But here formulation is explained only for 4-node tetrahedral element in similar way it can be derived for 10-node tetrahedral element. A tetrahedral i,j,m,p in space has been defined by x,y and z coordinates as illustrated in Figure 3.3.

The displacement ($\underline{U}$) at any point within the element is derived from the nodal displacements ($\underline{a}$) as given below:

$$\underline{U} = \underline{N}\,\underline{a} \tag{3.1}$$

Where,

$\underline{U} = \begin{Bmatrix} u \\ v \\ w \end{Bmatrix}$ where u,v and w are displacements in x, y and z directions.

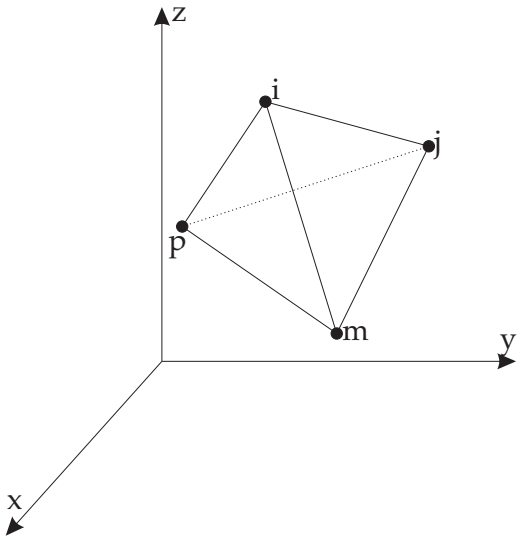

Figure 3.3: Tetrahedral element i,j,m,p in 3D space

$\underline{a} = \begin{Bmatrix} a_i \\ a_j \\ a_m \\ a_n \end{Bmatrix}$ where i,j,m,p denote the nodes and every nodal displacement has three components in x, y and z directions as $\underline{a}_i = \begin{Bmatrix} u_i \\ v_i \\ w_i \end{Bmatrix}$.

$\underline{N}$ = shape function matrix = $\begin{bmatrix} N_i I, N_j I, N_m I, N_p I \end{bmatrix}$ where N_i, N_j, N_m, N_p are shape functions for nodes i,j,m,p respectively and I is an Identity matrix of order 3×3.

The strains at any point can be found out from the known displacement at all points within the element by following relationship:

$$\underline{\varepsilon} = \begin{Bmatrix} \varepsilon_{xx} \\ \varepsilon_{yy} \\ \varepsilon_{zz} \\ \gamma_{xy} \\ \gamma_{yz} \\ \gamma_{zx} \end{Bmatrix} = \begin{Bmatrix} \frac{\partial u}{\partial x} \\ \frac{\partial v}{\partial y} \\ \frac{\partial w}{\partial z} \\ \frac{\partial u}{\partial y} + \frac{\partial v}{\partial x} \\ \frac{\partial v}{\partial z} + \frac{\partial w}{\partial y} \\ \frac{\partial w}{\partial x} + \frac{\partial u}{\partial z} \end{Bmatrix} = \begin{bmatrix} \frac{\partial}{\partial x}, 0, 0 \\ 0, \frac{\partial}{\partial y}, 0 \\ 0, 0, \frac{\partial}{\partial z} \\ \frac{\partial}{\partial y}, \frac{\partial}{\partial x}, 0 \\ 0, \frac{\partial}{\partial z}, \frac{\partial}{\partial y} \\ \frac{\partial}{\partial x}, 0, \frac{\partial}{\partial z} \end{bmatrix} \begin{Bmatrix} u \\ v \\ w \end{Bmatrix} = \underline{L}\underline{U} = \underline{L}\underline{N}\underline{a} = \underline{B}\underline{a} \qquad (3.2)$$

Where,

$\underline{B}$ = Strain interpolation matrix

$\underline{L}$ = Differential operator matrix

For elastic behavior of material, the stresses ($\underline{\sigma}$) can be determined by stress-strain relationship according to Hook's law:

$$\underline{\sigma} = \underline{D^e}(\underline{\varepsilon} - \underline{\varepsilon}_0) + \underline{\sigma}_0 \tag{3.3}$$

Where,

$\underline{D^e}$= Elasticity matrix of order of 6×6 that means this matrix contains total 36 independent constants but due to symmetry these will be 21. The value of these constants depends on material properties.

$\underline{\varepsilon}_0$= initial strains due to temperature changes, shrinkage, crystal growth, and so on

$\underline{\sigma}_0$= initial residual stresses

The nodal forces ($\underline{q}$) which are statically equivalent to the boundary stresses and distributed body forces $\underline{b}$ on the element can be determined by following equation (*Zienkiewicz and Taylor (2000)*):

$$\underline{q} = \underline{K}\,\underline{a} + \underline{f} \tag{3.4}$$

Where,

$\underline{K}$ = Stiffness matrix = $\int_V \underline{B}^T \underline{D^e}\,\underline{B} dV$, where V = Volume of material within element

$\underline{f}$= $-\int_V \underline{N}^T \underline{b} dV - \int_V \underline{B}^T \underline{D^e}\,\underline{\varepsilon}_0 dV + \int_V \underline{B}^T \underline{\sigma}_0 dV$= Forces due to body forces, initial strain and initial stress respectively.

3.1.3 Basic formulation for Dynamic behavior

The equation which defines the time-dependent motion in a volume under the influence of a (dynamic) load can be expressed as:

$$\underline{M}\,\underline{\ddot{u}} + \underline{C}\,\underline{\dot{u}} + \underline{K}\,\underline{u} = \underline{f} \tag{3.5}$$

Where,

$\underline{f}$ = Load vector $\underline{\ddot{u}}, \underline{\dot{u}}, \underline{u}$ = Acceleration, velocity and displacement respectively $\underline{M}$= Mass matrix = sum of all element masses

$\underline{K}$= Stiffness matrix = $\int_V \underline{B}^T \underline{D}^e \underline{B} dV$ (for elastic behavior) = $\int_V \underline{B}^T \underline{D}^{ep} \underline{B} dV$ (for elastoplastic behavior) $\underline{C}$= Material damping matrix that can be determined by Rayleigh damping formulation

The damping in numerical analysis dissipates the energy under dynamic loading. Material damping in dynamic calculation can be caused by viscosity of soil, friction or plastic deformations. Damping due to plastic deformations can be simulated by various plastic models but damping due to other factors is modeled by Rayleigh Damping. In this formulation, damping matrix is function of mass matrix and stiffness matrix.

$$\underline{C} = \alpha \underline{M} + \beta \underline{K} \tag{3.6}$$

Where, α and β are Rayleigh damping coefficients. These coefficients are related to the following relationship:

$$\xi = \frac{\alpha}{2\omega} + \frac{\beta}{\omega} \quad \text{and} \quad \omega = 2\pi f \tag{3.7}$$

Where,

ξ=Damping ratio which defines the system is Overdamped ($\xi > 1$) or Critically damped ($\xi = 1$) or Underdamped ($\xi < 1$).

ω = Angular frequency in rad/s and f = Frequency in Hz (1/s).

By solving equation 3.7 for two different target frequencies (ω_1 and ω_2) and corresponding target damping ratios (ξ_1 and ξ_2), the Rayleigh damping coefficients can be obtained from following expressions:

$$\alpha = 2\omega_1\omega_2 \frac{\omega_1\xi_2 - \omega_2\xi_1}{\omega_1^2 - \omega_2^2} \quad \text{and} \quad \beta = 2\frac{\omega_1\xi_1 - \omega_2\xi_2}{\omega_1^2 - \omega_2^2} \tag{3.8}$$

It is suggested by *Laera and Brinkgreve (2015)* that target damping ratios $\xi_1 = \xi_2$ should be taken and generally, chosen between 0.5 and 2%. According to *Hudson et al. (1994)* the first target frequency should be equal to the fundamental frequency of the whole

soil layer and the second target frequency should be equal to closest odd number given by the ratio of the fundamental frequency of the input signal at the bedrock and the fundamental frequency of the whole soil layer. The fundamental frequency (f) of the whole soil layer can be expressed as:

$$f = \frac{v_s}{4H} \tag{3.9}$$

Where,

v_s = Shear wave velocity = $\sqrt{\frac{G}{\rho}}$ where G is Shear modulus of soil in unit of kN/m^3 and ρ is the density of soil in unit of kg/m^3.

H = Thickness of soil layer in m

Time integration schemes i.e. Explicit and Implicit are used for numerical calculations of dynamics. The explicit integration has simple formulation, but its process is not robust and has limitations on the time step. The implicit method is more complicated, but it is more reliable method and produces more accurate results. So in PLAXIS 3D, Newmark implicit integration scheme is used. According to this scheme, the displacement ($u^{t+\Delta t}$) and the velocity ($\dot{u}^{t+\Delta t}$) at $t + \Delta t$ are expressed respectively as:

$$u^{t+\Delta t} = u^t + \dot{u}^t \Delta t + \left(\left(\frac{1}{2} - \alpha \right) \ddot{u}^t + \alpha \ddot{u}^{t+\Delta t} \right) \Delta t^2 \tag{3.10a}$$

$$\dot{u}^{t+\Delta t} = \dot{u}^t + \left((1 - \beta) \ddot{u}^t + \beta \ddot{u}^{t+\Delta t} \right) \Delta t \tag{3.10b}$$

Where,

u^t and $\dot{u}^t$ = the displacement and the velocity at time t respectively

$\ddot{u}^{t+\Delta t}$ and $\ddot{u}^t$ = the accelerations at time $t + \Delta t$ and t respectively

Δt = Time step

α and β = Newmark's coefficients

For unconditional stable solution, the following condition should be satisfied:

$$Newmark\ \beta \geq 0.5 \quad \text{and} \quad Newmark\ \alpha \geq 0.25(0.5 + \beta)^2 \tag{3.11}$$

3.2 Modeling of soil material

General

In continuum mechanics, stress at a point is defined by stresses components acting on three mutually perpendicular planes passing through that point. These stress components consist of one normal stress and two shear stresses components on each plane. In this study, the state of stress or these orthogonal planes are defined in Cartesian coordinate system. Figure 3.4 shows different stress components on every plane of a cubic element.

The different stress components acting on a plane can be represent as a stress vector

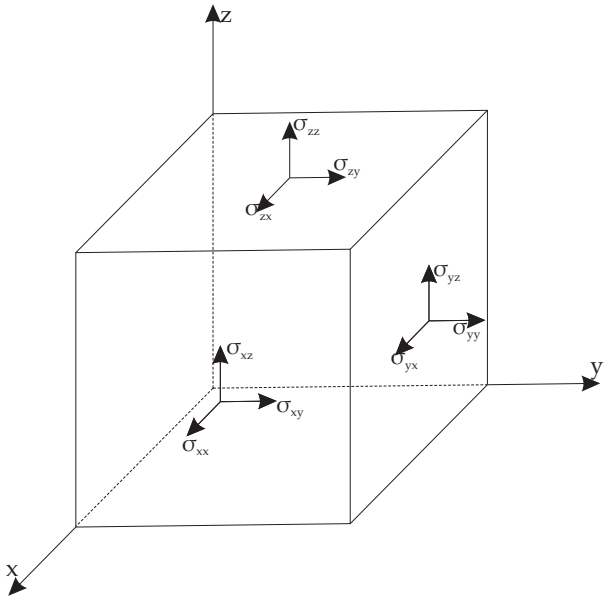

Figure 3.4: Stress components on a cube element in 3D space

acting on each plane of cubic element.

$$\underline{t_x} = \left\{ \begin{array}{c} \sigma_{xx} \\ \sigma_{xy} \\ \sigma_{xz} \end{array} \right\}; \qquad \underline{t_y} = \left\{ \begin{array}{c} \sigma_{yx} \\ \sigma_{yy} \\ \sigma_{yz} \end{array} \right\}; \qquad \underline{t_z} = \left\{ \begin{array}{c} \sigma_{zx} \\ \sigma_{zy} \\ \sigma_{zz} \end{array} \right\} \tag{3.12}$$

Where, σ_{xx} indicates the normal stress component in direction of x-axis and acting on plane which is perpendicular to x-axis. σ_{xy} and σ_{xz} denote the shear stress components

acting on plane which is perpendicular to x-axis, in direction of y-axis and z-axis respectively, similarly for others. This implies that subscripts describe the working direction of stress components. The first subscript indicates the axis perpendicular to the plane on which stress component act and second subscript indicates direction of stress component.

The total stress state of cubic element can be presented by combining all stress vectors. This matrix formulation containing nine stress components is known as Stress tensor which is given below:

$$\underline{\sigma} = \begin{bmatrix} t_x \\ t_y \\ t_z \end{bmatrix} = \begin{bmatrix} \sigma_{xx} & \sigma_{xy} & \sigma_{xz} \\ \sigma_{yx} & \sigma_{yy} & \sigma_{yz} \\ \sigma_{zx} & \sigma_{zy} & \sigma_{zz} \end{bmatrix} \tag{3.13}$$

For moment equilibrium of the element, the following shear stress relationships are required:

$$\sigma_{xy} = \sigma_{yx} \qquad \sigma_{yz} = \sigma_{zy} \qquad \sigma_{zx} = \sigma_{xz} \tag{3.14}$$

Which implies that only six components are required to define the whole stress state of an element or elastic soils.

The deformation of any body is defined by strain. Every stress components on cubic element faces is related to the associated components of strain. If the displacements in x-,y-and z-direction are u,v and w respectively, the strain components are given by:

Normal strain components,

$$\varepsilon_{xx} = \frac{\partial u}{\partial x}; \qquad \varepsilon_{yy} = \frac{\partial v}{\partial y}; \qquad \varepsilon_{zz} = \frac{\partial w}{\partial z} \tag{3.15}$$

Infinitesimal shear strain components:

$$\varepsilon_{xy} = \varepsilon_{yx} = \frac{1}{2}\left(\frac{\partial u}{\partial y} + \frac{\partial v}{\partial x}\right); \qquad \varepsilon_{yz} = \varepsilon_{zy} = \frac{1}{2}\left(\frac{\partial v}{\partial z} + \frac{\partial w}{\partial y}\right); \qquad \varepsilon_{zx} = \varepsilon_{xz} = \frac{1}{2}\left(\frac{\partial w}{\partial x} + \frac{\partial u}{\partial z}\right); \tag{3.16}$$

Engineering shear strain components:

$$\gamma_{xy} = \gamma_{yx} = \left(\frac{\partial u}{\partial y} + \frac{\partial v}{\partial x}\right); \qquad \gamma_{yz} = \gamma_{zy} = \left(\frac{\partial v}{\partial z} + \frac{\partial w}{\partial y}\right); \qquad \gamma_{zx} = \gamma_{xz} = \left(\frac{\partial w}{\partial x} + \frac{\partial u}{\partial z}\right); \tag{3.17}$$

The strain components can be expressed as strain tensor as given below:

$$\underline{\varepsilon} = \begin{bmatrix} \varepsilon_{xx} & \varepsilon_{xy} & \varepsilon_{xz} \\ \varepsilon_{yx} & \varepsilon_{yy} & \varepsilon_{yz} \\ \varepsilon_{zx} & \varepsilon_{zy} & \varepsilon_{zz} \end{bmatrix} = \begin{bmatrix} \sigma_{xx} & \frac{\gamma_{xy}}{2} & \frac{\gamma_{xz}}{2} \\ \frac{\gamma_{yx}}{2} & \sigma_{yy} & \frac{\gamma_{yz}}{2} \\ \frac{\gamma_{zx}}{2} & \frac{\gamma_{zy}}{2} & \sigma_{zz} \end{bmatrix} \tag{3.18}$$

The strain components can be easily visualized by considering 2D strain in the x-y plane as shown in Figure 3.5.

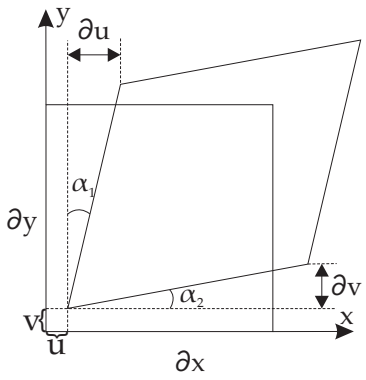

Figure 3.5: Plain strain deformation in square element

Stress-strain relationship

The stress-strain relationship at some point in continuum mechanics can be formulated as following:

$$\underline{\sigma} = \underline{D\varepsilon} \tag{3.19}$$

Where,

$\underline{\sigma}$ = Stress vector

$\underline{D}$ = Stiffness matrix

$\underline{\varepsilon}$ = Strain vector

Different stress-strain response occur for different materials but in general some specific response are available as shown in Figure 3.6.

Curves "a" and "b" represent the elastic behavior of material, but curve "a" describes

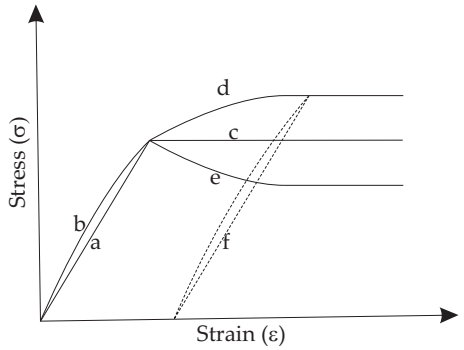

Figure 3.6: Stress-strain curves

the linear elastic behavior and "b" nonlinear elastic behavior. Curves "c", "d" and "e" represent the plastic behavior of material, where "c" shows perfect plastic, "d" and "e" show respectively strain hardening and strain softening behaviors. Curve "f" describes the elastic unloading or reloading behavior of material.

The stress-strain relationships are known as *constitutive models* and are specific for each material. All constitutive models manly describe the stiffness matrix and formulations of relationship with considering the behavior of material. Since stress-strain behavior of soil is very complicated becasuse soil is a non-linear, multi-phase, stress-dependent and time-dependent material, so various models are defined for different behavior of soils. Most of them are available in PLAXIS 3D. If a particular model is not present, that model can be used as user defined model. Some models relevant to this study are described as following:

3.2.1 Linear elastic model

Many materials behave elastic up to a certain level of stress. This elastic behavior can be expressed as linear variation as shown in Figure 3.7 . The simplest linear elastic behavior is called hyper-elasticity, i.e. the material elastic behavior is independent of the load history. This model is based on Hooke's law which describes the isotropic linear elastic

behavior of material. In PLAXIS 3D only two input elastic parameters that are Effective Young's modulus E (elasticity modulus) and Effective Poisson's ratio ν are used to define this model.

This model does not simulate any important facts of soil behavior. So it has limited use

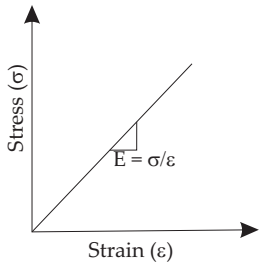

Figure 3.7: Linear elastic stress-strain curve

for analyzing geotechnical problems. But this model is more suitable for structural element materials e.g. steel, concrete, etc which often behave isotropic linear elastic in lower stress states. The following expression shows the stiffness matrix in terms of Effective Young's modulus E and Effective Poisson's ratio ν for isotropic linear elastic material.

$$\underline{D} = \frac{E}{(1+\nu)(1+2\nu)} \begin{bmatrix} 1-\nu & \nu & \nu & 0 & 0 & 0 \\ \nu & 1-\nu & \nu & 0 & 0 & 0 \\ \nu & \nu & 1-\nu & 0 & 0 & 0 \\ 0 & 0 & 0 & \frac{(1-2\nu)}{2} & 0 & 0 \\ 0 & 0 & 0 & 0 & \frac{(1-2\nu)}{2} & 0 \\ 0 & 0 & 0 & 0 & 0 & \frac{(1-2\nu)}{2} \end{bmatrix} \tag{3.20}$$

3.2.2 Mohr-Coulomb model

Since, any material behave elastic upto a certain stress level, after that plastic deformation takes place. So to define the plastic deformation, theory of plasticity is included. Mohr-Coulomb model is the most popular model which defines the plasticity of material. It is a linear elastic perfectly plastic model. The linear elastic part is described by Hooke's law while the perfectly plastic part is represented by Mohr-Coulomb failure criterion.

When plastic deformations occur, some permanent deformations known as irreversible strains is presented in material. A function, called yield function (f) is introduced which describes whether this deformations occur or not. When this function is equal to zero, plastic yielding will occur. If the yield function is plotted in 3D principal stress space, it forms a yield surface. In the space enclosed by this surface, the behavior is purely elastic and all strains are reversible. If the yield surface changes with plastic strain, the material will be harden or soften during plastic straining. So, perfectly plastic model is a constitutive model with fixed yield surface.

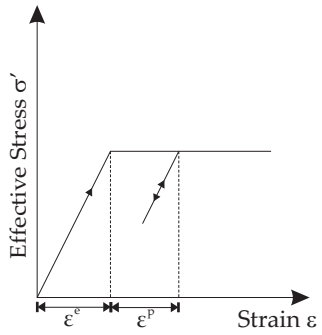

Figure 3.8: Linear elastic perfect plastic stress-strain curve

Stress-strain relationship for linear elastic perfectly plastic behavior

Figure 3.8 shows linear elastic perfectly plastic stress-strain response. The stress-strain relation can be expressed as following:

$$d\underline{\sigma}' = \underline{D}^{ep} \; d\underline{\varepsilon} \tag{3.21}$$

Where,

$d\underline{\sigma}'$ = Total incremental effective stress vector

$\underline{D}^{ep}$ = Elasto-plastic stiffness matrix

$\underline{\varepsilon}$ = Total incremental strain vector

The total incremental strain can be decomposed into elastic part and plastic part as-

$$d\underline{\varepsilon} = d\underline{\varepsilon}^e + d\underline{\varepsilon}^p \tag{3.22}$$

Since, the total incremental effective stress is related to the incremental elastic strain by Hooke's law. Then,

$$d\underline{\sigma}' = \underline{D}^e \; d\underline{\varepsilon}^e = \underline{D}^e \; (d\underline{\varepsilon} - d\underline{\varepsilon}^p) \tag{3.23}$$

As per classical plasticity theory, incremental plastic strain is proportional to derivative of yield function with respect to effective stresses. This shows that the incremental plastic strains can be represented as vectors perpendicular to yield surface. This classical approach is referred to as associated plasticity. However, for Mohr-Coulomb type yield function, this theory overestimates dilatancy. Therefore, instead of yield function, a plastic potential function (q) is defined where $q \neq f$ and this approach is known as non-associated plasticity. Now, incremental plastic strain can be expressed as following:

$$d\underline{\varepsilon}^p = \lambda \frac{\partial q}{\partial \underline{\sigma}'} \tag{3.24}$$

λ is plastic scalar multiplier.

$$\text{For} \qquad f < 0, \qquad \lambda = 0 \qquad \text{(Elasticity)} \tag{3.25a}$$

$$\text{For} \qquad f = 0, \qquad \lambda > 0 \qquad \text{(Plasticity)} \tag{3.25b}$$

From above written equations, the following relation can be expressed:

$$d\underline{\sigma}' = \underbrace{\left(\underline{D}^e - \frac{\alpha}{\beta} \underline{D}^e \frac{\partial q}{\partial \underline{\sigma}'} \frac{\partial f^T}{\partial \underline{\sigma}'} \underline{D}^e \right)}_{\underline{D}^{ep}} \; d\underline{\varepsilon} \tag{3.26a}$$

Where,

$$\beta = \frac{\partial f^T}{\partial \underline{\sigma}'} \underline{D}^e \frac{\partial q}{\partial \underline{\sigma}'} \tag{3.26b}$$

Where α is used as switch parameter: for elastic and plastic behavior $\alpha = 0$ and 1 respectively.

Formulation of Mohr-Coulomb model:

From equations 3.26a and 3.26b, it can be seen that in stress-strain relationship, elasto-

plastic stiffness matrix is a function of elastic stiffness matrix which is already defined in equation 3.20 and derivatives of yield function and plastic potential function with respect to effective stresses. For evaluation of elasto-plastic stiffness matrix, yield function and plastic potential function are required to express. Therefore, different models have different expression of stiffness matrix. Mohr-Coulomb yield condition is an extension of Coulomb friction law and obeys this law in any plane within the material. It consists of six yield functions which depend on principal stresses. Mohr-Coulomb failure criterion is illustrated in Figure and expressed in equation 3.27a.

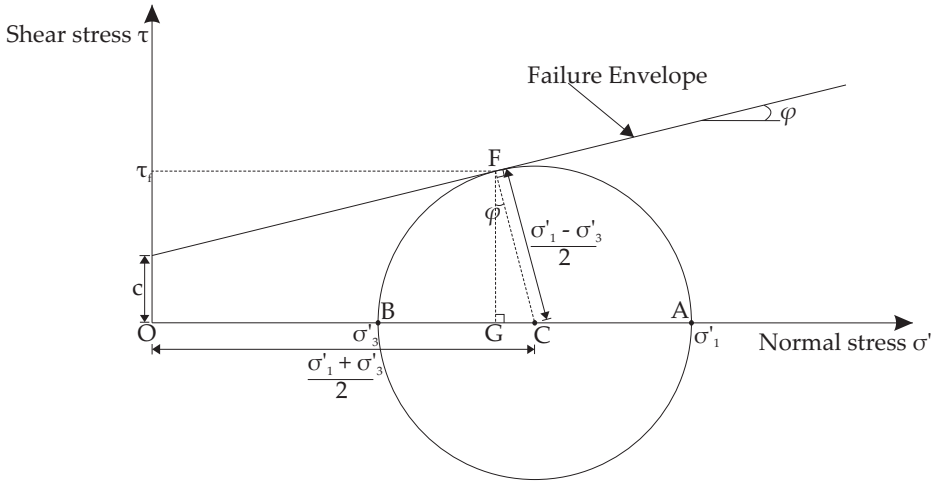

Figure 3.9: Graphical representation of Mohr-Coulomb failure criterion

$$\tau_f = c + \sigma'_n \tan\varphi \tag{3.27a}$$

From figure 3.9, equation 3.27a can be expressed in terms of principle stresses.

$$\frac{\sigma'_1 - \sigma'_3}{2} = \frac{\sigma'_1 + \sigma'_3}{2}\sin\varphi + c\cos\varphi \tag{3.27b}$$

Since six yield functions exist in this model. One of the yield function can be expressed like this:

$$f = \frac{\sigma'_1 - \sigma'_3}{2} - \frac{\sigma'_1 + \sigma'_3}{2}\sin\varphi - c\cos\varphi \leq 0 \tag{3.28}$$

Similarly, six plastic potential functions are also defined for this model. One of them is given below:

$$q = \frac{\sigma'_1 - \sigma'_3}{2} - \frac{\sigma'_1 + \sigma'_3}{2}\sin\psi \tag{3.29}$$

Where,

τ_f = Failure Shear stress

c = Cohesion of soil

φ = Friction angle

ψ = Dilatancy angle

σ'_n = Effective normal stress

σ'_1 = Effective major principal stress

σ'_3 = Effective minor principal stress

When plastic behavior occurs, all yield functions have zero value. And these functions create a fixed hexagonal cone in principal stress space as illustrated in Figure 3.10.

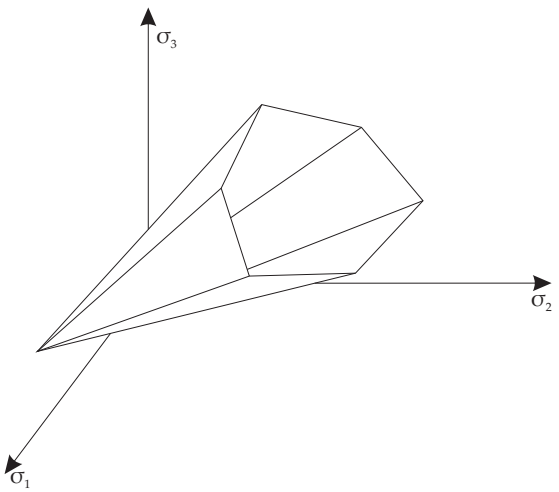

Figure 3.10: Mohr-Coulomb yield criterion in the principle stress space

Input Parameters:

For Mohr-Coulomb model, the input parameters are divided into two categories:

Basic Parameters

There are five following basic input parameters:

1. **Young's modulus (E)**

   Different Young's modulus have been defined for different behavior of material e.g. E_0 (tangent modulus-the initial slope of the stress-strain curve from triaxial

test), E_{50} (the secant modulus at 50% of the maximum stress level occurred in a triaxial test), E_{ur} (Young's modulus for soil when unloading and reloading occur) as shown in figure 3.11.

PLAXIS recommend that for modeling of initial loading, E_{50} should be used as

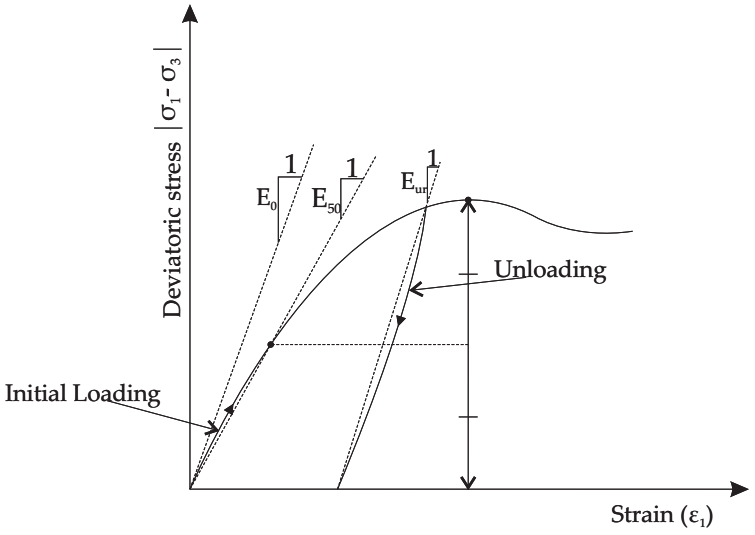

Figure 3.11: Definition of E_0, E_{50} and E_{ur}

soil's stiffness. However, when soil has larger linear elastic range, instead of E_{50}, E_0 can be used as stiffness. But for unloading-reloading problems, one should use E_{ur} instead of E_{50}.

2. **Poisson's ratio (ν)**

   In PLAXIS, it is recommended to use poisson's ratio in the range 0.3-0.4 and 0.15-0.25 for loading and unloading conditions respectively. But if the drainage type is set to Undrained (A) or Undrained (B), effective poisson's ratio should be used and its value should be less than 0.35.

3. **Cohesion (c)**

   The cohesion parameter is mainly depend on the drainage type of soil. For Drained and Undrained (A) type soil, cohesion is used to model the effective cohesion (c') of soil and for Undrained (B) and Undrained (C) type soil, it is used to undrained shear strength (c_u) of soil. For cohesionless soil ($c = 0$), the results are not nu-

merically stable. Therefore, it is suggested to use a smaller value of cohesion say $c \approx 0.2$kPa.

4. **Friction angle (φ)**

   The friction angle is used to model effective friction of soil in combination with effective cohesion (c') for Drained and Undrained (A) soil behavior. The computational time increases exponentially with increase in the friction angle. Hence, higher value of friction angles should be avoided for preliminary calculations of a particular project. According to *Brinkgreve et al. (2013a) and Brinkgreve et al. (2015a)* computing time becomes larger for friction angle more than 35° .

5. **Dilatancy angle (ψ)**

   Soils expand or contract during shearing. This volume change during shearing can be explained by the dilatancy angle. Since, the plastic potential function depends on dilatancy angle from equation 3.29. So, dilatancy angle controls the plastic volumetric strain developed during plastic shearing. Figure 3.12 illustrates the dilatation of element during shear (i.e. plastic behavior).

   Apart from overconsolidated layers, clay soils show very low dilatancy (approx-

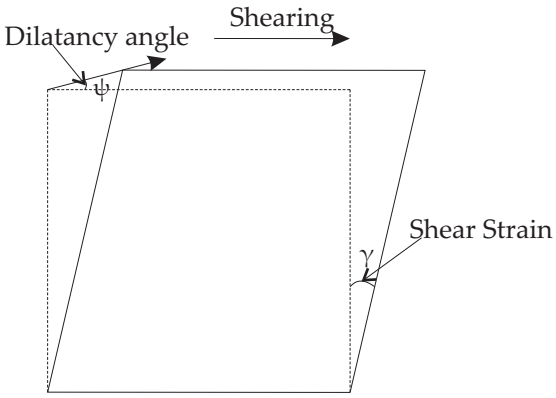

Figure 3.12: Volumetric change during shearing of an element

imately $\psi = 0$). For sand, the dilatancy angle depends on friction angle of soil. If friction angle is more than 30° ($\varphi > 30^\circ$), dilatancy angle can be evaluated as:

$$\psi = \varphi - 30^\circ \tag{3.30}$$

But if friction angle is less than or equal $30°$ ($\varphi \leq 30°$), dilatancy angle is mostly zero. A small negative value of dilatancy angle is acceptable for extremely loose sand.

Also other than these three advanced parameters such as increase of stiffness, increase of cohesion and tension cut off are also available to simulate more real behavior of soil.

Note that When Mohr-Coulomb model is used for dynamic calculation, special care should be taken. Because the stress cycles within the Mohr-Coulomb failure contour will define no (hysteretic) damping, nor accumulation of strains or pore pressure or liquefaction. In order to simulate the soil's damping characteristics in cyclic loading, Rayleigh damping is defined.

3.2.3 Hardening Soil model

The hardening soil model is an advanced model developed by *Schanz (1998)* and *Schanz et al. (1999)* for simulating the behavior of soft soils as well as stiff soils. This model is based on the hyperbolic model (*Duncan and Chang (1970)*) as shown in Figure 3.14 with implementation of some important features:

- Using of plasticity theory instead of elasticity theory;
- Including of dilatancy of soil;
- Establishing a yield cap as shown in Figure 3.13.

In contrast to earlier discussed models, the yield surface of this model expands due to plastic strain in principal stress space. This phenomena defines more realistic plastic behavior. As hardening takes place in this model and there are two types of hardening-Isotropic hardening and Kinematic hardening. Only isotropic hardening is included in this model of PLAXIS. Isotropic hardening is also divided into two parts i.e. Compression and Shear hardening. Compression and Shear hardening is used to model irreversible plastic strain due to primary compression and primary deviatoric loading respectively. Some basic features of this model are given below:

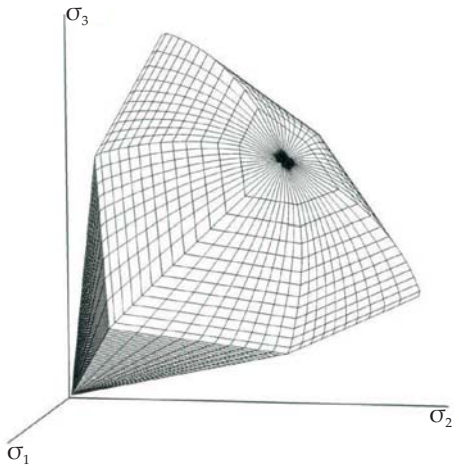

Figure 3.13: Representation of yield surface with cap in principal stress space for cohesionless soil, *Brinkgreve et al. (2013a) and Brinkgreve et al. (2015a)*

- Stiffness depends on stress according to a power law - m
- Plastic straining due to primary deviatoric loading - E_{50}^{ref}
- Plastic straining due to primary compression - E_{oed}^{ref}
- Elastic unloading / reloading - E_{ur}^{ref} , ν_{ur}
- Failure according to the Mohr-Coulomb failure criterion - c , φ and ψ

Hyperbolic Stress-Strain relationship

Based on the hyperbolic relationship between the vertical strain (ε_1) and the deviatoric stress (q) as shown in Figure3.14, the formulation of HS model can be described by:

$$-\varepsilon_1 = \frac{1}{E_i}\frac{q}{1-q/q_a} \quad \text{for} \quad q < q_f \tag{3.31}$$

Where,

q_a = Asymptotic value of the shear strength;

E_i = Initial stiffness that is related to E_{50} given by the equation:

$$E_i = \frac{2E_{50}}{2-R_f} \tag{3.32}$$

Where,

E_{50} is stiffness modulus which depends on confining pressure for primary loading and

is defined by following relation:

$$E_{50} = E_{50}^{ref} \left(\frac{c \cos \varphi - \sigma_3' \sin \varphi}{c \cos \varphi + p^{ref} \sin \varphi} \right)^m \tag{3.33}$$

Where E_{50}^{ref} is a reference stiffness modulus corresponding to the reference confining pressure p^{ref}. In PLAXIS by default p^{ref} is equal to 100kPa. Stress dependency of stiffness depends on exponent m. The value of m is 1 for soft clays, 0.5 for Norwegian sands and silts according to *Janbu (1963)*. *von Soos (1990)* suggests the range of m from 0.5 to 1.0. R_f is known as failure ratio of ultimate devaitoric stress (q_f) and Asymptotic value (q_a). Obviously value of R_f will be always less than 1 and in PLAXIS by default R_f is equal to 0.9. The ultimate devaitoric stress (q_f) is derived from Mohr-Coulomb failure criterion which involves strength parameters c and φ.

$$R_f = \frac{q_f}{q_a}; \qquad q_f = (c \cot \varphi - \sigma_3') \frac{2 \sin \varphi}{1 - \sin \varphi} \tag{3.34}$$

Where, σ_3' is minor principal stress (i.e. confining pressure in triaxial test)

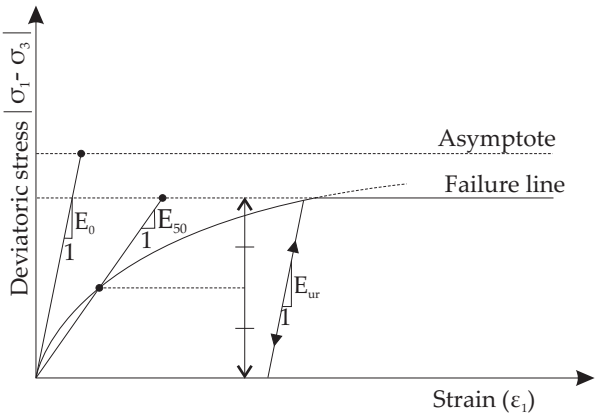

Figure 3.14: Hyperbolic stress-strain relationship, *Brinkgreve et al. (2013a) and Brinkgreve et al. (2015a)*

For unloading and reloading stress paths, another stress dependent stiffness modulus is used:

$$E_{ur} = E_{ur}^{ref} \left(\frac{c \cos \varphi - \sigma_3' \sin \varphi}{c \cos \varphi + p^{ref} \sin \varphi} \right)^m \tag{3.35}$$

Where E_{ur}^{ref} is a reference stiffness modulus for unloading and reloading corresponding to the reference confining pressure p^{ref}. By default in PLAXIS-

$$E_{ur}^{ref} = 3E_{50}^{ref} \tag{3.36}$$

Note: It is assumed that E_{ur} does not change. It will be a real elastic stiffness modulus.

Input Parameters

All input parameters of this model are defined in Table 3.2 and evaluation of them is explained in Table 3.1.

Table 3.1: Determination of input parameters of HS model

Parameters	**Evaluation**
E_{50}^{ref}	y-intercept in log(σ_3/p^{ref})-log(E_{50}) space
E_{oed}^{ref}	y-interceptin log(σ_1/p^{ref})-log(E_{oed}) space
E_{ur}^{ref}	y-intercept in log(σ_3/p^{ref})-log(E_{ur}) space
m	Slope of trend-line in in log(σ_3/p^{ref})-log(E_{50}) space
c	y-intercept of failure line from MC failure criterion
φ	Slope of failure line from MC failure criterion
ψ	Function of ε_a and ε_v
ν_{ur}	Default setting
K_0^{nc}	Default setting
R_f	$(\sigma_1 - \sigma_3)/(\sigma_1 - \sigma_3)_{ult}$

Note: The HS model better describes the soil behavior not only in terms of stress-strain relationship but also it includes stress dependency than Mohr-Coulomb model. But this model also have some limitations for dynamic calculations. Here also stress cycles within hardening contour will only generate elastic strains.

3.2.4 Hardening Soil model-Small Strain

Benz et al. (2009) and Benz (2007) explained in detail, the formulation and verification of the Hardening Soil model with Small Strain stiffness. The essential background of the model has been discussed in this section. In standard HS model, unloading/reloading behavior is assumed as linear elastic within yield surface. However, the strain range in which soils can be considered truly elastic is very small. Soil stiffness decreases non-linearly with increase in strain. This phenomena is illustrated in Figure 3.15. Because

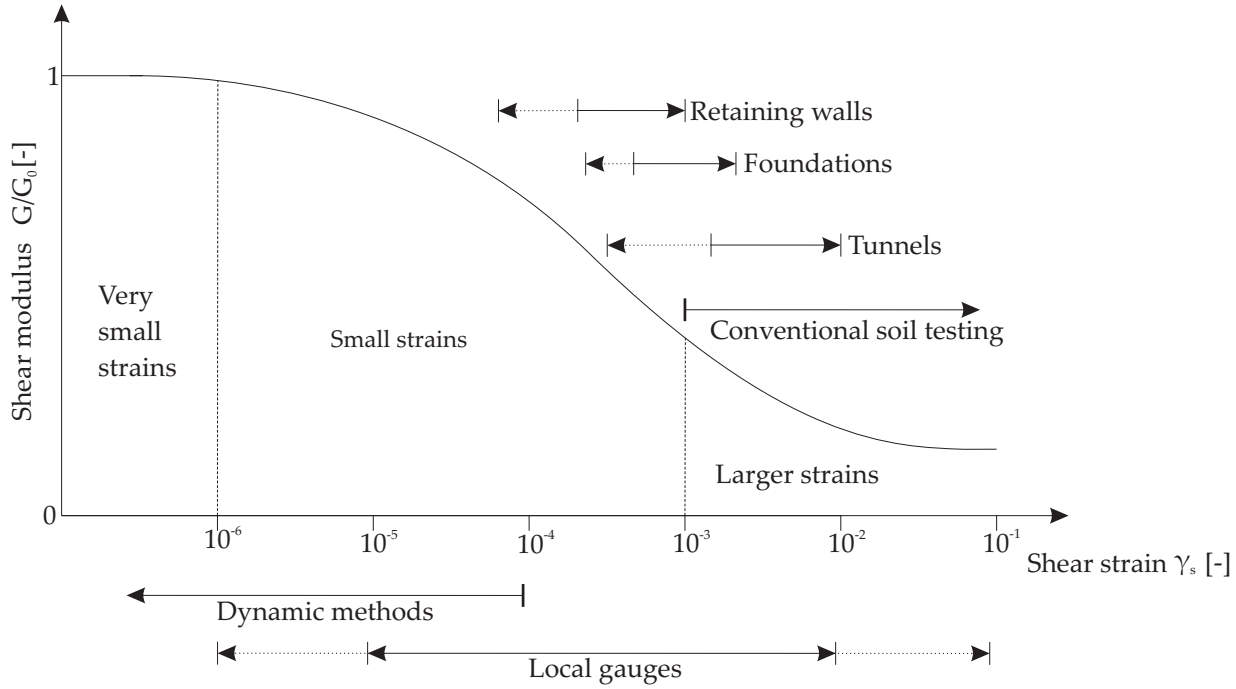

Figure 3.15: Secant shear modulus-shear strain behavior of soil with typical strain ranges for laboratory tests and structures, *Brinkgreve et al. (2013a) and Brinkgreve et al. (2015a)*

HSSmall model is based on HS model, therefore almost all parameters are same. Only two additional parameters are defined to explain variation of stiffness with strain:

1. Initial or very small strain shear modulus (G_0)
2. Shear strain ($\gamma_{0.7}$) at which secant shear modulus (G_s) is equal to 70% of G_0

The relationship between G_0 and $\gamma_{0.7}$ is based on hyperbolic law in which stiffness decreases with increase in strain due to loss of intermolecular and surface forces within soil

skeleton. Firstly it was defined by *Hardin and Drnevich (1972)*, then modified by *Santos and Correia (2001)* and given as:

$$\frac{G_s}{G_0} = \frac{1}{1 + a\left|\frac{\gamma}{\gamma_{0.7}}\right|} \qquad \text{where } a = 0.385 \tag{3.37}$$

By putting value of a and $\gamma = \gamma_{0.7}$, the value of $\frac{G_s}{G_0} = 0.722$. It shows that instead of 70%, 72.2% will be more accurate.

The stress-strain relationship can be expressed by secant shear modulus as:

$$\tau = G_s\gamma = \frac{G_s}{G_0} = \frac{1}{1 + 0.385\left|\frac{\gamma}{\gamma_{0.7}}\right|} \tag{3.38}$$

The tangent shear modulus (G_t) is evaluated by differentiating equation3.38 with respect to shear strain:

$$\frac{G_t}{G_0} = \frac{1}{\left(1 + 0.385\left|\frac{\gamma}{\gamma_{0.7}}\right|\right)^2} \tag{3.39}$$

Plotting the tangent shear modulus against shear strain according to equation3.39 shows that the decrement of tangent shear modulus tends to zero for infinite shear strains as shown in Figure3.16. Therefore a lower cut-off limit of G_t is set and equal to unloading/reloading stiffness (G_{ur}) which is calculated by material parameters E_{ur} and ν_{ur}.

$$G_t \geq G_{ur} \quad \text{where} \quad G_{ur} = \frac{E_{ur}}{2(1+\nu_{ur})} \quad \text{and} \quad G_t = \frac{E_t}{2(1+\nu_{ur})} \tag{3.40}$$

The cut-off shear strain $\gamma_{cut-off}$ can be evaluated as:

$$\gamma_{cut-off} = \frac{1}{0.385}\left(\sqrt{\frac{G_0}{G_{ur}}} - 1\right) \tag{3.41}$$

Not only tangent shear modulus G_t but also young's modulus E_t with constant ν_{ur} depends on stress and follows same power law as in HS model. For primary loading, the model uses same formulation as in HS model, where E_{ur} is replaced by E_t.

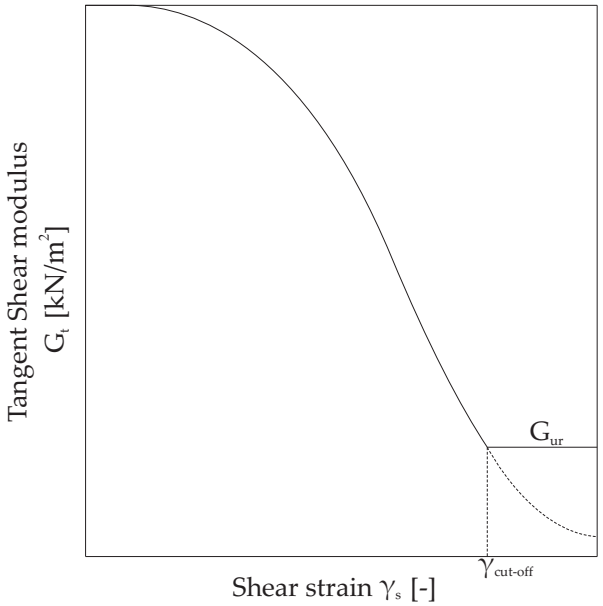

Figure 3.16: Cut-off in the tangent stiffness reduction curve as used in the HSSmall model

Hysteresis Behavior of Soil

A typical soil subjected to cyclic loading exhibits a hysteresis loop which is a graph between shear stress and shear strain for loading, unloading and reloading as shown in Figure 3.17. This hysteresis loop can be explained by HSSmall model. Shear modulus

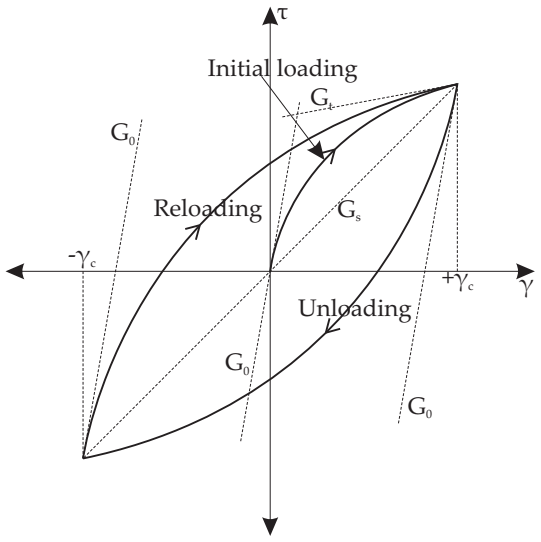

Figure 3.17: Hysteresis Behavior of Soil

starts with small strain shear modulus G_0 and decreases with increase in shear strain according to Figure3.15. When the load will be reversed, the shear modulus will restart from G_0 and will decrease again until the next load reversal. This implies that the stiffness of soil is defined by the inclination of hysteresis loop. Under dynamic loading, hysteresis behavior establishes a hysteresis damping component. This damping can be evaluated as damping ratio according to *Brinkgreve et al. (2007)*, as given below:

$$\xi = \frac{E_D}{4\pi E_S} \tag{3.42}$$

Where,

E_D is dissipated energy in one load cycle from $\gamma = -\gamma_c$ to $+\gamma_c$ and back to $-\gamma_c$ (where γ_c is maximum shear strain in one load cycle). It is equal to area of the hysteresis loop. E_S is energy stored at maximum shear strain γ_c.

Input Parameters

All parameters except G_0^{ref} and $\gamma_{0.7}$ of this model have been discussed in HS model. G_0^{ref} is the shear modulus at very small strain e.g. strain < 10^{-6} for reference confining pressure p^{ref}. It can be calculated from expression $G_0^{ref} = E_0^{ref}/(2(1+\nu_{ur}))$, because ν_{ur} is assumed constant and E_0^{ref} is small strain young's modulus. $\gamma_{0.7}$ is the threshold shear strain at which $G_s^{ref} = 0.722 G_0^{ref}$. It is to be supplied for initial loading.

Table 3.2: Input parameters of HS model in PLAXIS

	Parameters	Explanation
Basic Parameters	E_{50}^{ref}	Reference secant stiffness modulus in standard drained triaxial test
	E_{oed}^{ref*}	Reference tangent stiffness modulus for primary oedometer loading ($E_{50}^{ref} = 1.25E_{oed}^{ref}$)
	E_{ur}^{ref}	Reference unloading or reloading stiffness modulus (default $E_{ur}^{ref} = 3E_{50}^{ref}$)
	m	Power for stress-level dependency of stiffness
	c	Effective cohesion
	φ	Effective friction angle
	ψ	Dilatancy angle
Advanced Parameters	ν_{ur}	Poisson's ratio for unloading-reloading (default $\nu_{ur} = 0.2$)
	p^{ref}	Reference stress for stiffness modulus (default $p^{ref} = 100$kPa)
	K_0^{nc}	K_0-value for normal consolidation (default $K_0^{nc} = 1 - \sin\varphi$)
	c_{inc}	Increase of cohesion as defined in Mohr-Coulomb model
	R_f	Failure ratio (default $R_f = 0.9$)
	$\sigma_{tension}$	Tensile strength as defined in Mohr-Coulomb model (default $\sigma_{tension} = 0$)

$*$ E_{oed}^{ref} is used to define E_{oed} by following relationship:

$$E_{oed} = E_{oed}^{ref} \left(\frac{c\cos\varphi - \frac{\sigma_3'}{K_0^{nc}}\sin\varphi}{c\cos\varphi + p^{ref}\sin\varphi} \right)^m$$

3.3 Modeling of piles

Piles can be modeled in two dimension or three dimension, but for real interaction of piles with surrounding soils, it is required to model them in 3D. For modeling of piles two approaches such as Standard finite element approach and Embedded pile approach are used. In Standard finite element approach volume elements are used to model the piles. But when the large number of piles are used, this approach takes more time to analyze. So a new approach, Embedded pile approach, has been defined to model the piles in 3D model. Here we will discuss both the approaches to model piles in PLAXIS 3D.

3.3.1 Standard finite element approach

In this approach, the piles are modeled with volume elements in which the interaction with surrounding soil is modeled with interface elements. The roughness of the soil-structure interaction is defined with a strength reduction factor R_{inter}, which determines the interface strength with respect to soil strength. In PLAXIS 3D, the volume pile can be created as continuum with different shapes and sizes. Figure 3.18 shows window of inserting a solid function. The properties of volume pile are assigned as soil properties but with concrete properties.

One of main key issue with volume elements is that they cannot give the structural forces as output of analysis. But to get these forces, a beam element is inserted at the axial axis of the volume pile as shown in Figure 3.19. The properties of beam element will be same properties as volume pile except young's modulus. This beam element should have to be much softer than the volume pile for real behavior. For this *Dao (2011)* recommended that Young's modulus of beam element should be 10^6 times lower than that of volume pile. The deformation of beam element will be same as that of volume pile. But to obtain the actual result of structural forces in the pile, the force values of beam in PLAXIS output have to be multiplied by 10^6. But this issue has been solved in new version PLAXIS 3D AE.01 in which a cylindrical volume pile can gives structural forces directly.

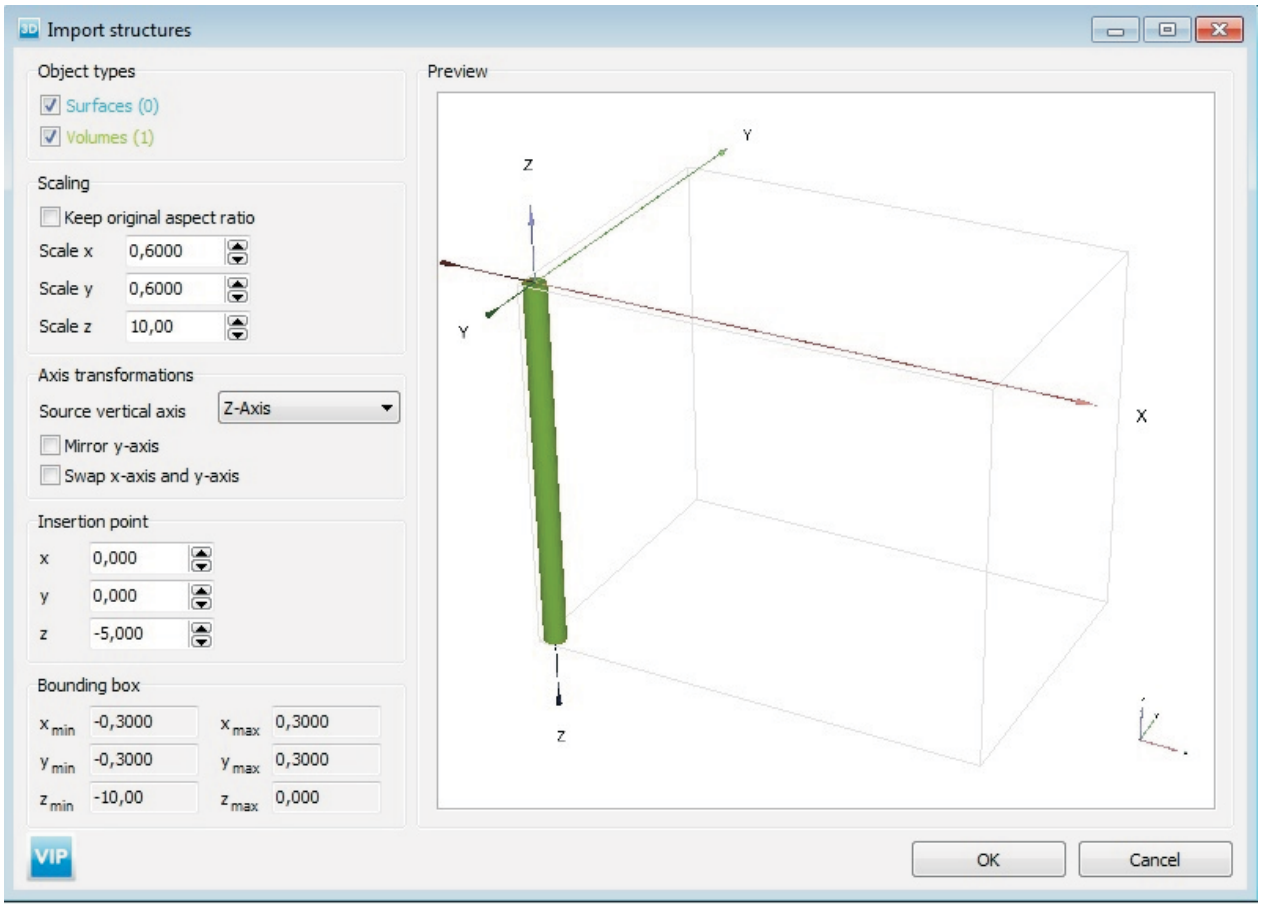

Figure 3.18: Inserting of Volume pile by solid function

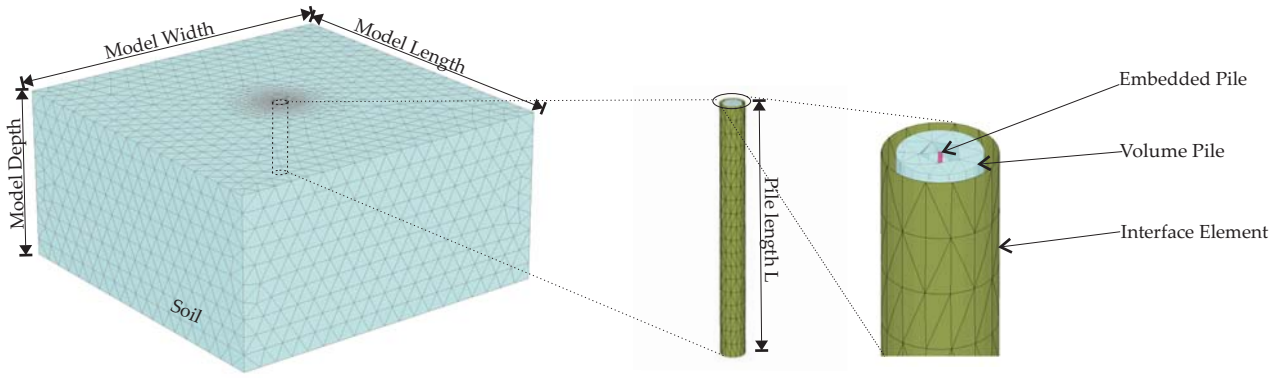

Figure 3.19: Standard finite element approach in PLAXIS 3D

3.3.2 The embedded pile approach

In this approach, the piles are modeled as embedded pile element that is considered as a beam element. This element can cross 10-node tetrahedral soil volume elements at any

place with any arbitrary orientation as shown in figure 3.20. When the embedded pile crosses the soil elements, additional nodes called "virtual" nodes are automatically generated inside these existing finite elements. An embedded pile consists of 3-node line elements with quadratic shape function. Each node has six degrees of freedom, i.e. three translations (u_x, u_y, u_z) and three rotationals ($\varphi_x, \varphi_y, \varphi_z$).

An elastic region having same diameter as pile (radius R_{eq}) is introduced arround em-

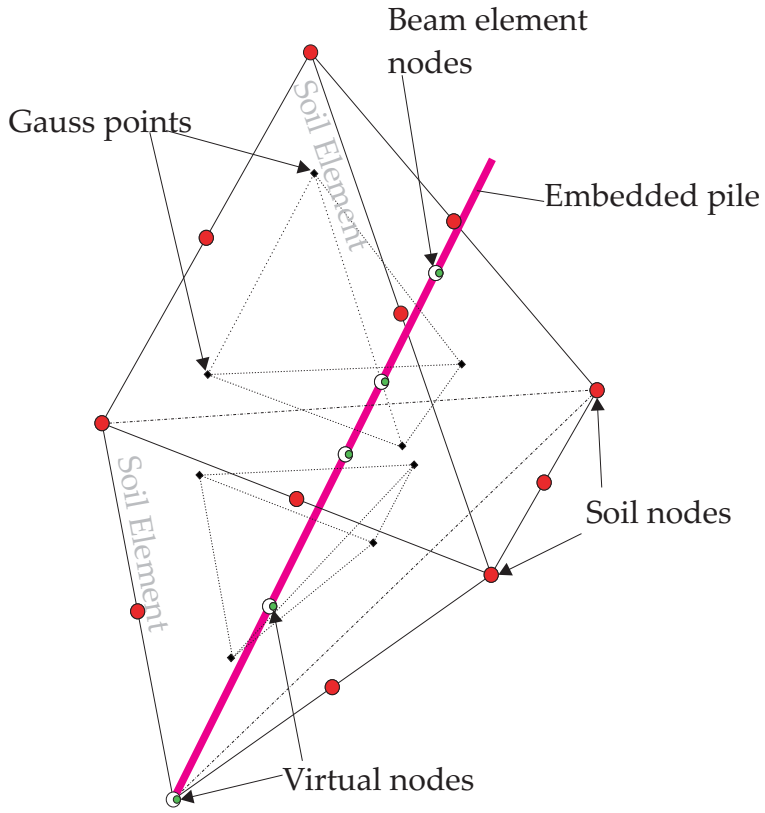

Figure 3.20: Embedded pile with a 10-node tetrahedral element, *Tschuchnigg and Schweiger (2015)*

bedded pile as shown in figure 3.21. This elastic region excluded the plastic soil behaviour in the vicinity of the pile element. The properties inside the elastic region is similar to the properties of surrounding soil. After loading, Gaussian points (Stress points) of the soil which fall inside the elastic region are forced remain elastic (linear elastic behavior) but has the same stiffness as the surrounding soil. By this region, the embedded pile behaves like a volume pile. The elastic region cosists of two sub-regions, one is elastic region along the pile shaft and second is elastic region above the pile and below the

pile base.

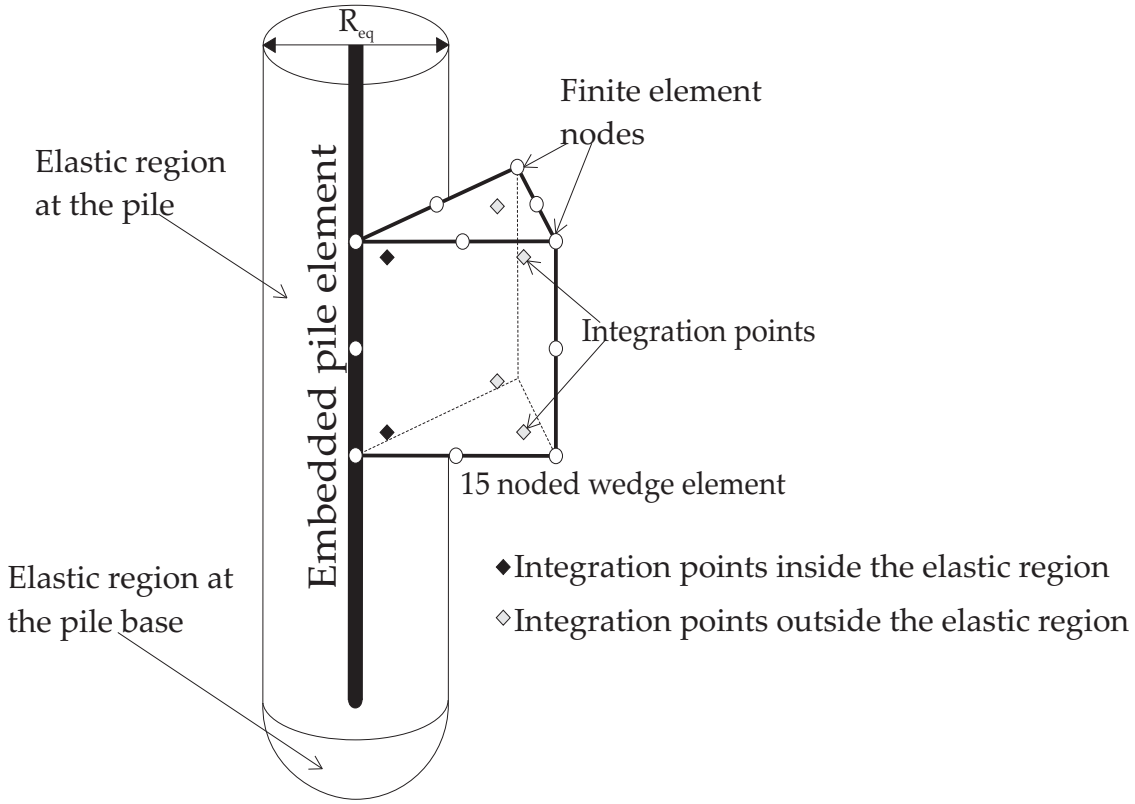

Figure 3.21: Schematic representation of the elastic region, *Tschuchnigg and Schweiger (2015)*

Input Parameters

In PLAXIS 3D, the embedded pile is defined in separate material data sets: the input parameters of an embedded pile are classified into three groups. The first group is related to the beam properties of pile and second group describes the interface element i.e. pile-soil interaction. The third group describes the connection of pile head with the solid finite elements.

Beam properties

Since embedded pile is considered as beam element, so it is modeled as linear elastic material. Linear elastic properties of embedded pile are defined by the Young's modulus E and the unit weight γ of pile material. Subsequently, geometric properties of the pile

are defined by two options. The first option is predefined shapes in which three shapes (i.e. Massive circular pile, Massive tube, Massive square pile) are already defined. The diameter, thickness or width is set up to defined these shapes. In predefined shapes, area (A) and moment of inertia I_2 and I_3 are calculated automatically. But in the second option which is user-defined, area and moment of inertia have to be set up directly. If the piles are not circular an equivalent radius is calculated.

$$R_{eq} = max \left\{ \sqrt{\frac{A}{\pi}}, \sqrt{\frac{I_2 + I_3}{A}} \right\} \tag{3.43}$$

Note that structural elements itself do not occupy the any volume and overlaps with the soil elements. Hence, at the time of assigning unit weight of structural elements, it should be subtracted by unit weight of soil in order to compensate for the overlap. For partial overlapping of elements, the reduction of unit weight should be proportional.
For dynamic behavior, two additional parameters are defined as material properties. These parameters are Rayleigh damping parameters α and β which describe the influence of mass and stiffness in damping of the system.

Pile-soil interaction

The pile-soil interaction is related to the relative displacement between the pile nodes and virtual nodes in the soil element. Interaction between embedded pile and surrounding soil is modeled by embedded interface element. This embedded interface element connect the virtual nodes inside soil elements and the nodes of the embedded pile. The embedded interface element is defined by elasto-plastic model. The interaction is described by skin resistance and tip resistance whose sum is known as the bearing capacity of embedded pile.
The skin resistance along embedded pile is given by following constitutive equation:

$$t^{skin} = K^{skin} \times \Delta u_{rel} \tag{3.44}$$

$$t^{skin} = \begin{bmatrix} t_s \\ t_n \\ t_t \end{bmatrix} \tag{3.45}$$

$$K^{skin} = \begin{bmatrix} K_s & 0 & 0 \\ 0 & K_n & 0 \\ 0 & 0 & K_t \end{bmatrix} \tag{3.46}$$

$$\Delta u_{rel} = \begin{bmatrix} u_s^p - u_s^s \\ u_n^p - u_n^s \\ u_t^p - u_t^s \end{bmatrix} \tag{3.47}$$

Where,

t^{skin} = Skin force vector along embedded pile at integration point

K^{skin} = Stiffness matrix of embedded interface elements

Δu_{rel} = Relative displacement vector between the soil and pile

t_s = Shear stress in axial direction

t_n and t_t = Normal stress in horizontal direction (normal on pile)

K_s = Elastic shear interface stiffness

K_n and K_t = Elastic normal interface stiffness

u^p = Displacement of pile node

u^s = Displacement of virtual soil node

Figure 3.22 gives an visualization of the embedded interface stiffness. The maximum skin resistance T_{max} is defined as capacity of interface to distinguish the behavior of interface. When shear force ts at particular point is less than T_{max} at that point ($|t_s| < T_{max}$), it behaves as elastic. Otherwise it behaves as plastic if ($|t_s| \geq T_{max}$). The maximum base resistance F_{max} is assigned by a non-linear spring at the base of an embedded pile. The base resistance of embedded pile is given by following constitutive equation:

$$F_{base} = K_{base} \ (u_{base}^p - u_{base}^s) \tag{3.48}$$

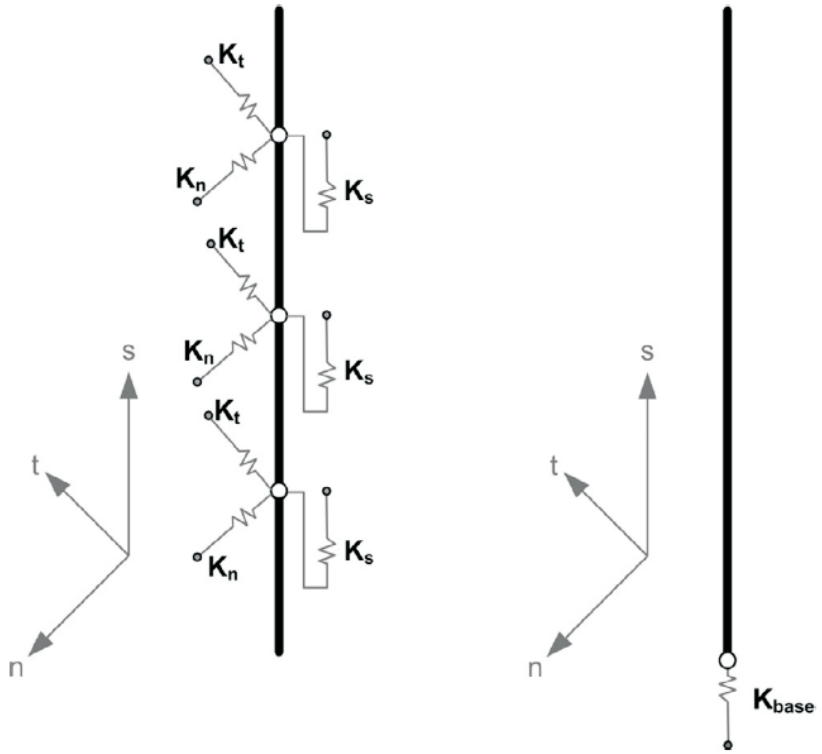

Figure 3.22: Embedded interface stiffness at the pile shaft(left) and the pile base(right), *Tschuchnigg and Schweiger (2015)*

Where,

F_{base} = Base resistance of the embedded pile

K_{base} = Spring stiffness at pile base

u^{p}_{base} = Displacement of last embedded pile node

u^{s}_{base} = Displacement of connected virtual node of soil

When the pile is pulled out, force at base of pile F_{base} will be zero (tension behavior). When pile undergoes into compression and force at base of pile F_{base} is equal or greater than maximum base resistanceF_{max}, failure can occur.

Whenever the maximum value of any force at an integration point is reached, relative displacements between the embedded pile and the surrounding soil occur.

The ultimate skin resistance is defined by three different options. First option is the linear distribution, where a constant or linear distribution exists by inserting two values $(T_{top,max}, T_{bot,max})$ This option is useful when pile is embedded in homogeneous soil. The

bearing capacity (Q_{pile}) can be defined as following equation:

$$Q_{pile} = F_{max} + \frac{1}{2} L_{pile}(T_{top,max} + T_{bot,ma}) \tag{3.49}$$

Second option is the multi-linear distribution, where a maximum skin resistance T_{max} is defined at certain position along the pile length L_{pile}. This option is useful when pile is embedded in non-homogeneous soil or multiple soil layers. The bearing capacity (Q_{pile}) is given by:

$$Q_{pile} = F_{max} + \sum_{i=1}^{n-1} \frac{1}{2}(L_{i+1} - L_i)(T_i + T_{i+1}) \tag{3.50}$$

In these two options, the bearing capacity of pile is an input to do analysis. The maximum bearing capacity can be defined by pile load test data or if pile load test data is not available, by classical approach.

The third option is layer dependent option. In this option, the ultimate skin resistance is defined with one input value T_{max}. The maximum shear stress ($t_{s,max}$) is related to the strength parameters of the soil (cohesion c and friction angle φ), interface strength reduction factor(R_{inter}) which is set up in the material data set of soil and the normal stress (σ_n^{avg})along interface. The value of R_{inter} affects the relative displacement between the pile and the soil.

$$t_{s,max} = (\sigma_n^{avg} \cdot \tan \varphi_i' + c_i) \cdot 2 \cdot \pi \cdot R_{eq} \tag{3.51}$$

$$\sigma_n^{avg} = \frac{\sigma_t + \sigma_n}{2} \tag{3.52}$$

Where,

σ_t and σ_n = Effective stresses of the surrounding soil perpendicular to the pile

When the third option is used, the embedded interface elements behave similar to standard zero thickness interface elements as used in the standard finite element approach, the main difference is that the interaction is modeled along a line element.

Output Parameters

After calculation, embedded pile gives Axial force N, Shear force Q_{12}, Shear force Q_{13}, Bending moment M_2, Bending moment M_3, Skin force T_{skin} (in axial pile direction) and lateral forces T_2 and T_3 as structural forces.

3.3.3 Validation of the embedded piles by previous research

Many researches have been done to validate the use of embedded pile. From these researches, it has been proved that embedded pile fulfills the following four criteria: 1) Realistic load-settlement behavior. 2) Realistic distribution of the ultimate skin friction and realistic mobilization of the skin friction. 3) Mobilization of the end-bearing capacity. 4) Robustness of numerical procedure. In this section, the results of some previous research and comparison of embedded pile with volume pile have been discussed.

Validation of the embedded pile subjected to vertical loading

Engin et al. (2007) modeled a pile load test carried out in Amsterdam in PLAXIS 3D Foundation using the embedded pile. In this case, the results of study were compared with measured data and also with volume piles. The pile was embedded in five different layers of soil. Figure 3.23 describes the geometry of PLAXIS models. For good comparison between results, mesh generation should be similar for both embedded and volume pile.

Figures 3.24 and 3.25 shows the comparison of the test results and results from numerical analysis. From the curves, it can be seen that the embedded pile is able to resemble the real behavior. Besides, the volume pile gives an overestimated pile capacity and embedded pile behaves softer than volume pile. However, the result of axial force distribution shows that embedded pile gives similar distribution as real pile.

Another study has been done by *Tschuchnigg and Schweiger (2015)* to check the behavior of embedded pile in vertically loaded pile group. The results of *Chow and Small (2008)*

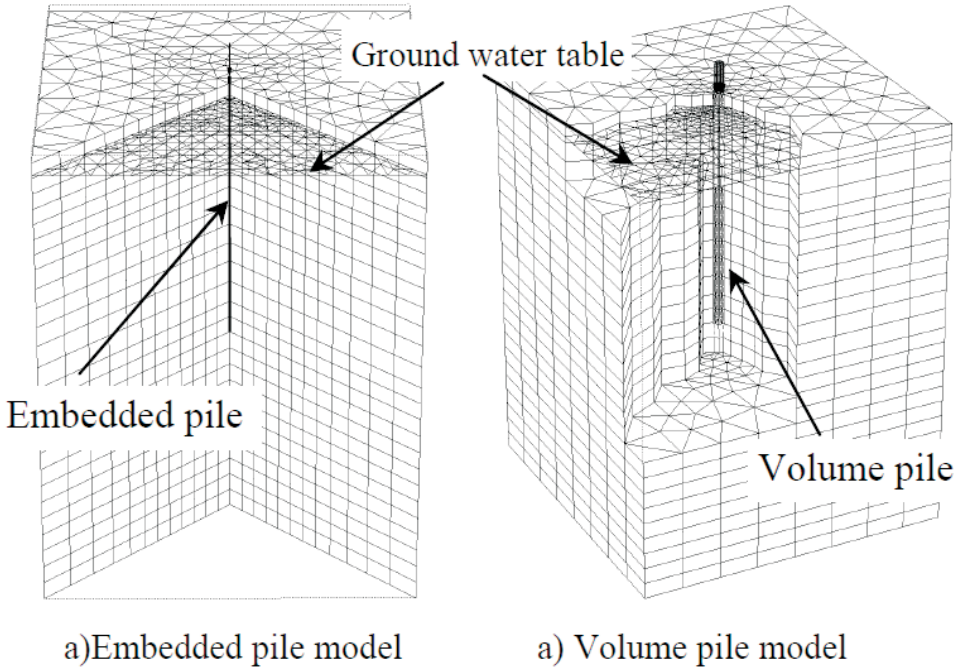

Figure 3.23: Model of Amsterdam pile load test in PLAXIS 3D Foundation, *Engin et al. (2007)*

was compared with the results of PLAXIS 3DF using embedded piles. Figure 3.26 shows the layout of piled raft foundation studied by 3.26. Piles were tested in homogeneous layer of soil.

Figure 3.27 illustrates the settlement along the cross section A-A and normal force distribution of pile P1 along pile length. Results show that settlement using with embedded pile are very similar to results from APRILS analysis (Analysis of Piled Rafts In Layered Soils) presented by *Chow and Small (2008)* and from standard finite element approach. The normal force distribution shows reasonable agreement with results computed with embedded pile concept.

Validation of the embedded pile subjected to horizontal loading

The same model presented by *Chow and Small (2008)* has been tested for horizontal loading. To make rigid connection with pile head, raft is model as plate element. Figure 3.28 shows the horizontal deflection and bending moments in center pile P1. The com-

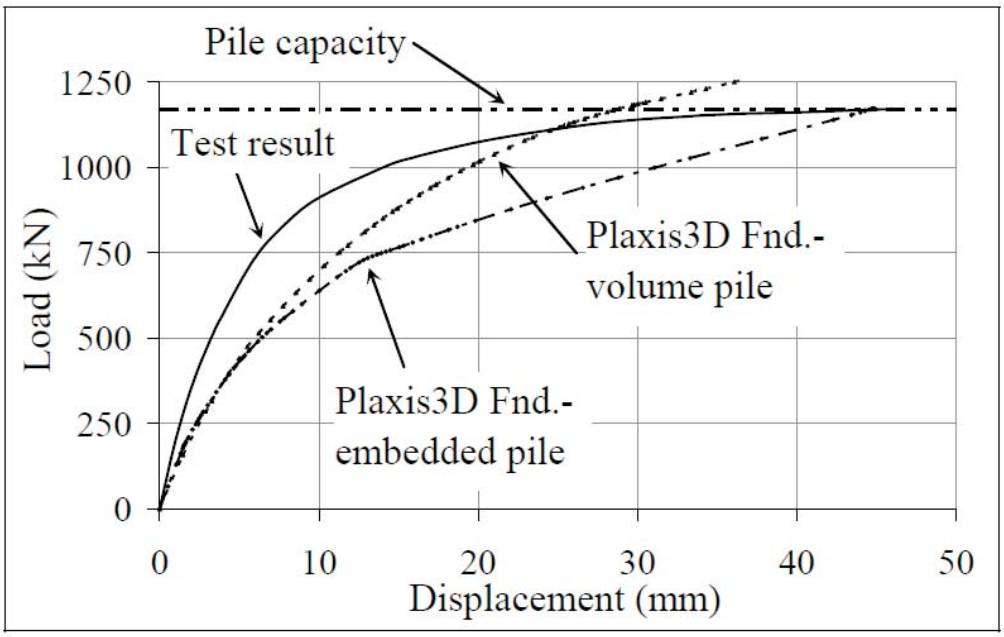

Figure 3.24: Load-displacement behavior of embedded pile, real test pile and volume pile, *Engin et al. (2007)*

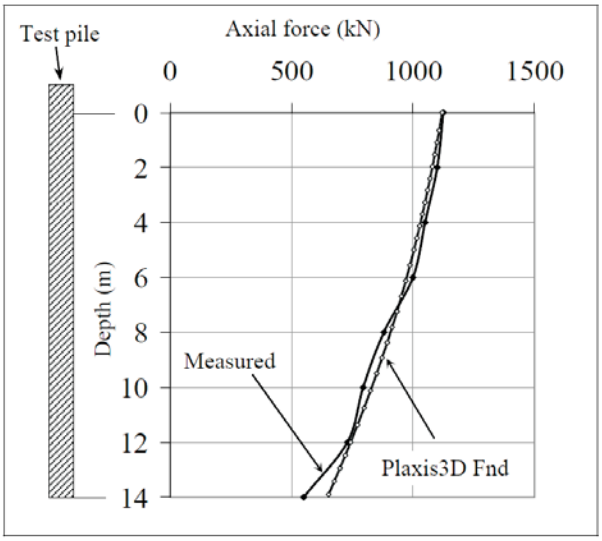

Figure 3.25: Axial force distribution with depth of embedded pile and real test pile, *Engin et al. (2007)*

puted horizontal deflection and bending moments of the embedded pile are in very good agreement with results presented by *Chow and Small (2008)* and from standard finite element approach.

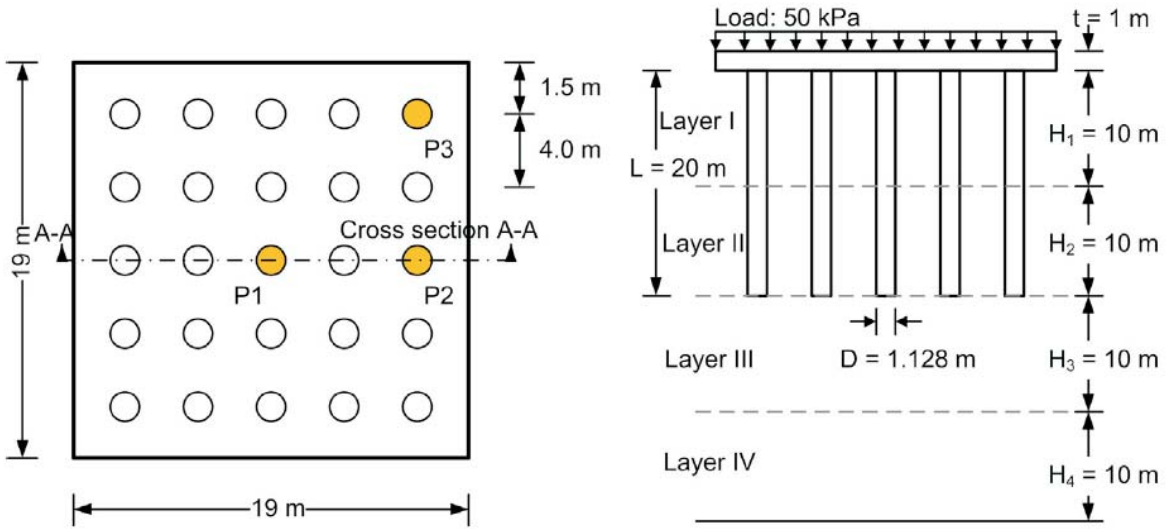

Figure 3.26: Layout of piled raft foundation studied by Chow and Small, *Tschuchnigg and Schweiger (2015)*

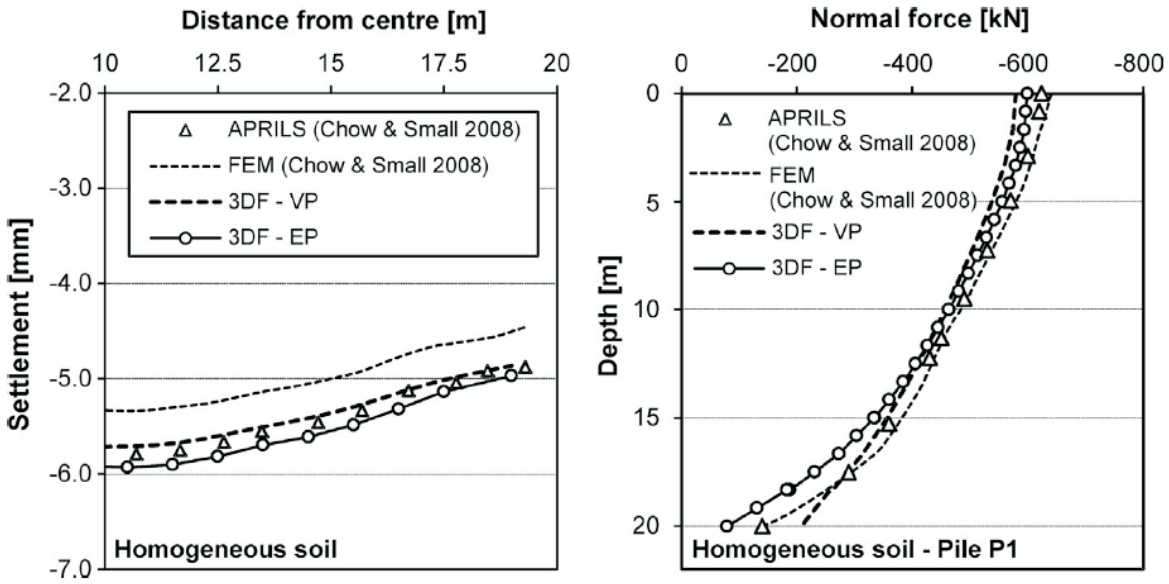

Figure 3.27: Differential settlements along cross section A-A (left) and normal force in pile P1 (right), *Tschuchnigg and Schweiger (2015)*

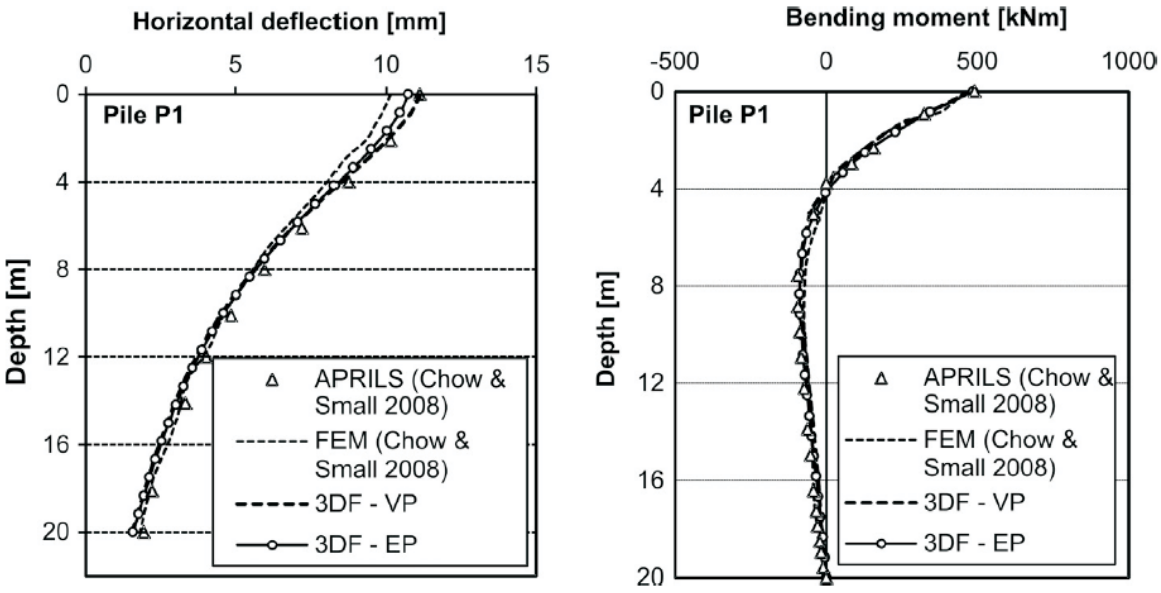

Figure 3.28: Horizontal deflection (left) and bending moments (right) of pile P1, *Tschuchnigg and Schweiger (2015)*

3.4 Modeling of raft

Raft is another structural element which have to model in this study. The ways of modeling of raft is similar to pile, because raft can also be modeled as volume or plate. The main difference between raft and pile is that pile is a line element and raft is a 2D element.

3.4.1 Raft model as a volume element

In similar manner, raft is modeled as volume element of any arbitrary shape as shown in Figure 3.29. In material data set of soil and interface, concrete properties are assigned instead of soil properties as in volume pile. To define real soil-structure interaction, raft is modeled with interface element. The strength reduction factor R_{inter} is main parameter which describes the interaction of raft with surrounding soil. With this model also, the structural forces can not be calculated. However, by using softer plate element in the center of raft, forces can be got in PLAXIS output.

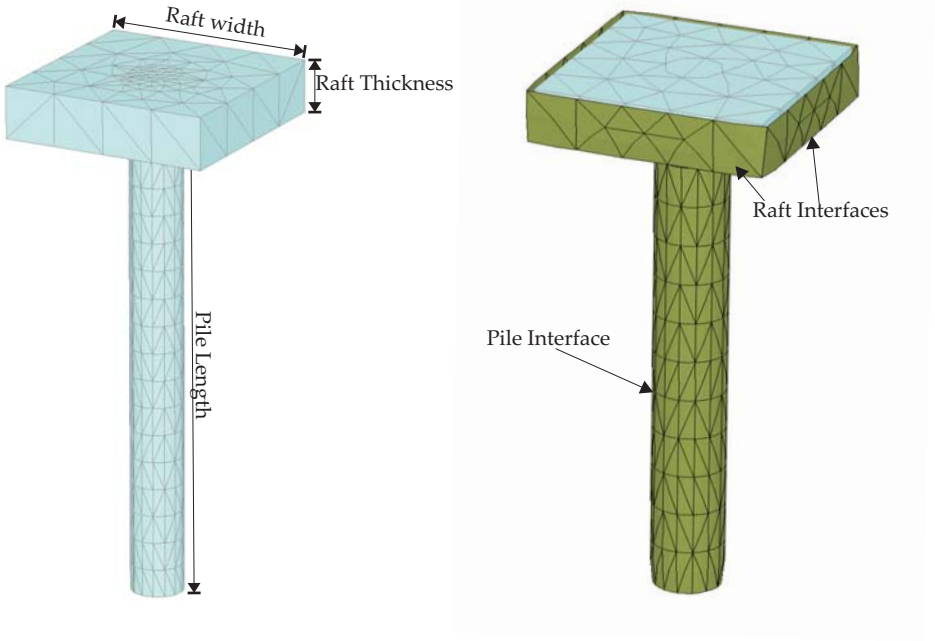

Figure 3.29: Raft as volume element without interface element (left) and with interface (right)

3.4.2 Raft model as a plate element

In this approach, the raft is modeled as a plate element which is an inbuilt structural element in PLAXIS 3D. It is used to model 2D structures in the ground with significant flexural rigidity (bending stiffness). In PLAXIS 3D, plate is created as geometric surface created. A plate element consists of 6-node triangular elements with six degrees of freedom at each node: three translations (u_x, u_y, u_z) and three rotationals ($\varphi_x, \varphi_y, \varphi_z$). The plate elements are based on Mindlin's plate theory (Bathe, 1982). In this theory, plate deflections can be due to shearing as well as bending. Also, the element can change length when an axial force is applied. For soil-structure interaction, raft is modeled with interface element similar to volume element as shown in Figure 3.30. For input parameters

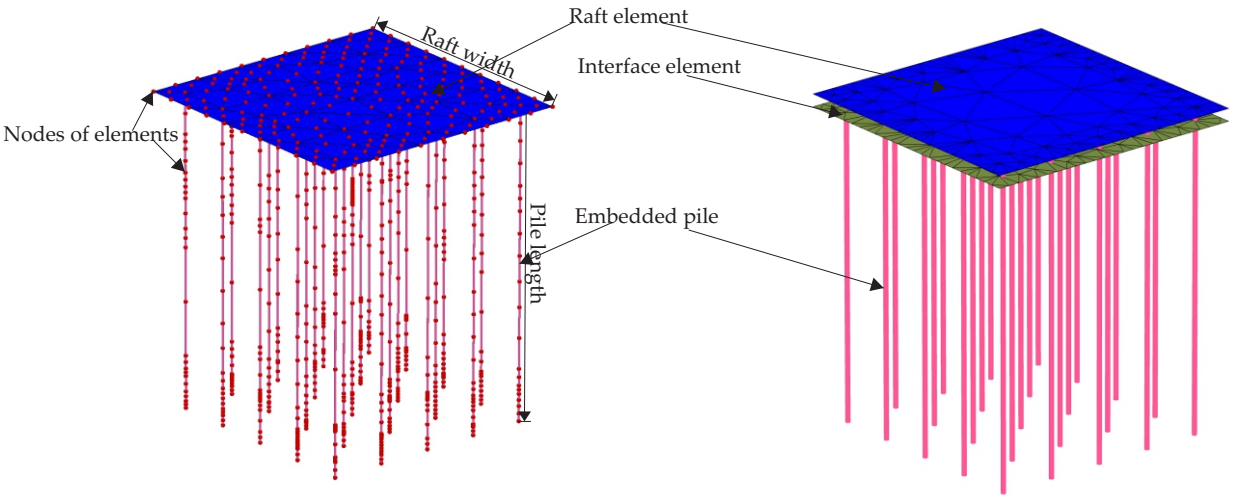

Figure 3.30: Piled Raft foundation in which raft as plate element without interface element (left) and with interface (rigth)

of plate, a separate material data set is available in PLAXIS 3D. Plate properties can be classified into two following groups:

General properties

General properties are thickness of plate and unit weight of plate material (Note volume and overlapping concept is also applicable for plate element).

End bearing of plates

In soil embedded structures, the vertical load is resisted by wall friction and tip resistance. The tip resistance depends on thickness or cross-sectional area of tip. In vertical plate structures (e.g. slender, walls, etc), if thickness is very small (tends to zero), structures have no end bearing. However, the end bearing can be considered by selecting the option of end bearing in material data set window. After selecting this option, a zone in the soil volume elements surrounding the bottom of plate is generated in which any type of soil plasticity is excluded (elastic zone) similar to embedded pile. The size of this elastic zone is determined by following equation:

$$D_{eq} = \sqrt{\frac{12EI}{EA}} \tag{3.53}$$

Stiffness properties

Plate stiffnesses will be linear. In PLAXIS 3D, plate can behave as orthotropic or anisotropic. The plate behavior is defined by following parameters:

Where,

E_1 = Young's modulus in first axial direction

E_2 = Young's modulus in second axial direction

G_{12} = In-plane shear modulus

G_{13} = Out-of-plane shear modulus related to shear deformation over first direction

G_{23} = Out-of-plane shear modulus related to shear deformation over second direction

ν_{12} = Poisson's ratio

If isotropic option is selected, only E_1 and ν_{12} options are required to assign because E_1 = E_2 and G_{12} = G_{13} = G_{23} = $\frac{E}{2(1+\nu_{12})}$.

For dynamic behavior, here also Rayleigh damping parameters α and β are defined.

In PLAXIS 3D output, plate gives axial forces N_1 and N_2, shear forces Q_{12}, Q_{23} and Q_{13} and moments M_{11}, M_{22} and M_{12} as shown in Figure 3.31.

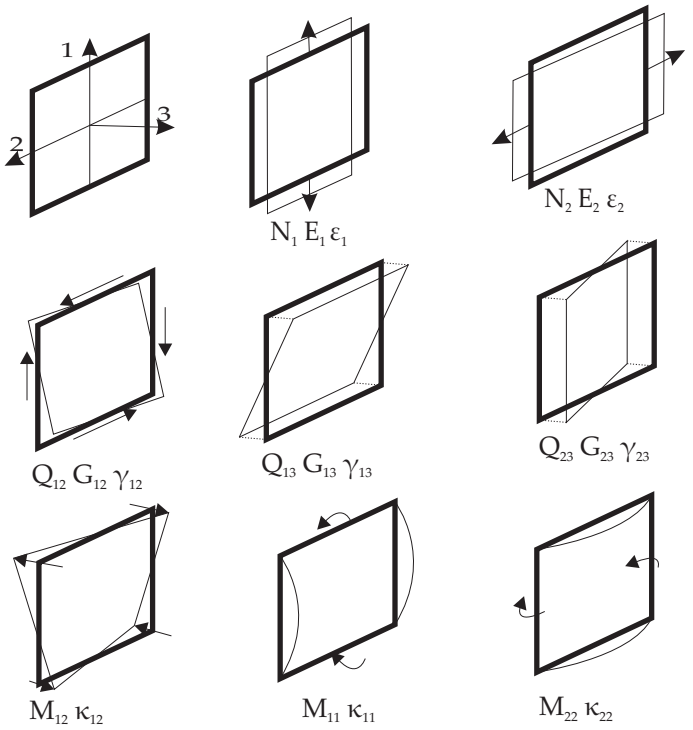

Figure 3.31: Positive normal forces (N), shear forces (Q) and bending moments (M) for a plate based on local system of axes

3.5 Modeling of Geogrid

Geogrids (or geotextiles) are flexible elastic materials that are often used to reinforce the soil. These elements have only axial stiffness and cannot sustain compressive force. In PLAXIS 3D, a special tension element called geogrid are used to model these elements. After meshing, a geogrid element consists of 6-node triangular surface elements with three translations degrees of freedom at each node (u_x, u_y, u_z). The length of the element can be changed after application of tensile load. Figure 3.32 shows the typical representation of the geogrid element.

Two options of geogrid material types are available i.e. Elastic and Elastoplastic. For elastic material only stiffness properties required but for elastoplastic material additional strength properties are needed. PLAXIS 3D also allows isotropic, orthotropic as well as behavior in geogrid.

Properties of geogrid can be divided into following two categories:

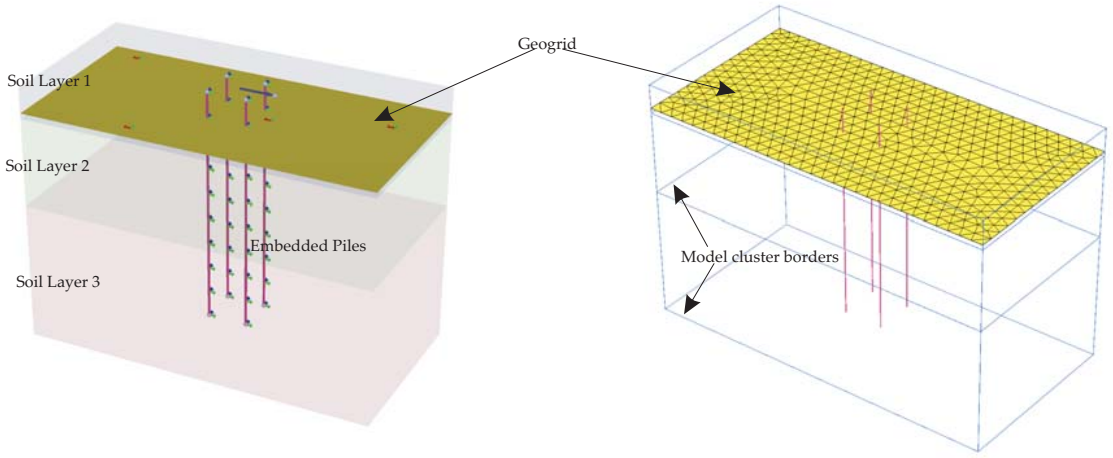

Figure 3.32: Representation of pile foundation on reinforced soil with geogrid before meshing(left) and after meshing(right)

3.5.1 Stiffness Properties

Three stiffnesses are defined for geogrid. First is axial(normal) elastic stiffness in plane (EA_1), second is axial elastic stiffness out of plane (EA_2) and last is shear stiffness in plane (GA). For isotropic material, $EA_1 = EA_2$ and $GA = EA_1/2$. The stiffness is usually provided by the manufacturer.

3.5.2 Strength Properties

This parameter is activated when geogrid behaves as elastoplastic material (or in case of plasticity). Two input values are required to define the strength of geogrid these are the maximum forces (force per unit width) in plane ($N_{p,1}$) and out of plane ($N_{p,2}$). Axial forces(N_p) are calculated at the stress points of the geogrid elements. If N_p is exceeded, stresses are redistributed according to the theory of plasticity, so that the maximum forces are complied with. This will result in irreversible deformations. For isotropic material, $N_{p,1} = N_{p,2}$.

3.6 Modeling of soil-structure interaction

The soil-structure interaction is simulated by using interface elements. Without interface elements, it is constrained that the adjacent structure and soil element will have to move together. There will be no relative displacement(slipping or gapping) between them. Interface can be generated next to plate, geogrid and between two soil volumes.

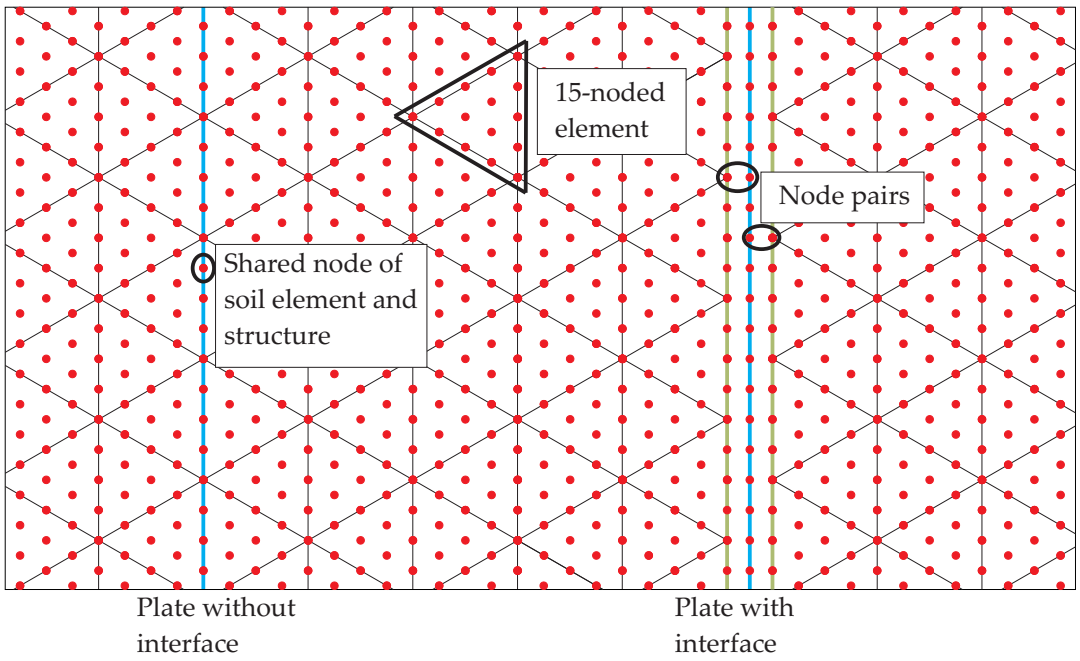

Figure 3.33: Visualization of nodes in different elements adopted from (From Plaxis Knowledge Base)

In PLAXIS 3D after meshing, interfaces are composed of 12-node interface elements. Interface elements consist of node pairs. From a node pair, one node is associated to the structure and other one is associated to the soil. The interaction between these two nodes defines the soil-structure interaction. It consists of two elastic perfectly plastic springs. One spring models the gap displacement and other one models slip displacement between these nodes. Figure 3.33 represents the Connectivity plot of a soil-structure connection with and without interface.

In two conditions interface element node pairs are 'degenerated' to single nodes. One is when the interface ends and other one is when one structural element is connected perpendicularly to other structural element (e.g. a plate is connected to a beam). In second

condition it is happened to avoid the disconnection between both structural elements. The problem of stress oscillation exists due abrupt change in boundary condition and at corners of stiff structures. This problem can be solved by assigning additional interface elements inside the soil body with strength reduction factor (R_{inter} which will be defined in properties of interface) is equal to 1. These interface elements increase the flexibility of the finite element mesh.

3.6.1 Properties of an interface

The interface properties such as Material mode, permeability condition and Virtual thickness factor can be set in Object explorers as:

Material mode

There are two option available to set the interface properties. One option is that the properties can be assigned from adjacent soil and by default this option is selected. In second option, a material data set can be assigned directly to an interface. In these option several parameters are entered. These parameters depend on the constitutive model which is selected to describe the behavior of surrounding soil. It is also possible to use different constitutive model for the surrounding soil and the interface elements. For all models except Modified Cam-Clay model and User-defined models, the main parameter is strength reduction factor (R_{inter}). Following parameters are required to define the material data set of interface:

Strength reduction factor (R_{inter})

The strength reduction factor (R_{inter}) is used to define the strength of interface. The behavior of interface is described by an elasto-plastic model. The Mohr-Coulomb criterion is used to define the failure of the interface. The interface strength parameters can be calculated by following relationship:

$$c_i = R_{inter}\ c_i \tag{3.54}$$

$$\tan\varphi_i = R_{inter} \ \tan\varphi_{soil} \tag{3.55}$$

$$\psi_i = 0^\circ \quad \text{for} \quad R_{inter} < 1, \quad \text{otherwise} \quad \psi_i = \psi_{soil} \tag{3.56}$$

All used symbols have as usual meaning and subscript i denotes for interface. The value of R_{inter} is defined by three options - Rigid, Manual and Manual with residual strength. When the first option is used, there will be no reduction in strength of interface compared to surrounding soil strength and all parameters will be same except poission's ratio. The value of $R_{inter} = 1$. By default this option is activated. In second option, the value of R_{inter} is entered manually. For real soil-structure interaction, the interface will be less stronger and more flexible than soil. For it the value of $R_{inter} < 1$. The suitable value of R_{inter} for an interaction can be chose from various literature available. If no detailed information is available, value of R_{inter} may be assumed of the order of $2/3$. Generally, the reduction of strength is more for cohesive soil than for cohesionless soil and that means R_{inter} value is higher for cohesionless soil. When the interface strength is reached to its limit value as defined by R_{inter}, the interface strength reduce to a residual strength as defined by $R_{inter,residual}$. $R_{inter,residual}$ is activated when third option is selected.
The elastic and plastic behavior of interface can be differentiate by following conditions:

$$\text{For elastic behavior} \quad |\tau| < -\sigma_n \tan\varphi_i + c_i \tag{3.57}$$

Where τ is shear stress and σ_n is normal stress on interface.

$$\text{For plastic behavior} \quad |\tau| = -\sigma_n \tan\varphi_i + c_i \tag{3.58}$$

When the interface behaves as elastic then both slipping (relative movement parallel to the interface) and gapping or overlapping (i.e. relative displacements perpendicular to the interface) can be expected to occur and these can be expressed as:

$$\text{Elastic gap} = \frac{\sigma_n}{K_n} \quad \text{where} \quad K_n = \text{normal interface stiffness} = \frac{E_{oed,i}}{t_i} \tag{3.59}$$

$$\text{Elastic slip} = \frac{\tau}{K_s} \quad \text{where} \quad K_s = \text{shear interface stiffness} = \frac{G_i}{t_i} \tag{3.60}$$

Where t_i is virtual thickness of the interface and is equal to the multiplication of virtual thickness factor and average element size ($t_i = \delta_v \times ES_{avg}$). The shear interface stiffness (G_i) and oedometric interface stiffness ($E_{oed,i}$) depend on the defined soil stiffness G and E_{oed} respectively as:

$$E_{oed,i} = 2G_i \frac{1-\nu_i}{1-2\nu_i} \tag{3.61}$$

$$G_i = R_{inter}^2 G_{soil} \tag{3.62}$$

Where poission's ratio of interface ν_i is equal to 0.45.

Virtual interface thickness (t_i)

The virtual interface thickness is one of the main properties of interface and has imaginary dimension. The elastic deformation is directly proportional to the virtual thickness. So for small elastic deformation, it should be small. But if it is too small, numerically ill-condition may occur. As earlier defined $t_i = \delta_v \times ES_{avg}$, by default the value of δ_v is 0.1. It can be changed in Object explorers and when very large normal stresses occur, a reduce value of δ_v may be used.

3.7 Modeling of Dynamic loading

The input values and multipliers are used to define the dynamic load in PLAXIS 3D. A dynamic impulse at each time step is the multiplication of multiplier and input value as:

$$F_x(t) = M(t)\ F_{x,input} \tag{3.63}$$

Where $F_x(t)$ is the dynamic load at time t, $M(t)$ is multiplier at that time and $F_{x,input}$ is the load which is set in a phase prior to dynamic phase.

3.7.1 Multipliers

Multipliers are defined in the Dynamic multipliers under the Attributes library in the Model explorer. There are two types of multipliers defined i.e. Load multipliers and

Displacement multipliers which can be assigned to the dynamic component of a load or to a prescribed displacement respectively. In each multipliers, the signal are defined in two ways i.e. Harmonic signal and Signal from table. Dynamic loading only in Displacement multiplier can be specified into three types such as Displacements, Velocities and Accelerations.

Drift Correction

If in Displacement multiplier signal from table is used with acceleration data type, an extra option of drift correction is available. When acceleration is used as prescribed motion, for obtaining displacement time history will be integrated and with one time integration velocity will be obtained. Due inequality of area above and below the horizontal axis in acceleration history, there will be a nonzero residual constant velocity in velocity history. This residual velocity will result in a steadily increasing displacement history. This phenomena is represented visually in Figure3.34.

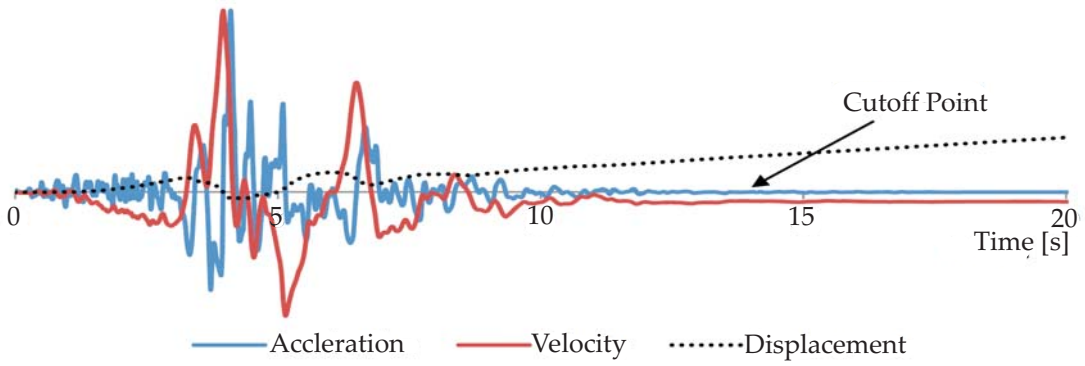

Figure 3.34: Acceleration, velocity and displacement histories with drift

To remove this drift or make the final displacement zero, the drift correction option have to be selected. It applies a lower value of frequency motion from the starting of the phase of the calculation and corrects the acceleration accordingly. For this correction the phase time should be same as the input signal's time interval.

3.7.2 Harmonic signal

Harmonic loads are expressed by following equation:

$$F = \hat{M}\hat{F}\sin(\omega t + \phi_0) \tag{3.64}$$

Where,
$\hat{M}$ = Amplitude multiplier
$\hat{F}$ = Input value of load
ω = Circular frequency in rad/sec and $\omega = 2\pi f$ with f = Frequency in Hz
ϕ_0 = Initial phase angle in degrees
Three input parameters i.e. Amplitude of dynamic load ($= \hat{M}\hat{F}$), Frequency in Hz and Initial phase angle in degrees are required to define harmonic signal.

3.7.3 Signal from Table

Besides harmonic signal, signal can be generated in a table form or imported from a file. These table or file consists of two columns i.e. Time and Multiplier. File should be in format of plain ASCII or in Strong motion CD-Rom (SMC) format. SMC files should be used in combination with prescribed boundary displacements at the bottom of a geometry model.

3.8 Simulation of Boundary conditions

The modeling of boundary conditions is very important for numerical analysis specially in dynamic analysis. Two types such as Deformation boundaries and Dynamic boundaries are introduced in PLAXIS 3D. The deformation boundaries can be free or fix in one or two or all three direction. These can be applied by two ways. In one way, PLAXIS 3D provides automatically standard boundary conditions for different elements as illustrated in Figure 3.35. According to *Brinkgreve et al. (2013b) and Brinkgreve et al. (2015b)*, for soil volumes these standard boundary conditions mean:

- Vertical model boundaries normal to x-direction (i.e. parallel to the yz-plane) are fixed in x-direction (u_x = 0) and free in y- and z-direction.
- Vertical model boundaries normal to y-direction (i.e. parallel to the xz-plane) are fixed in y-direction (u_y = 0) and free in x- and z-direction.
- Vertical model boundaries normal to neither x- nor y-direction are fixed in x- and y-direction (u_x = u_y = 0) and free in z-direction.
- The model bottom boundary is fixed in all directions ($u_x = u_y = u_z = 0$).
- The 'ground surface' is free in all directions.

But in new version of PLAXIS 3D AE.01, all possible options such as Free, Normally fixed, Horizontally fixed, Vertically fixed and Fully fixed are available in standard boundary conditions but by default options according above defined conditions are activated. In another way, fixities and/or prescribed displacements on points, lines and surfaces

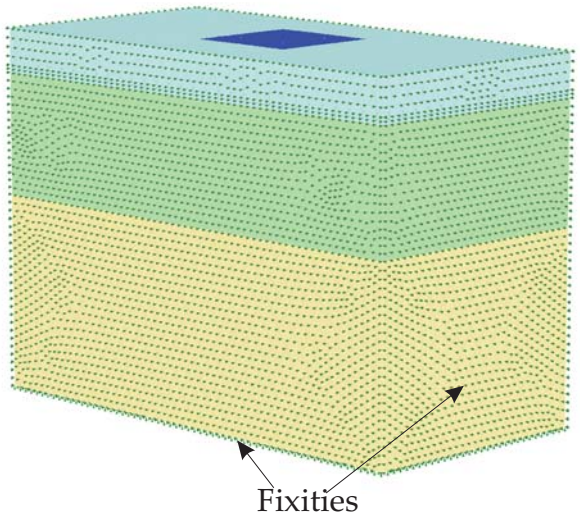

Figure 3.35: Schematic representation of standard fixities on soil model boundaries

in a certain direction can be introduced by user. When the default boundaries and the user defined boundaries conflict, the user defined boundaries take preference over the standard boundary conditions.

In dynamic calculations, stress waves reflect inside the soil body and distort the computed results. To stop reflection of waves or to simulate the far field behavior of model, absorbing boundaries may be applied as defined below:

Viscous boundaries

Viscous boundaries provide the dampers which absorb the outgoing wave energy i.e. an increase in stress on the boundary without rebounding. This option is generally used when the dynamic source is inside the mesh. If bottom boundary of the model is modeled as viscous for seismic analysis, the input seismic history must be a loading history. The normal and shear stress components absorbed by a damper in x-direction are expressed as:

$$\sigma_n = C_1 \rho V_p \dot{u}_x \tag{3.65a}$$

$$\tau = -C_2 \rho V_s \dot{u}_y \tag{3.65b}$$

Where,

ρ = Density of material

V_p and V_s = Pressure wave velocity and shear wave velocity, respectively

C_1 and C_2 = Relaxation coefficients that are used to improve the wave absorption on the viscous boundaries. These coefficients correct the dissipation in direction perpendicular to the boundary and tangential direction, respectively. If the waves strike perpendicular to the boundary, relaxation is unnecessary ($C_1 = C_2 = 1$). But when waves come in arbitrary direction, C_2 has to be adjusted to improve the absorption, from experience $C_1 = 1$ and $C_2 = 0.25$ (*Brinkgreve et al. (2015c)*).

Chapter 4

Numerical Analysis

The numerical model used in this study is validated by back analysis of experimental study conducted by *Taha (2014)*. In this experimental study, the author performed many model tests and also numerical analysis on pile foundation in soil strengthened by geosynthetics. He investigated the behavior of geosynthetic reinforced pile foundation system under static horizontal loading and harmonic or seismic loading. Figures 4.2 and 4.3 illustrate the experimental set up for both type of loading. Here all numerical calculations have been performed in Finite Element Method (FEM) based PLAXIS 3D.

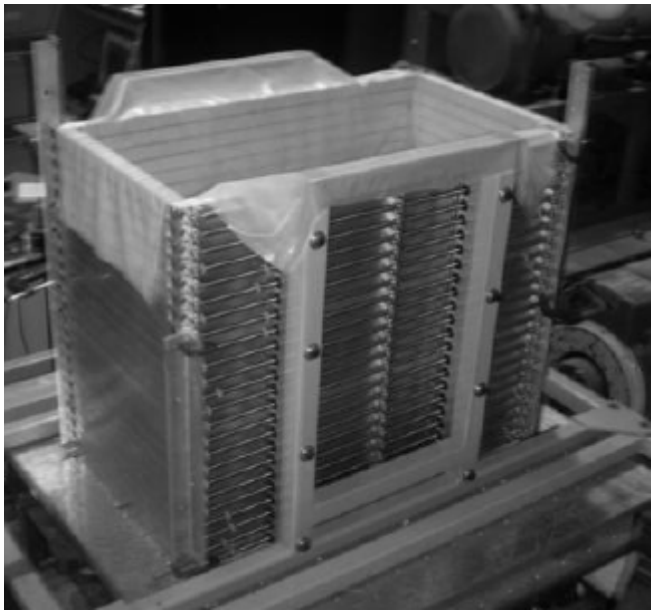

Figure 4.1: Laminar soil container lined with latex sheet *Taha (2014)*

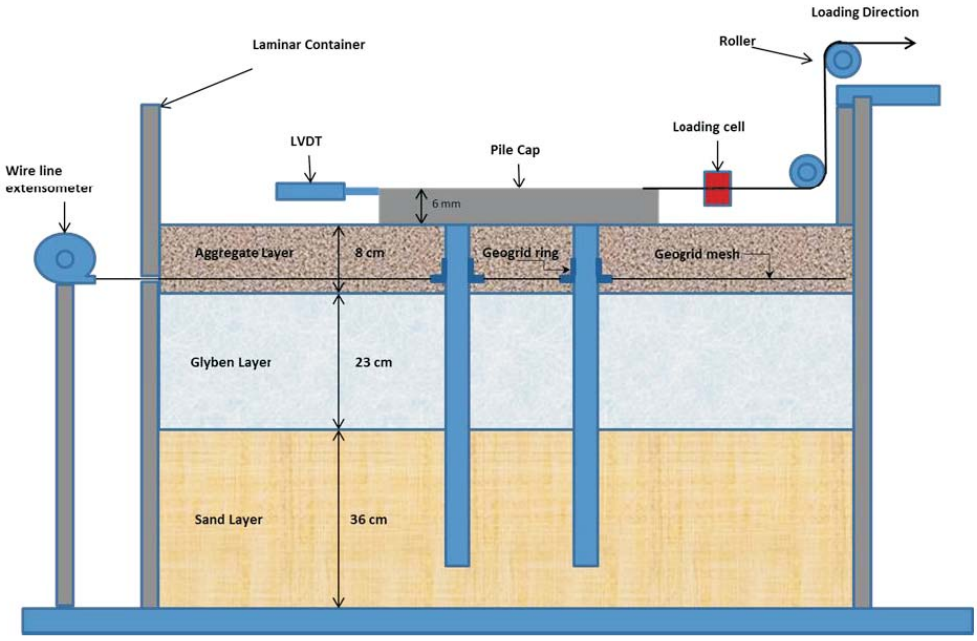

Figure 4.2: Experimental set up for static horizontal test *Taha (2014)*

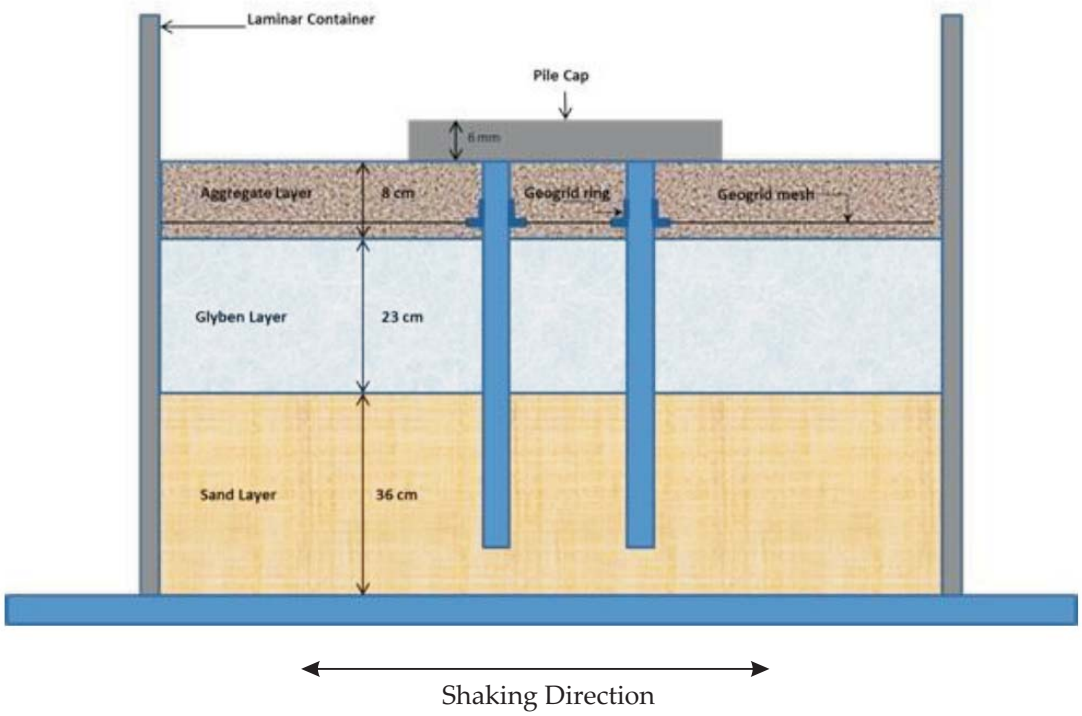

Figure 4.3: Experimental set up for dynamic loading *Taha (2014)*

4.1 Numerical Model

The numerical model consists of 10-node tetrahedral elements to simulate the soil volume, 6-node plate elements to simulate the pile cap (raft), 6-node geogrid elements to model the geosynthetics and 3-node embedded pile element to simulates piles. The pile-soil interfaces are simulated as embedded interface elements (as described earlier in Numerical Basis Chater) having the strength equal to the some percentage of the adjacent soil shear strength. The simulation of raft-soil interaction has been done by an interface element.

Figure4.4 explains the geometry of different elements used in model. The model is defined in 3D space, the dimensions of model are length = 900 mm, width = 450 mm and hight = 670 mm as shown in Figure4.4a. The model is divided into three layers as: Glyben layer (an artificial clay according to *Turan et al. (2009), Turan et al. (2007) and Turan et al. (2011)*) is sandwiched between two layers i.e Aggregate layer (top) and Sand layer (bottom). Depths of each layer are 80mm, 230mm and 360mm respectively. A geogrid mesh is placed within the aggregate layer at a depth of 3.5 times of pile diameter (66 mm). A horizontal point load is applied at center of the plate in x-direction to measure the horizontal displacement of foundation in x-direction. Standard fixities which fixes the bottom boundary in all directions and vertical boundaries in normal directions, are imposed to the boundaries around the soil volume in static loading. In experiment, a latex sheet has been used inside the box to prevent penetration of soil into gaps and make watertight arrangement for saturated soil as shown in figure 4.1. To model this type of boundary conditions, plates having latex sheet properties has been created around the boundaries of numerical model.

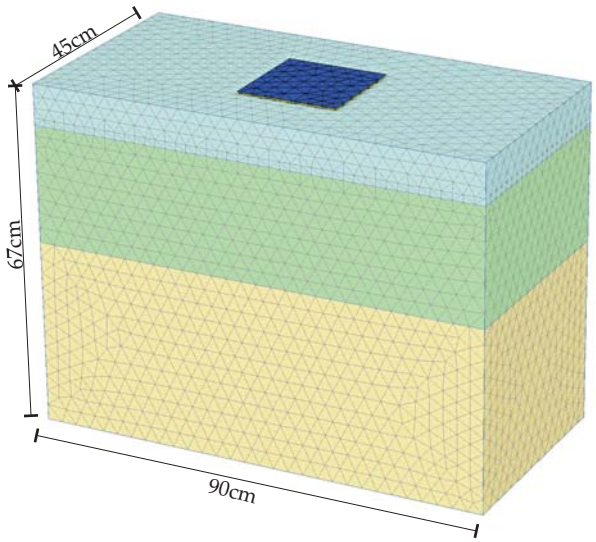

(a) 3D visualization after meshing

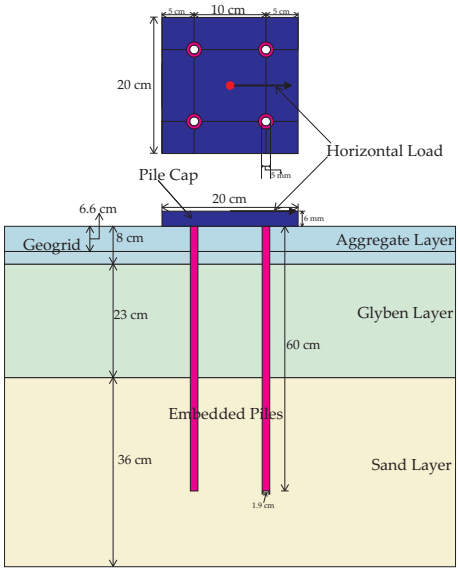

(b) Cross sectional and top view

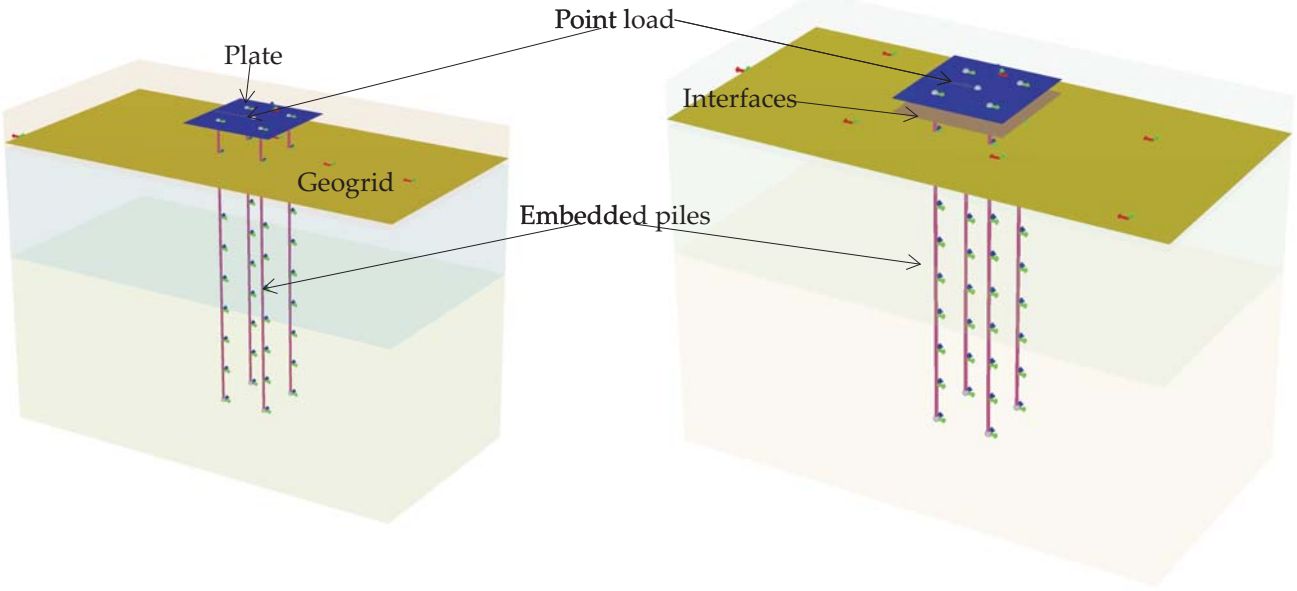

(c) 3D visualization of structural

(d) 3D visualization of structural elements with interfaces

Figure 4.4: Numerical model of Soil and pile-cap-geogrid system

4.2 Properties of elements

In model test acrylic tubular piles have been rigidly connected to aluminum raft. Most of the material properties of each element have been taken from *Taha (2014)*. The properties which are not given have been used with suitable value from different resources. These are defined in the Tables 4.1, 4.2 and 4.3 given below:

Table 4.1: Properties of Geogrid (*Taha (2014)*)

Parameters	**Unit**	**Geogrid**
Material type	-	Elastic
Material behavior	-	Isotropic
Axia elastic stiffness (EA)	kN/m	110

Table 4.2: Properties of Embedded Piles (*Taha (2014)*)

Parameters	**Unit**	**Embedded Piles**
Young's modulus (E)	kN/m^2	3.2×10^6
Unit weight (γ)	kN/m^3	0.01
Pile type		Predefined
Predefined pile type	-	Circular tube
Diameter	mm	19
Thickness	mm	7
Skin Resistance type	-	Layer dependent
Maximum skin resistance allowed along the pile (T_{max})	kN/m	1
Base Resistance (F_{max})	kN	1

Type of soil parameters depends on constitutive models for soil. The author have used Mohr-Coulomb model for numerical study but for present study advanced constitutive model (HS Small model) will also be used. However initially soil is modeled as Mohr-

Table 4.3: Properties of Pile cap (raft) (*Taha (2014)*)

Parameters	**Unit**	**Raft (Plate)**
Cross Section	$mm \times mm$	200×200
Thickness (d)	mm	6
Unit weight (γ)	kN/m^3	26.48
Material Type and Behavior	-	Linear and Isotropic
Young's modulus (E)	kN/m^2	69×10^6
Poission's ratio (ν)	-	0.334

Coulomb model. After validating with M-C model, analysis is performed with Hardening soil model with small strain stiffness (HSSMALL). The analysis with HSSMALL is divided into two parts: in first (say HSSMALL Analysis I) only Glyben is modeled as HSSMALL and others are M-C model but in next analysis (say HSSMALL Analysis II) both top layer and Glyben are modeled as HSSMALL and sand remains as M-C model. The interface used around plate has the properties from adjacent soil. No interaction between geogrid and soil has been considered because interlocking behavior of geogrid. All the properties of soils for these two models are defined in the following Table 4.6 and 4.4. For dynamic calculation sand has been modeled as linear elastic because with non-linear model analysis takes more time. And also for dynamic properties of soils several laboratory tests results given by *Taha (2014)* are presented in Appendix A.

Table 4.4: Final material properties of soils for Hardening soil model with small strain stiffness (*Taha (2014)*)

Parameters	**Unit**	**Top Aggregate**	**Bottom Aggregate**	**Glyben**
Material model	-	HS Small	HS Small	HS Small
Drainage type	-	Drained	Drained	Undrained(B)
Unit weight (γ_{sat})	kN/m^3	16.1	16.1	13.8
Secant stiffness modulus in standard drained triaxial test (E_{50}^{ref})	kN/m^2	2783	4680	800
Tangent stiffness modulus for primary oedometer loading (E_{oed}^{ref})	kN/m^2	2188	3573	850
Unloading / reloading stiffness modulus (E_{ur}^{ref})	kN/m^2	8350	14.04×10^3	8000
Power for stress-level dependency of stiffness (m)	-	1.0	1.0	1.0
Poisson's ratio (ν)	-	0.2	0.2	0.2
Cohesion (c)	kN/m^2	-	-	15
Friction angle (φ)	$\circ$	50	50	-
Shear strain ($\gamma_{0.7}$)	kN/m^2	34.79×10^3	58×10^3	3770
Shear modulus at very small strains (G_0^{ref})	-	7×10^{-5}	7×10^{-5}	6×10^{-4}
K_0^{nc} determination	-	Automatic	Automatic	Automatic
Lateral earth pressure coefficient (K_0^{nc})	-	0.234	0.234	1
Damping (ξ)	%	2	2	10

Table 4.5: Properties of sand for linear elastic model (*Taha (2014)*)

Parameters	**Unit**	**Sand**
Material model	-	Linear elastic
Drainage type	-	Drained
Unit weight (γ)	kN/m^3	17.35
Young's modulus (E)	kN/m^2	11.51×10^3
Poission's ratio (ν)	-	0.3
Damping (ξ)	%	10

Table 4.6: Material properties of soils for Mohr-Coulomb model (*Taha (2014)*)

Parameters	**Unit**	**Aggregate**	**Glyben**	**Sand**
Material model	-	Mohr-Coulomb	Mohr-Coulomb	Mohr-Coulomb
Drainage type	-	Drained	Undrained(B)	Drained
Unit weight (γ_{unsat})	kN/m^3	16.1	13.8	17.35
Young's modulus (E)	kN/m^2	2746.2	2623.2	8377.2
Poisson's ratio (ν)	-	0.15	0.2	0.3
Cohesion (c)	kN/m^2	-	10	-
Friction angle (φ)	$\circ$	50	-	40
Dilatancy angle (ψ)	$\circ$	20	-	10
K_0 determination	-	Automatic	Automatic	Automatic
Lateral earth pressure coefficient (K_0)	-	0.234	1	0.357
Strength reduction factor (R_{inter})	-	0.7	0.1	0.7

4.3 Simulation Process

For numerical analysis, the model has to be divided into elements. For that in PLAXIS 3D automatic mesh generation option is available. In this back analysis, medium meshing is used in final calculation and for measuring the influence of different parameter coarse meshing is used because to get quick results of influences. Generally for accuracy of results the mesh should be finer but it should not be very much finer since it will take more computing time. The calculation is executed in 15 phases to simulate the geostatic equilibrium, construction procedure and incremental application of lateral load. The geostatic equilibrium is achieved in initial phase in which gravity loading has been used to calculate the initial stresses. Whole construction procedure is completed in 6 phases to simulate exact procedure used in experimental study explained in Table 4.7. The horizontal load is applied in incremental form in 8 phases. It starts from 100N and increased by 100N at each loading phase until a maximum load of 800N. Note that some numerical calculations in which soil is modeled as Mohr-Coulomb model with static loading are carried out in old version PLAXIS 3D 2013.01 and others are executed in updated version PLAXIS 3D AE.01.

Table 4.7: Constrution procedure used in numerical analysis

Phase No.	**Activation of element**
1	Embedded piles
2	Glyben layer
3	Lower Aggregate layer
4	Geogrid
5	Upper Aggregate layer
6	Plate and interface

For dynamic loading, the test is performed on shake table and 1-D motion was applied from base in longitudinal direction so to simulate 1-D shaking of lamina, at the vertical boundaries of the model, special fixities have been generated which fix the translation

of model in Y direction while free in X and Z directions. A harmonic loading of $16Hz$ frequency and $0.06g$ amplitude has been applied at base of model as shown in Figure 5.11 and Figure 4.6 describes two harmonic signals that have been used in numerical analysis and experiment. In this HSSMALL analysis II has been used and large relative displacement between pile cap and top aggregate layer was observed, therefore, to simulate this interaction, an interface element having strength properties 1% of soil strength, has been introduced at the bottom of pile cap. In contrast, since geogrid interlocks the surrounding soil, that interlock behaviour restricts the relative translation between them. To simulate these two interaction the aggregate layer has been split into two layers 3 cm and 5 cm in which the reduced interface strength has been assigned to the top layer and the rigid interface layer has been assumed at the bottom.

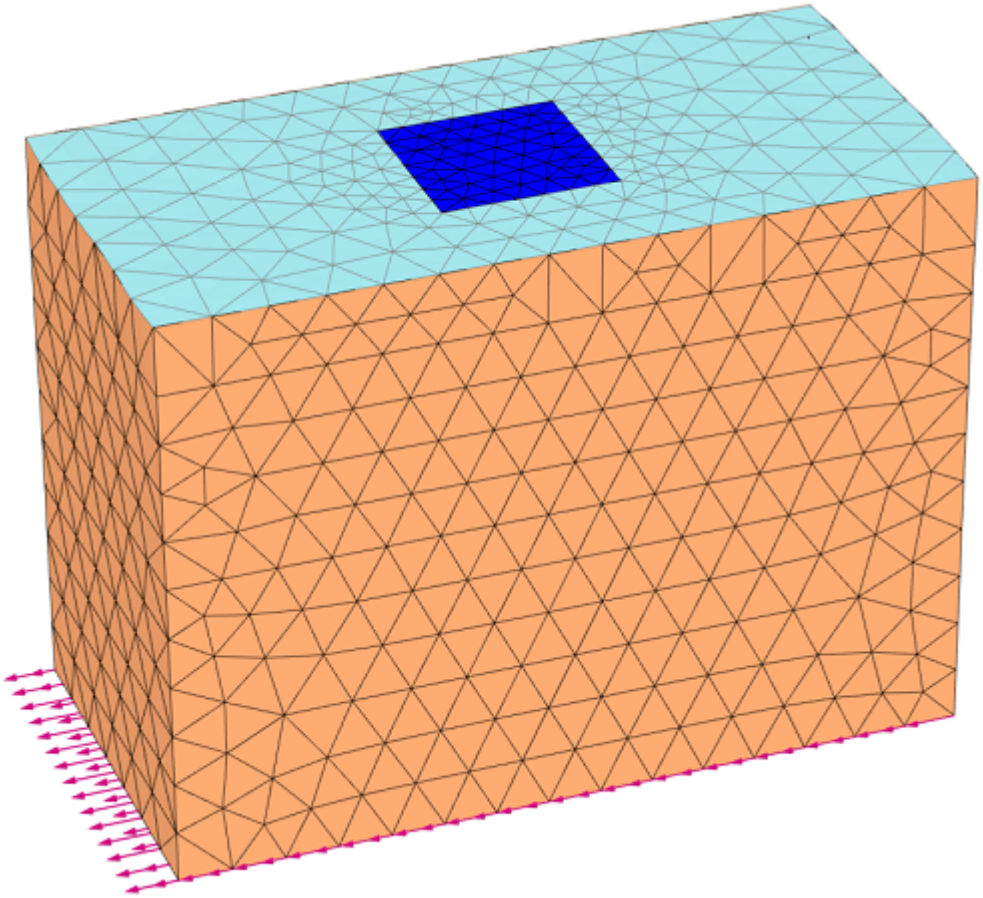

Figure 4.5: Numerical model for dynamic loading

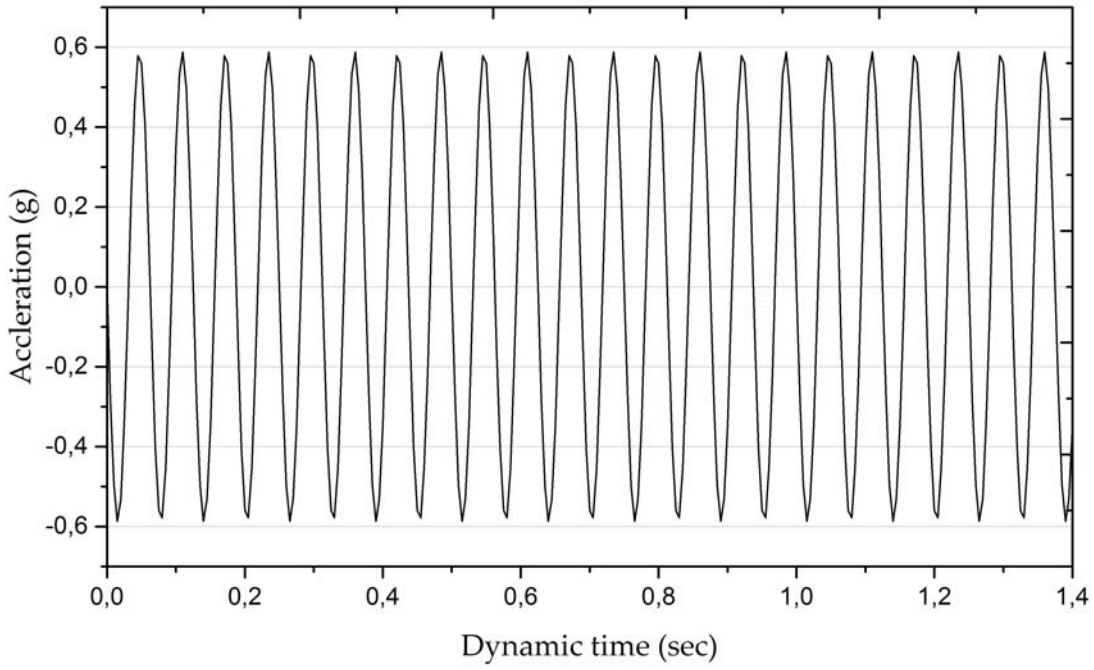

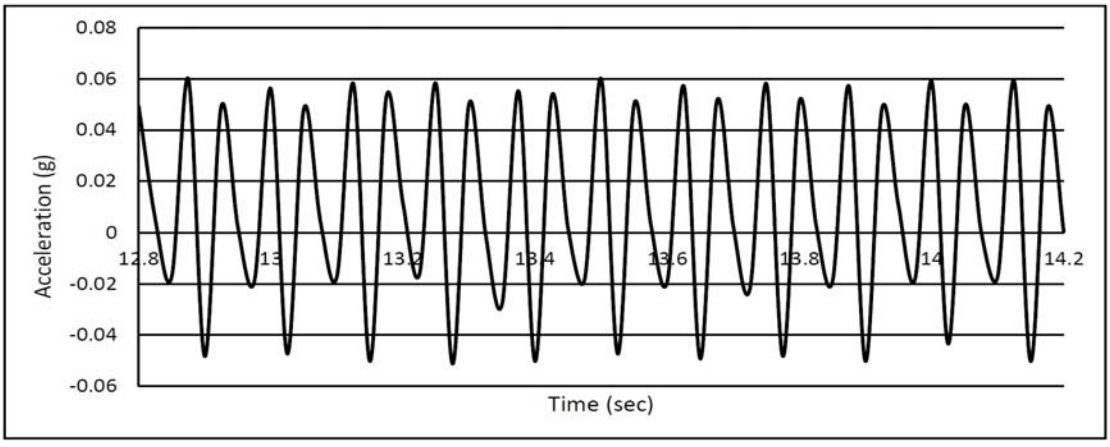

Figure 4.6: First figure is for harmonic loading and second is from shake table loading

4.4 Results and comparison with the experimental data of numerical analysis

STATIC HORIZONTAL ANALYSIS

After completion of calculation, results are measured from Output window of PLAXIS

3D. The results are presented in form of load-displacement response of the model. The horizontal displacement of foundation is the main observation for this study. It can be measured by three ways i.e. taking horizontal displacement of the node of plate at which load is acting, maximum horizontal displacement of plate and average horizontal displacement of plate. The observation from all three cases have been made and it is found from Figure 4.7 that there is no significant change in average value and node value. But maximum value is slightly higher than other values. So, node value has been taken for further study.

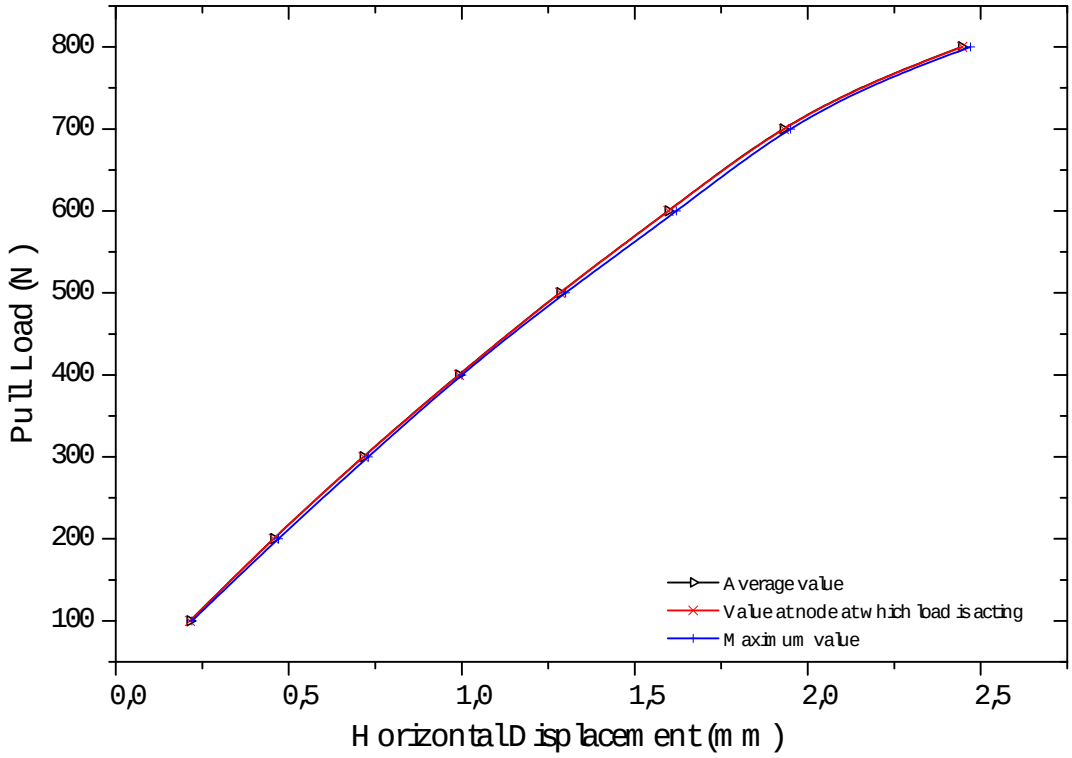

Figure 4.7: Comparison of different options to measure the value of horizontal displacement

To obtain results similar to experimental results, the effect of different has been investigated as following:

4.4.1 Influence of Meshing

In PLAXIS 3D, the calculation results depend on the mesh coarseness. To examine the mesh dependency, four types of mesh (such as "Very Coarse" mesh, "Coarse" mesh, "Medium" mesh and "Fine" mesh) have been implemented in the model. Different numbers of mesh elements have been generated for different meshing as given in Table 4.8. Very fine meshing option is also available but it is not used because analysis took very high computational time. From the Figure 4.8 it can be seen that with increase in coarseness of mesh, there will be decrease in displacement.

Table 4.8: Mesh generation

Type of mesh	**Number of elements**	**Number of nodes**
Very coarse	8388	11796
Coarse	20661	28659
Medium	67559	92363
Fine	161879	219668
Very fine	500075	675329

4.4.2 Influence of Interface element

The effect of interaction between different structural elements and soil has been checked simultaneously. Total 4 model has been prepared with abbreviations RIPI, RPI, RIP and RGIP where R-Raft, P-Pile and I-Interaction for example RPI means that only pile-soil interaction is available (no Raft-soil interaction). The material properties of interface elements are provided from surrounding soil having $R_{inter} = 0.9$ in all cases. Figure 4.9 illustrates that the existence of interfaces between all structure elements and soil gives more displacement and results are closer to experimental results.

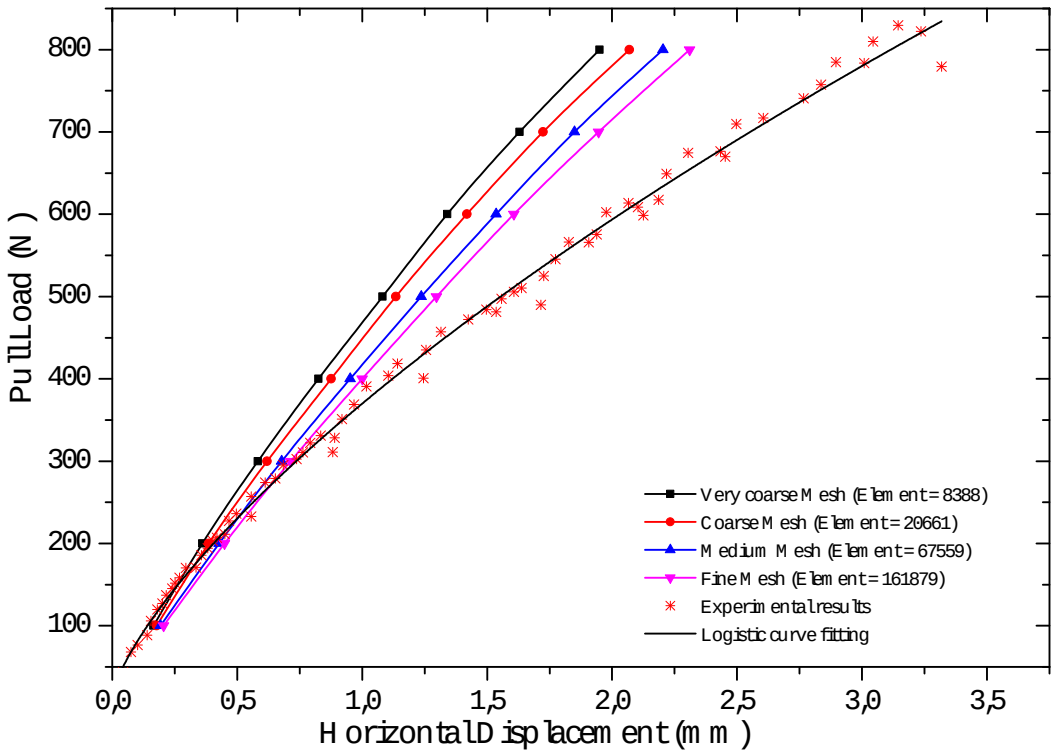

Figure 4.8: Effect of meshing

4.4.3 Influence of Strength reduction factor (R_{inter})

As the value of R_{inter} defines the soil-structure interaction, so three different R_{inter} values i.e. 0.7, 0.8 and 0.9 has been used to check the influence of R_{inter}. With reducing the value of R_{inter} more displacement are occurring and a better correlation with experimental results is obtained as presented in Figure 4.10.

4.4.4 Influence of the presence of geogrid

With using a layer of geogrid in upper fill, it has been observed that lateral deformation foundation is reduced about 12%. When geogrid uses, it interlocks soil molecule to move. It can also been seen in Figure 4.11 that with higher load the difference increases.

DYNAMIC ANALYSIS

The acceleration response of the raft center has been measured. The comparison of results with experimental has been made for the period from 3.5 to 5.5 seconds. It has

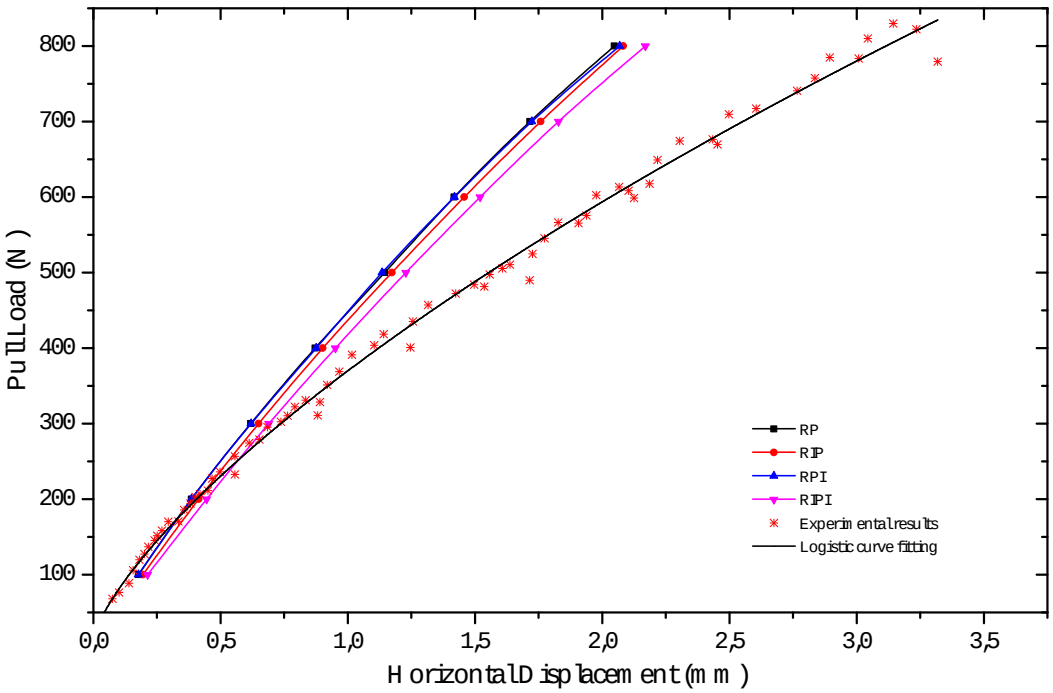

Figure 4.9: Effect of different soil-structure interaction and their combination

observed that the results are very similar to experimental results as shown in Figure 4.12. But at particular interval the amplitude of numerical analysis were coming higher from experimental. It can be because of applied loading as shown in Figure4.6. Since the author applied shake table data which lesser amplitude at the same time at which the amplitude is coming higher. And the response of raft is around 0.2g which 3.33 times higher than the applied load.

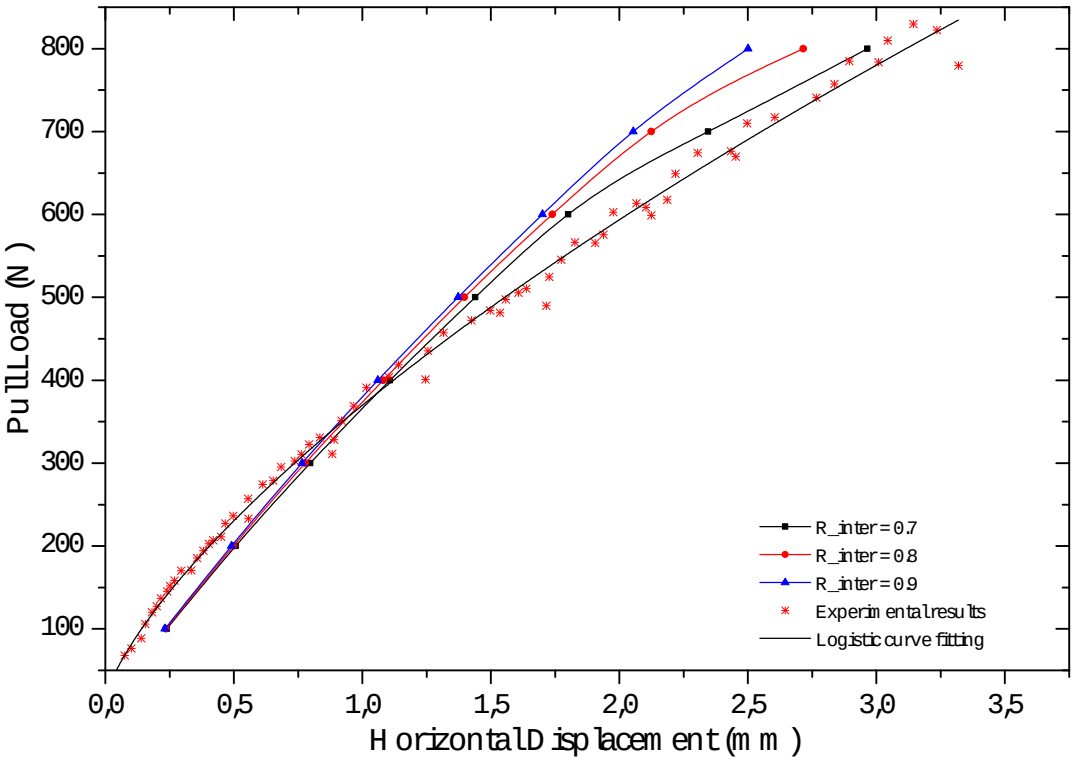

Figure 4.10: Variation of Strength reduction factor (R_{inter})

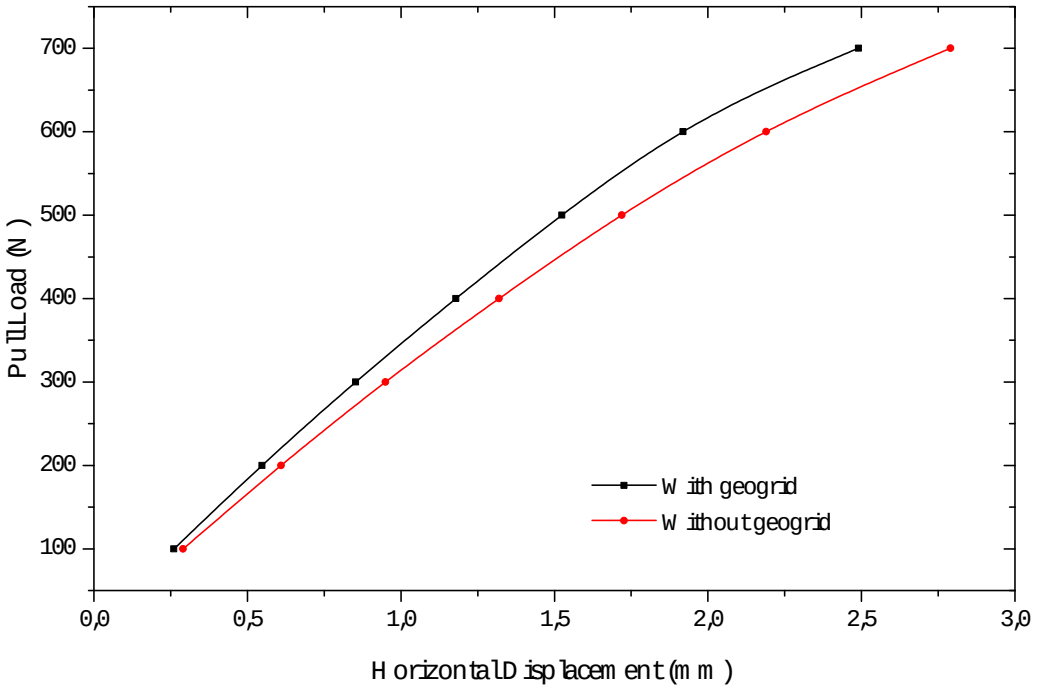

Figure 4.11: Effect of geogrid

4.5 Conclusion of the Back Analysis

From comparative study, it seems that all parameters have a great effect in calculation of horizontal displacement of foundation under static horizontal loading. For obtaining the results similar to experimental results the optimum values of parameters such as $R_inter = 0.7$, medium meshing and both raft and pile-soil interactions have been considered for Mohr-Coulomb model and but for Hardening soil model with small strain stiffness, final values of parameters have been listed in Table 4.4.

From these chosen values final static analyses have been carried out with geogrid and without geogrid and all results as illustrated in Figures 4.13 and 4.14 are in good agreement with the experimental results for both the constitutive models and also in dynamic analysis, the response of raft is similar as reported experimentally. These results define that used model is numerically stable, it can be used for further study.

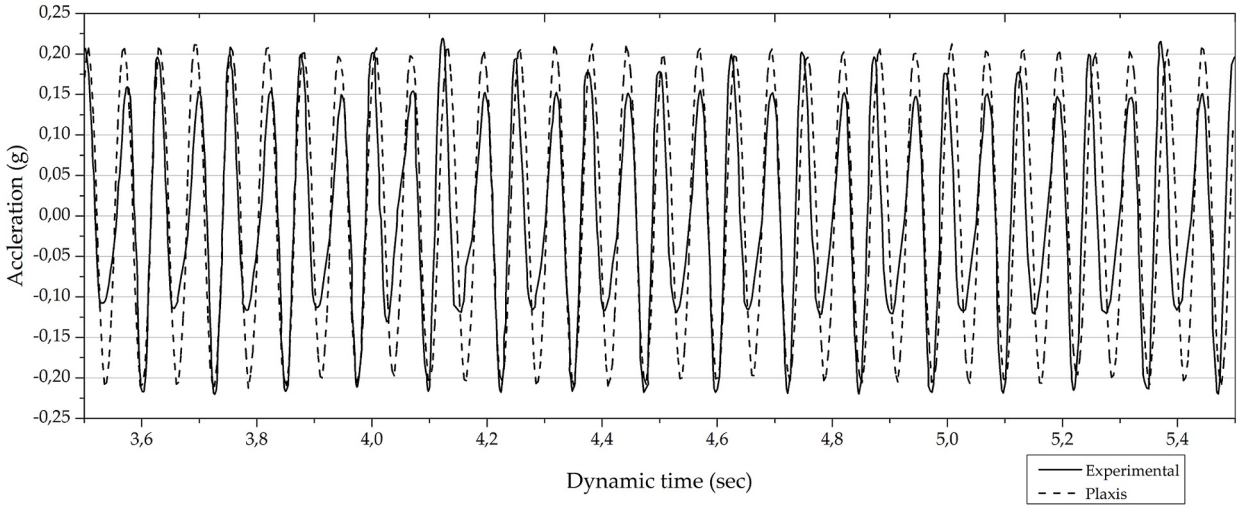

Figure 4.12: Comparison of the acceleration response of raft with experimental study

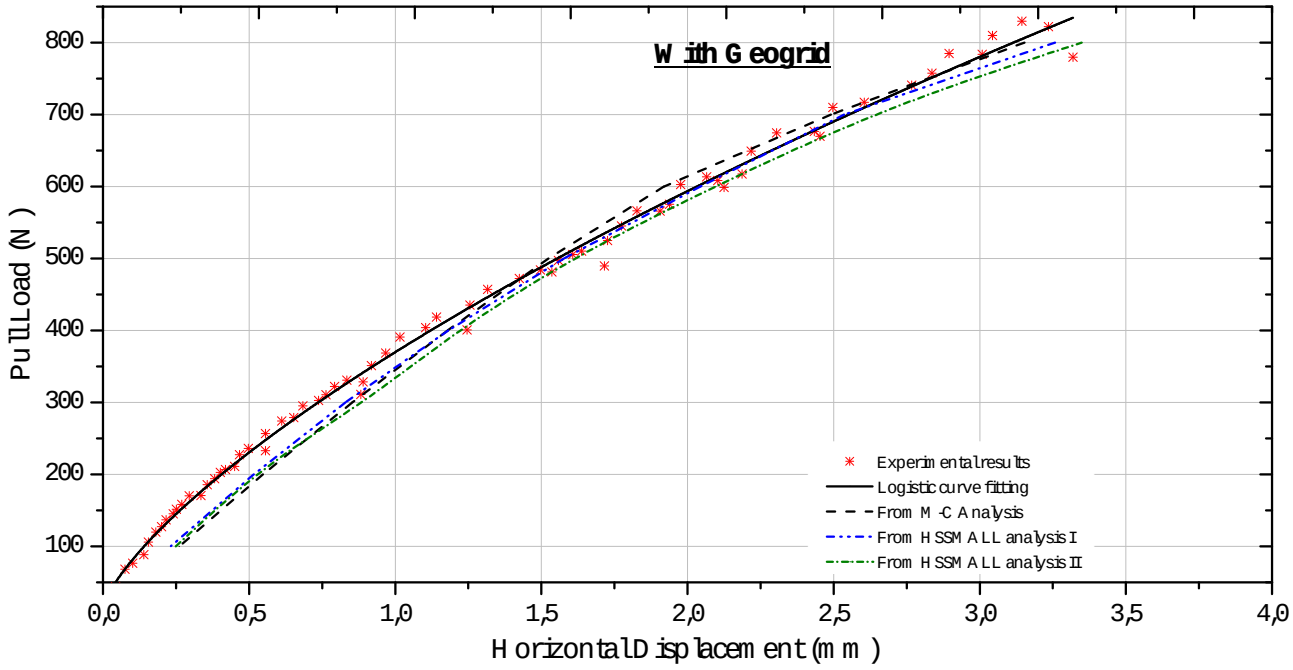

Figure 4.13: Comparison of all static analysis with experimental study when Piled raft foundation is founded on soil reinforced with geogrid

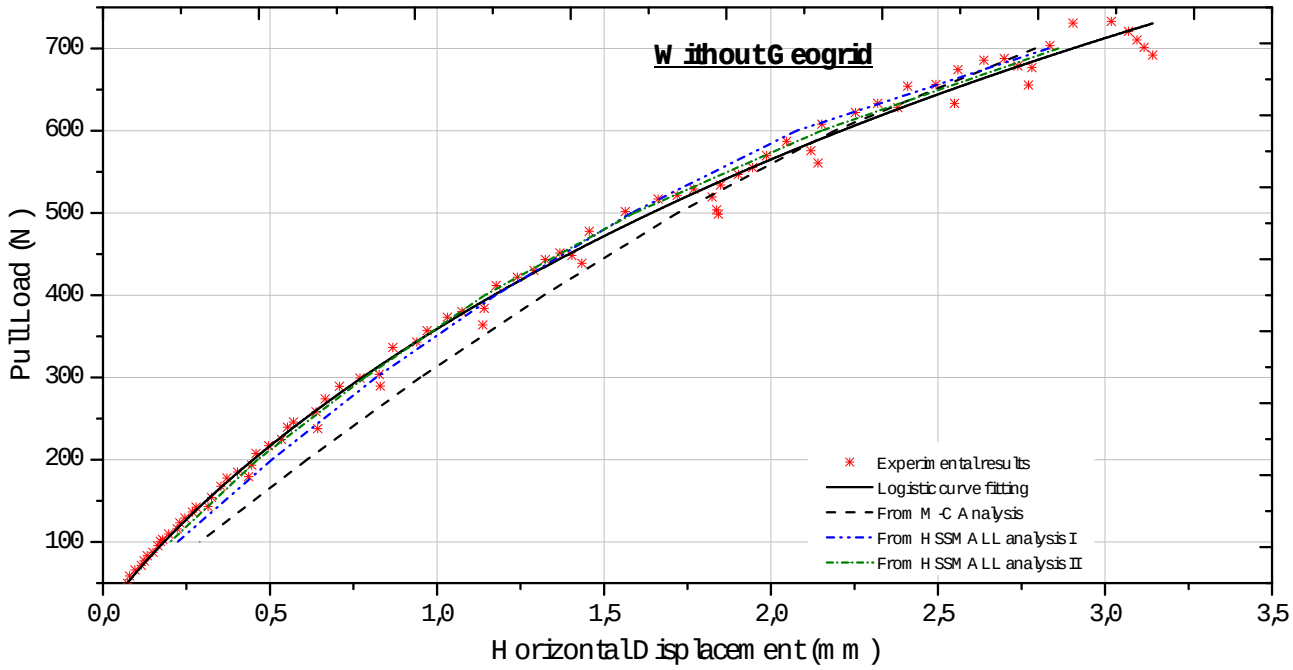

Figure 4.14: Comparison of all static analysis with experimental study when Piled raft foundation is founded on soil without geogrid

Chapter 5

Results and Discussion

The main study is to compare the behavior of disconnected piled raft foundation (DPRF) with connected piled raft foundation (CPRF) under dynamic loading for that same calibrated model has been used with similar loading. To model disconnected system an interposed layer has been provided between piles and raft. Here this layer has same properties as sand which is used as bottom layer. Numerical analysis has been performed under different load types such as static vertical load and horizontal load, dynamic horizontal load (harmonic signal). The influence of various thickness and stiffness of interposed layer in DPRF has been investigated. Geogrid has also been introduced in interposed layer to provide lateral confinement.

5.1 Static vertical load

A numerical analysis has been performed for vertical loading of $250N$ and $625N$ corresponding to prototype loading $2000kN$ and $5000kN$ as scale relationship described in Table A.1. The loading has been applied uniformly on the raft. The thickness of interposed layer $7mm$ and standard elementary boundary condition has been introduced as shown in Figure 5.1.

From Figure 5.2, it is observed that the settlement of raft in DPRF system is more in comparison of CPRF system. But for $625N$ loading, CPRF gives 4 times more settlement than for $250N$, while DPRF gives 2 times more settlement. And maximum bending moment in raft is generating at pile position in both cases but value of maximum bending moments

are $42Nm/m$ and $22Nm/m$ in CPRF and DPRF systems for $625N$ loading, respectively as shown in Figures 5.5 and 5.6. This observation shows that the bending moment is much higher in connected case.

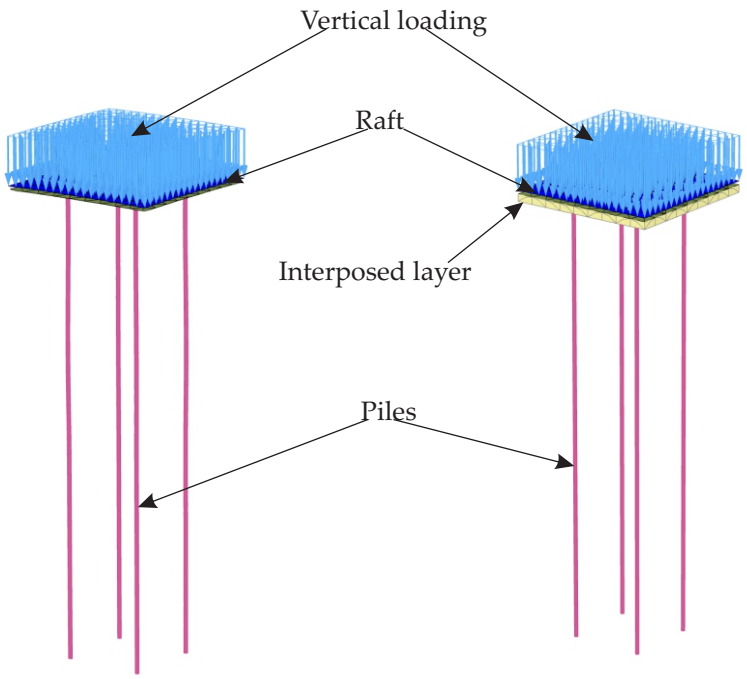

Figure 5.1: Schematic representation of Connected (left) and Disconnected (right) Piled Raft system

Similarly for piles, the bending moment at pile head is approximately zero in disconnected system as represented in Figure 5.3(a). The Figures 5.3(b) and 5.3(c) illustrate the axial load and skin friction distribution along the pile, in which it is observed that in connected system higher axial load are generated and in disconnected system axial load initially increases upto a certain depth then decrease. So the maximum value occurs at certain depth below (or at a plane) at which skin friction changes from negative to positive. This negative skin friction occurs above this plane because in this portion surrounding soil settles more than pile, that soil applies a downward drag as illustrated in Figure 5.4. This plane is called neutral plane because of zero skin friction. The similar behavior explained by *Fioravante and Giretti (2010)*, *Tradigo et al. (2014)* and *Tradigo et al. (2015)*.

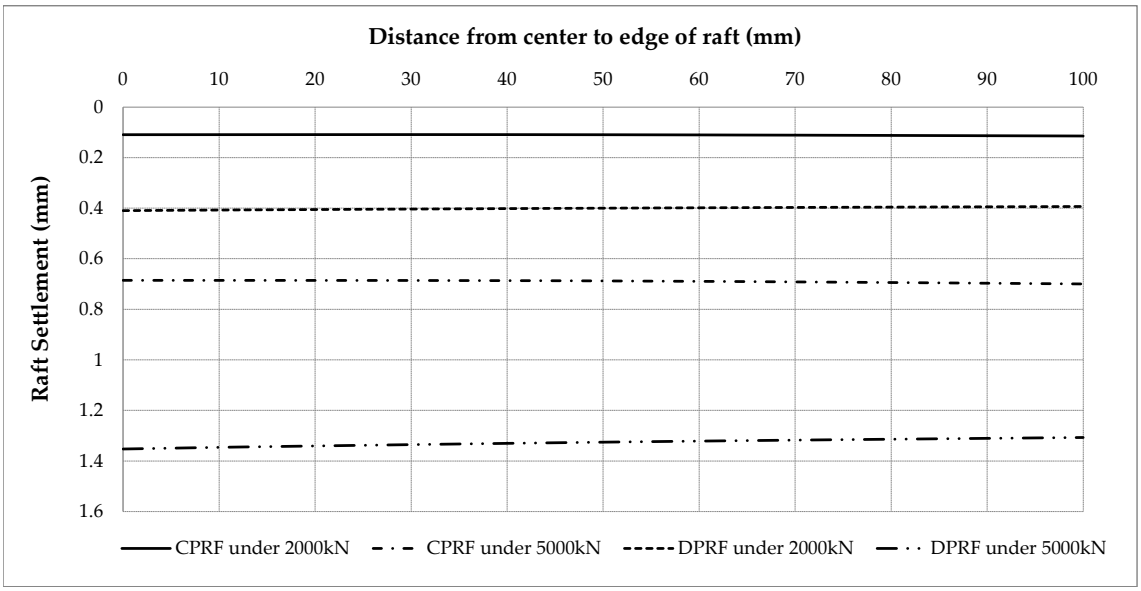

Figure 5.2: Comparison of raft settlement in CPRF with DPRF under different vertical loads

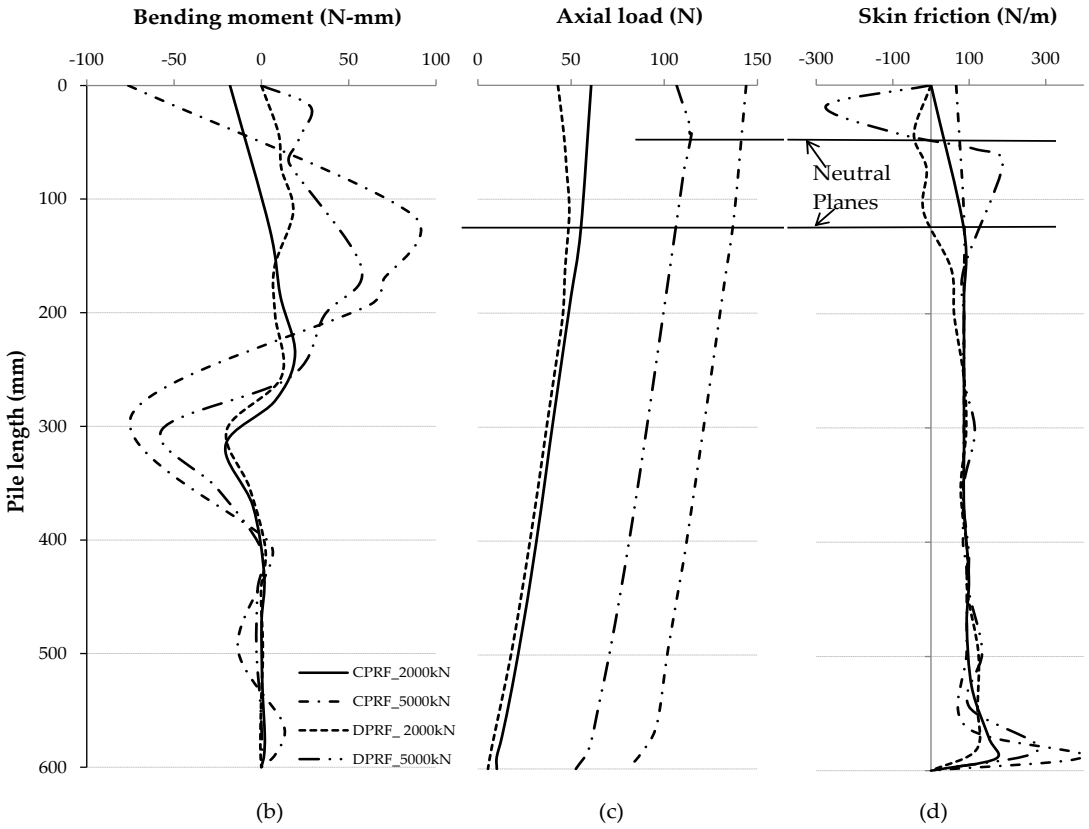

Figure 5.3: Comparison of (a) Bending moment, (b) Axial load and (c) Skin friction along the pile in CPRF with DPRF under different vertical loads

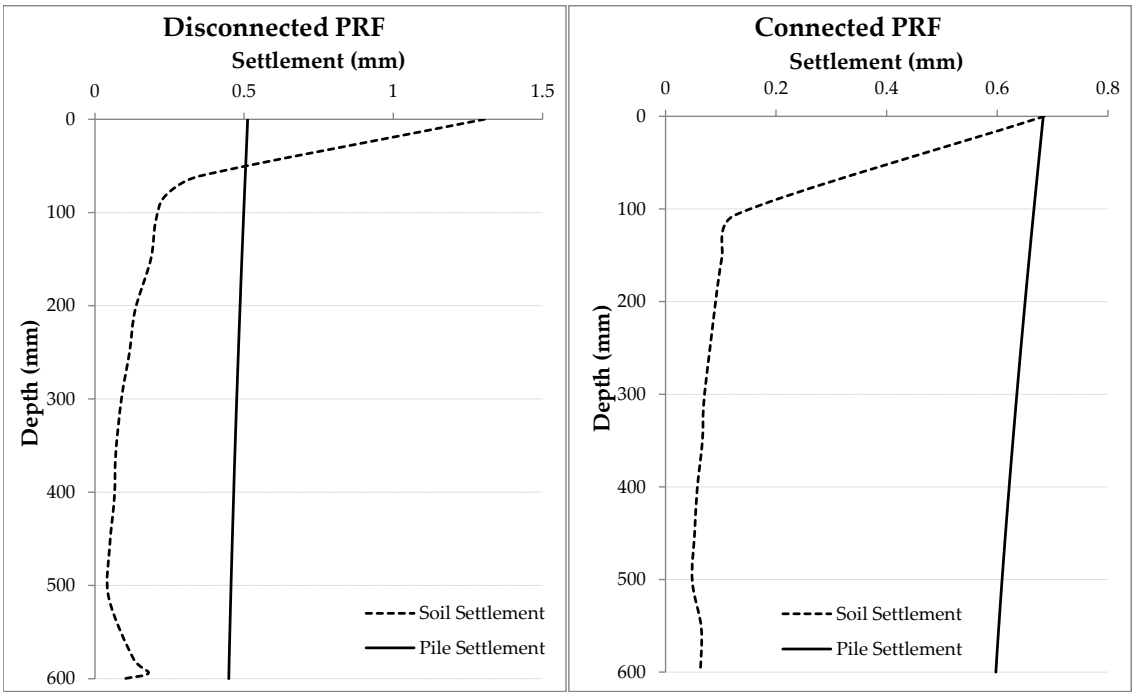

Figure 5.4: Vertical displacement of soil and pile for both system under $625N$ vertical load

5.1.1 Influence of thickness and Stiffness of interposed layer

In disconnected system, load transfer mechanism is the main finding, because a granular interposed layer is introduced for disconnection and this layer also help to distribute the loads. Therefore, the thickness and stiffness of this layer are the key points and influence of these parameters has been checked. The value of stiffness is varied from $5000KPa$ to $25000KPa$ with in increment of $5000KPa$ and similarly thickness from $5mm$ to $25mm$ with $5mm$ increment.

From the Figure 5.7, it is observed that with increase in the stiffness of layer and decrease in thickness causes decrement in the raft settlement and increment in axial load. And also rate of decrement in raft settlement decreases with increase in stiffness. As stiffness decreases, increment in the depth of neutral plane is observed in Figure 5.7(c), that same concept explained by $Lianget\ al.\ (2003)$. So, an optimum value of thickness and stiffness has to be selected for interposed layer.

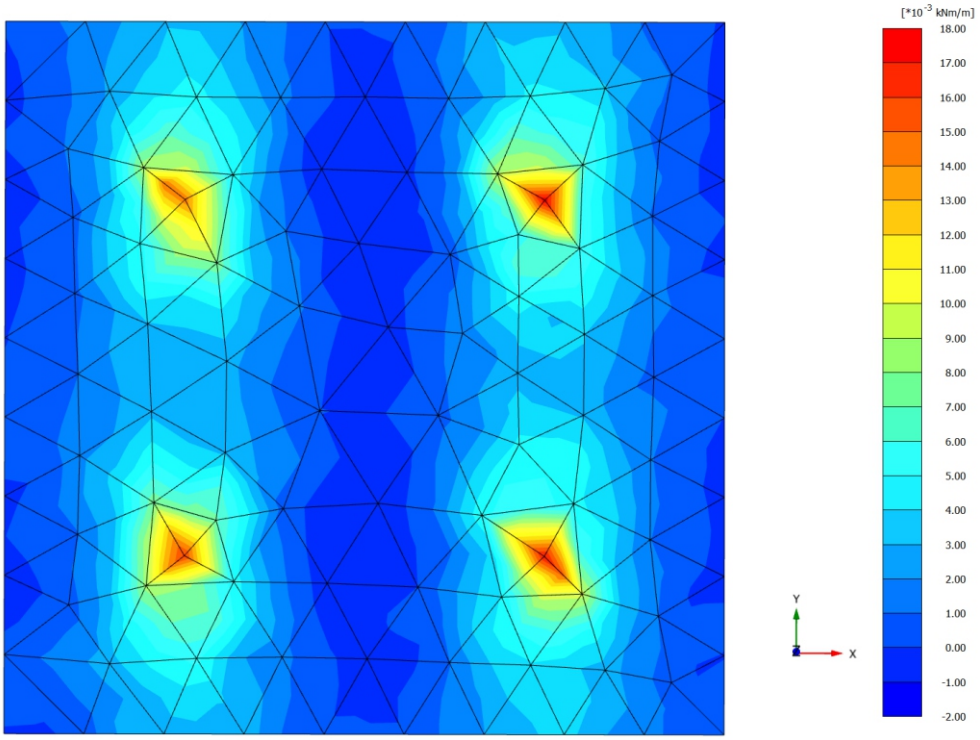

(a) CPRF under 250N

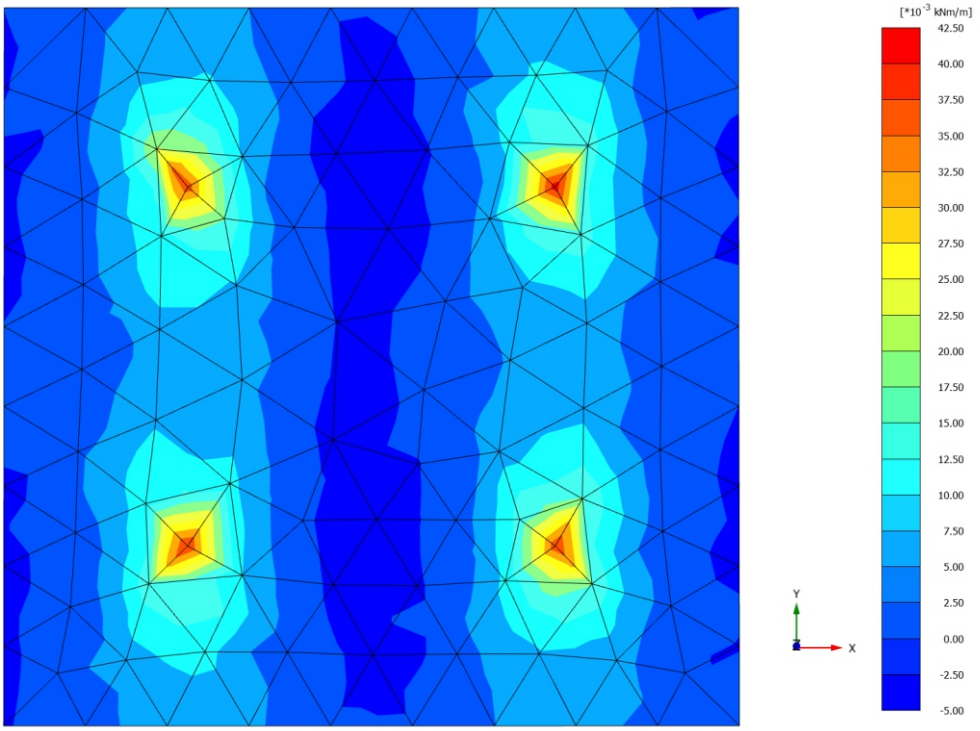

(b) CPRF under 625N

Figure 5.5: Bending moment distribution in raft in CPRF under vertical load

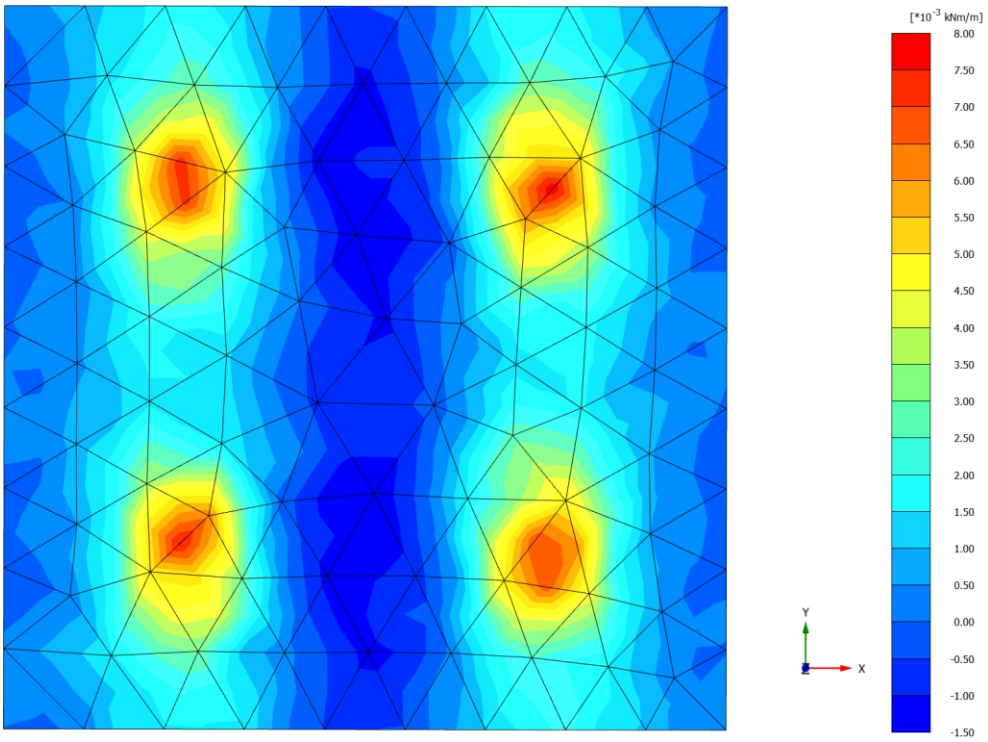

(a) DPRF under 250N

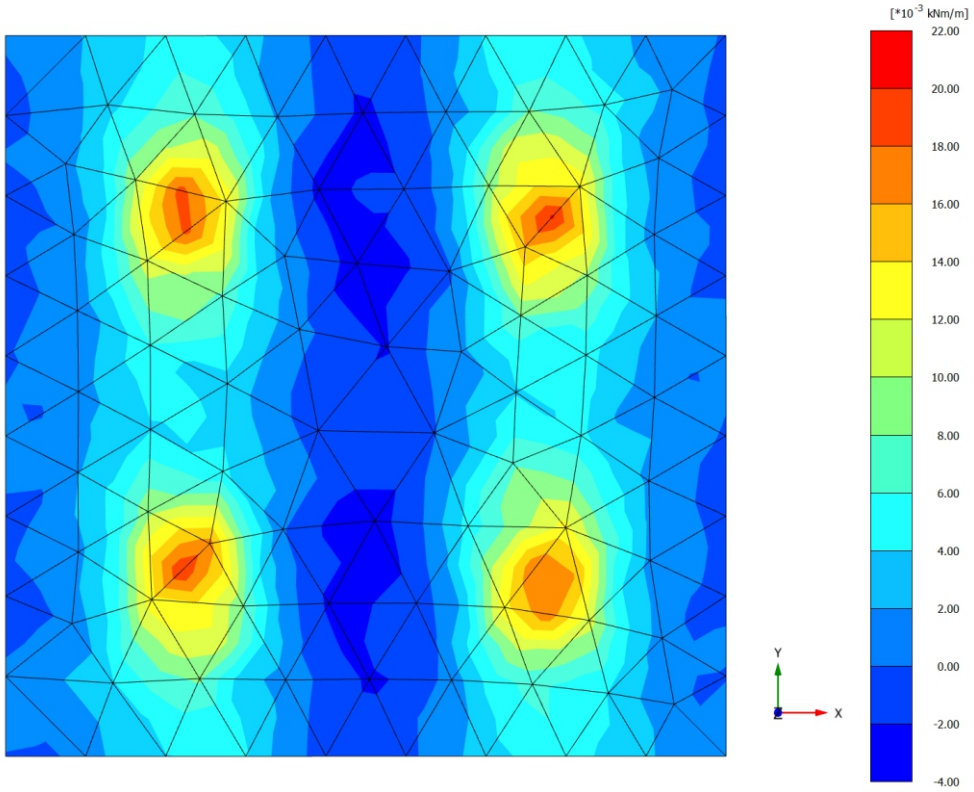

(b) DPRF under 625N

Figure 5.6: Bending moment distribution in raft in DPRF under vertical load

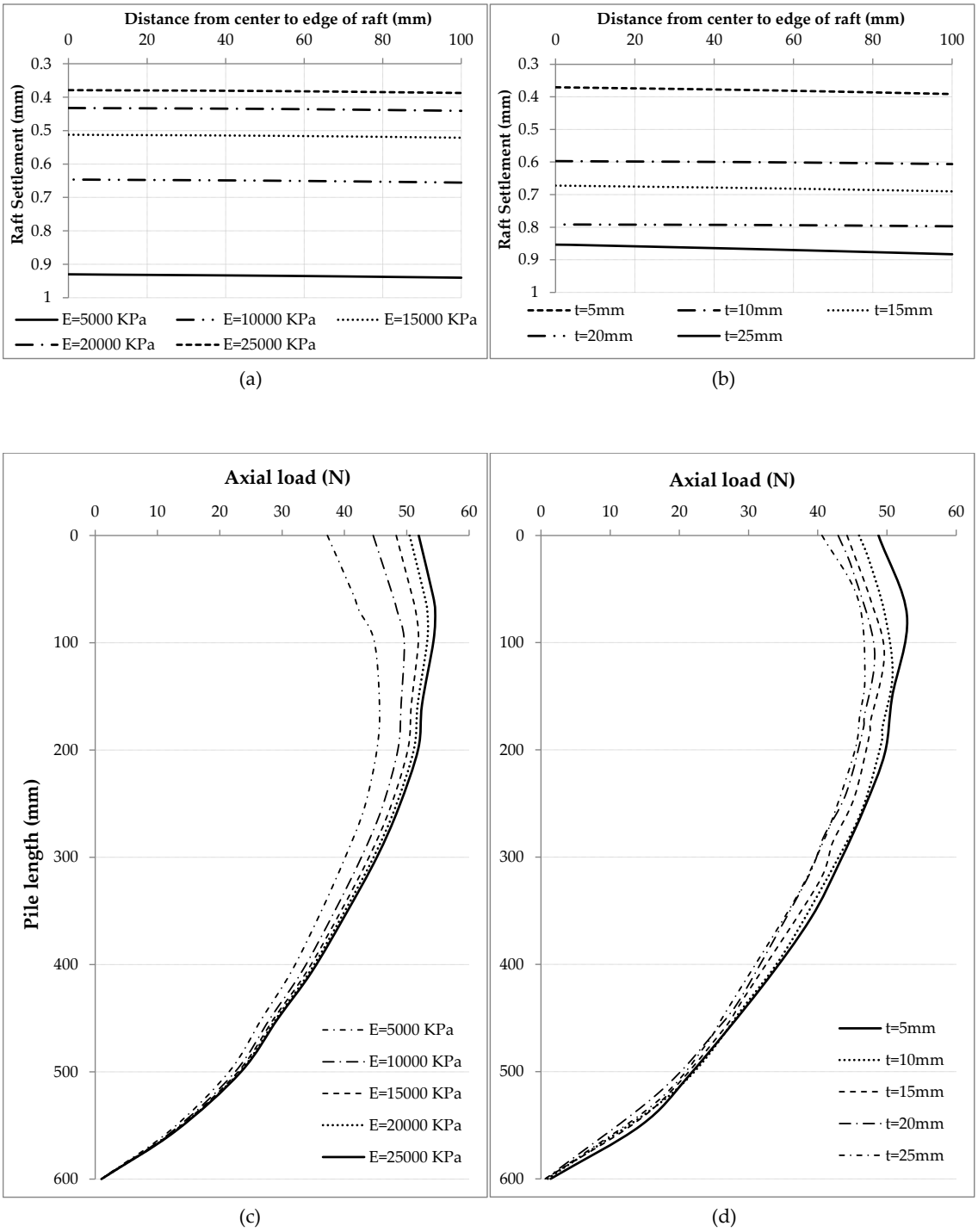

Figure 5.7: Influence of thickness and stiffness of interposed layer on axial load and raft settlement under $250N$ vertical load

5.2 Static vertical and horizontal load

The model has also been analyzed under static horizontal load as "base shear" which is applied on the raft. Since the base shear usually varies from 10 to 30% of vertical load, therefore, the influence of different horizontal loads that are varied from 10 to 30% with 5% increment of $250N$ vertical load, has been investigated. The thickness and stiffness of interposed layer are $10mm$ and $15000KPa$ used respectively.
The Figure 5.8 illustrates that in disconnect system more horizontal displacements are generated while less shear forces are produced at pile head. The horizontal displacement in piles in disconnected system approximately 64% increases but the decrement in shear force approximately 80% has been observed. Similarly in case raft, maximum horizontal displacement in disconnected system is 3 times of connected system as illustrated in Figure 5.9(a). But Figure 5.9(b) shows that maximum shear force in raft is much lesser in comparison of connected system. And also with increase in horizontal load, maximum horizontal displacement in raft increases linearly in both systems but rate in disconnected system is more. Likewise, maximum shear force increases linearly with high rate in connected system while no major variation of has been observed in disconnected system.

5.2.1 Influence of Geogrid introduced in interposed layer

To reduce the horizontal displacement in DPRF, a geogrid, same as used in calibrated model, has been introduced in interposed layer. The isotropic geogrid, having same axial stiffness $110kN/m$ has been introduced and engineering properties are defined in Table A.2. The geogrid layer is laid at a depth of $9mm$ from the bottom of raft.
Figure 5.9(a) and 5.9(c) illustrate that the horizontal displacement in disconnected system decreases arround 6 to 10% by introducing geogrid layer for this geometric model. Moreover, a significant reduction in the settlement of raft has been observed arroun 44% as shown in Figure 5.9(e). But shear forces increase due presence of geogrid that can be because of interlocking behavior of geogrid as represented in Figure 5.9(b) and 5.9(d).

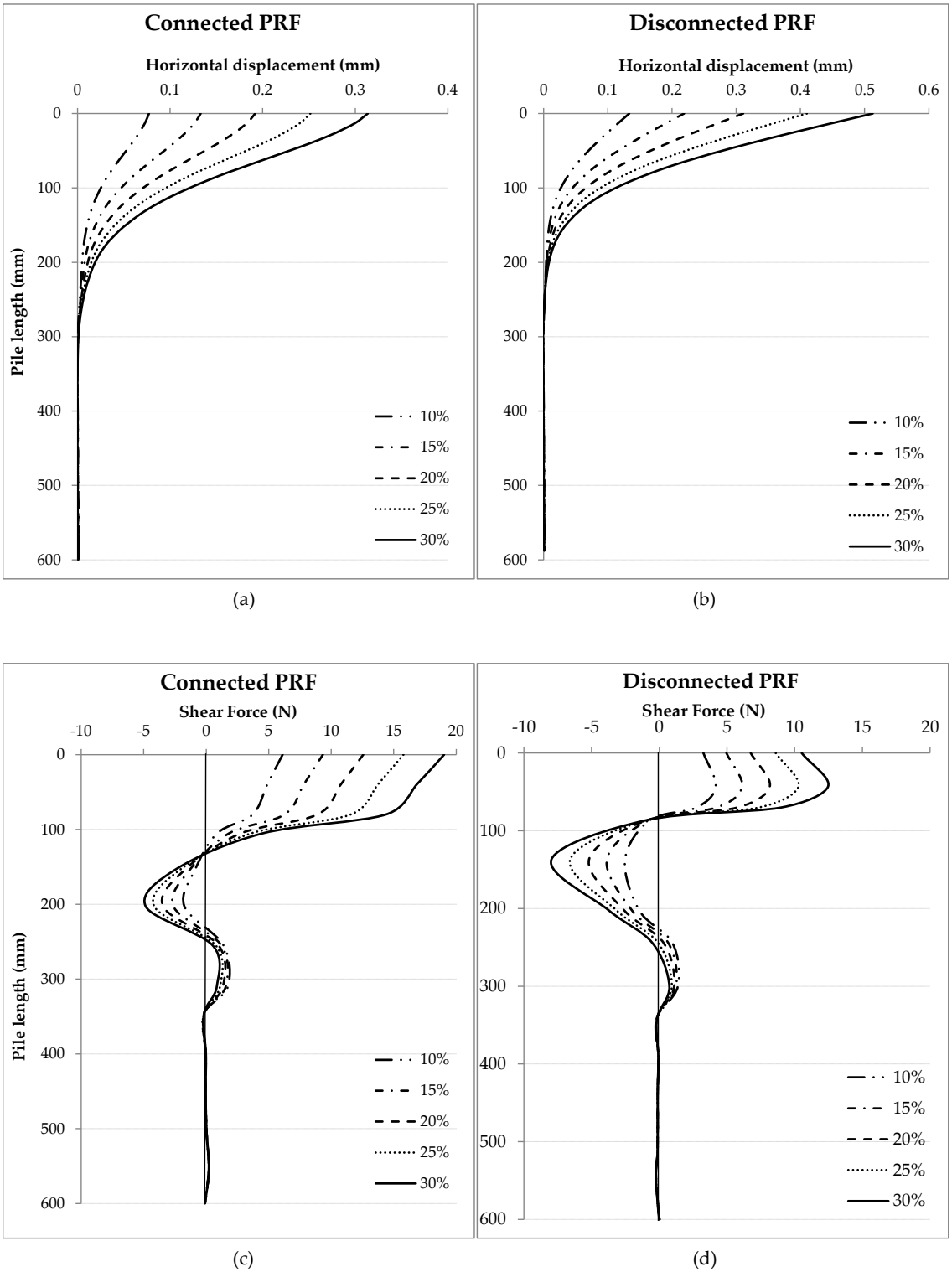

Figure 5.8: Comparison of horizontal displacement and shear force along the pile under different horizontal loads

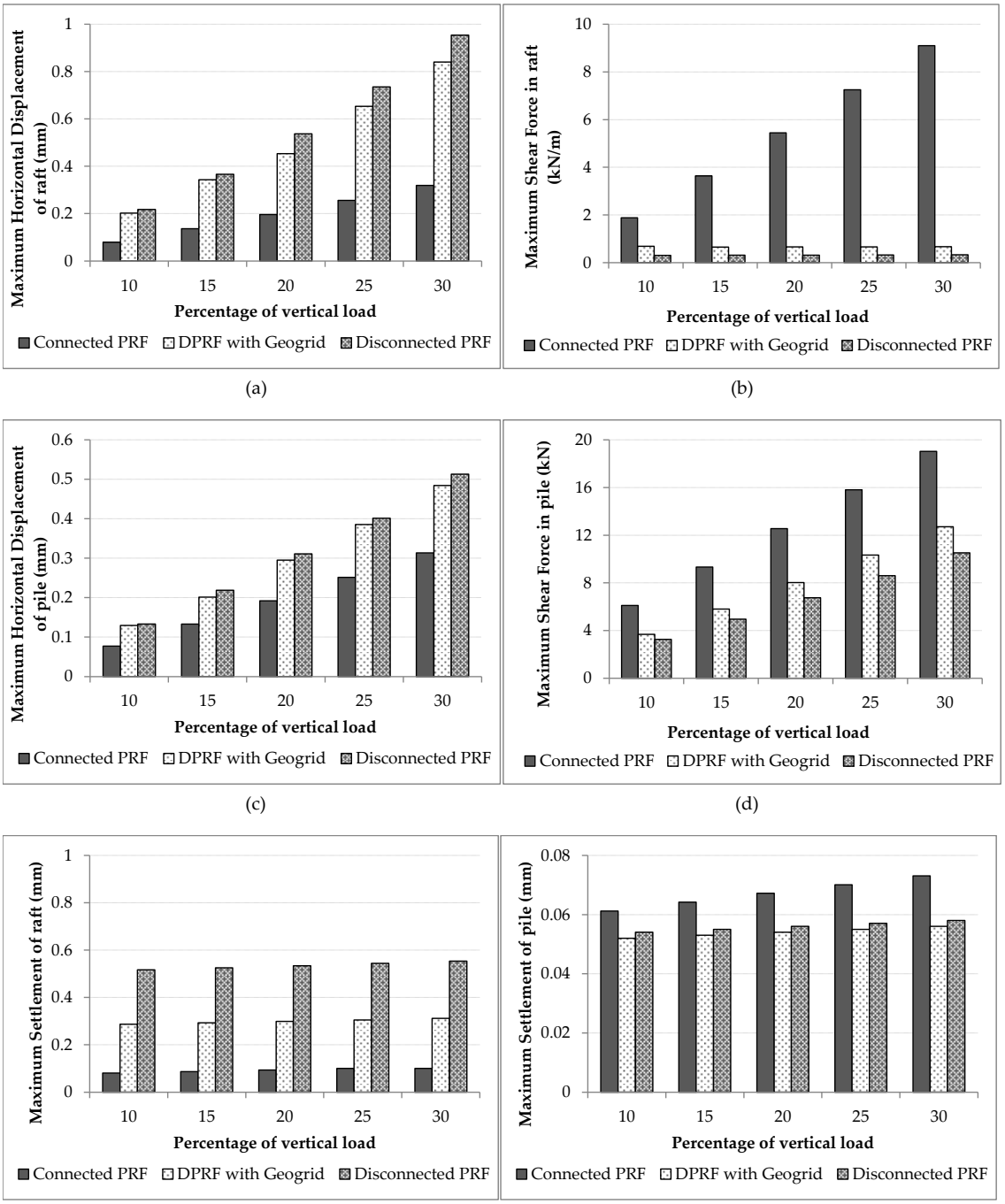

Figure 5.9: Influence of Geogrid on horizontal displacement, settlement and shear force under different horizontal loads

5.3 Dynamic horizontal Load

The influence of dynamic loading has also been investigated in DPRF. For dynamic loading, a harmonic signal, having $16Hz$ frequency and $0.06g$ amplitude of acceleration has been applied from the base of model in the horizontal direction (i.e. x-direction) for $2sec$ duration. 1D shaking has been simulated using elementary boundary condition as used in calibrated model.

From Figure 5.11, it is observed that both the systems have similar variation of horizontal displacement of the pile and raft and acceleration response with time, but disconnected system shows higher value in all cases.

Moreover, the horizontal displacement along the pile is differ in upper portion i.e. above $250mm$, of pile after that displacement is same for both systems. In this upper portion, the connected system are giving less horizontal displacement in comparison of connected system as shown in Figure 5.10. The axial load and bending moment both are coming less in DPRF. Due to this there will be less stress concentration at pile head. Here, maximum axial load are generating at the middle of pile for both the systems. That defines upto center of pile negative skin friction are acting.

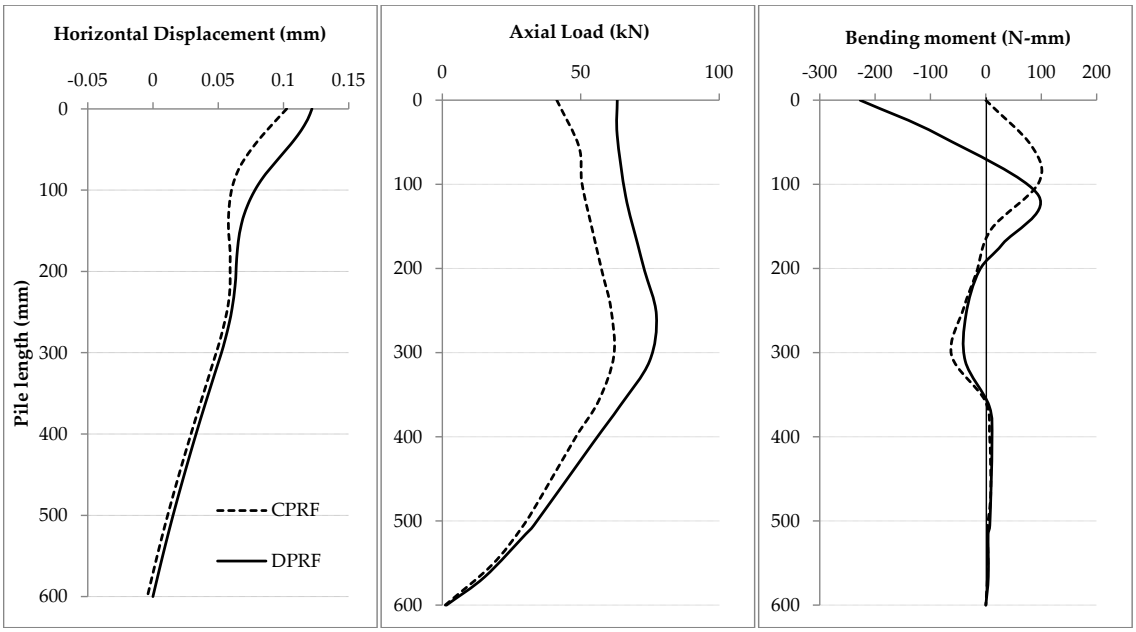

Figure 5.10: Representation of horizontal displacement, axial load and bending moment distribution along the pile under dynamic horizontal load at $2sec$

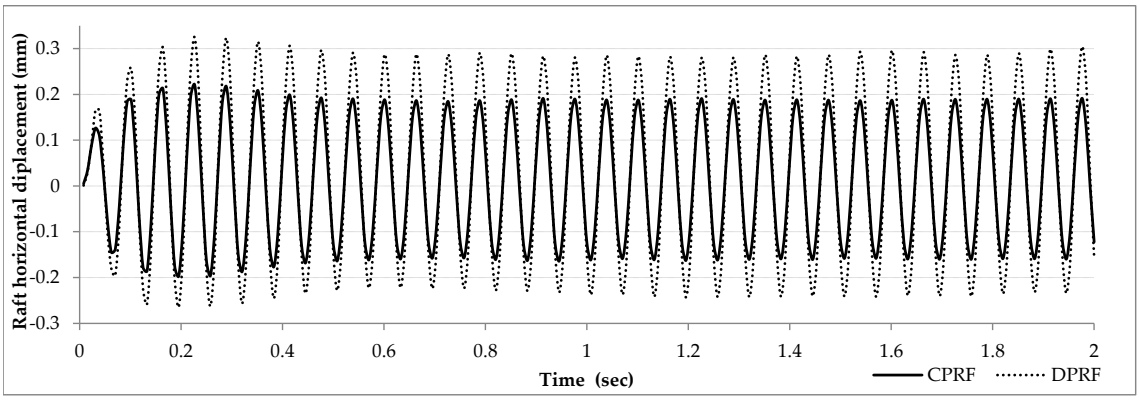

(a)

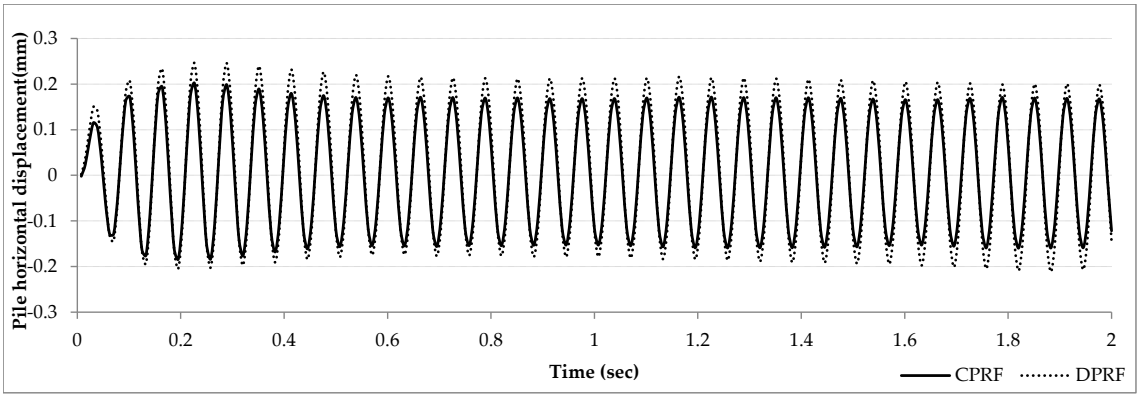

(b)

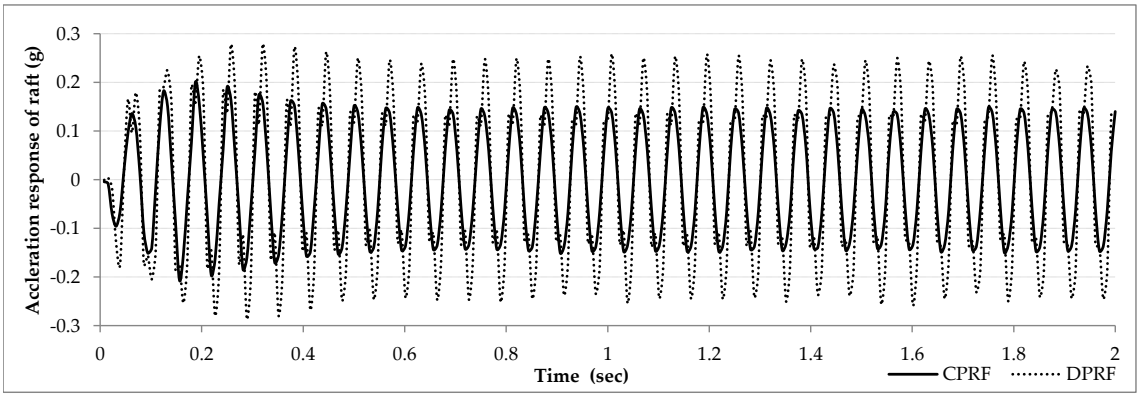

(c)

Figure 5.11: Representation of variation of horizontal displacement of pile head and raft and acceleration response of raft with time for both systems

Chapter 6

Conclusions

Generally, for heavy loading or poor soil condition, settlement reducing piles are provided under the raft to reduce the large deformations. These piles are structurally connected to the raft and also shared some part of load. But due to generation high stresses at the connection, a alternative approach i.e. by disconnecting them from the raft with an interposed layer, has been investigated in this work.

The feasibility of Disconnected piled-raft foundation (DPRF) over the Connected piled-raft foundation (CPRF) have been investigated under different load conditions. A 3D model of piled raft system has been numerically analyzed in finite element software PLAXIS 3D 2013. The soil are simulated using advanced constitutive model i.e. Hardening Soil model with small strain stiffness because this model shows the real hysteresis behavior of soil under dynamic loading. Also piles are modeled using an embedded pile approach because usually large number of piles are used in foundation, to analyze them numerically becomes more complex and takes more computational efforts in 3D model. Initially, the model has been calibrated from an experimental model test carried out by *Taha (2014)* on pile raft foundation and then same model has been used for further study. From numerical analysis study following conclusions can be made:

- From the calibration analysis all numerical results of horizontal displacement and acceleration response are in good agreement to the experimental test results.
- The results show the improve behavior of DPRF over CPRF in respect of bending moment and shear force distribution resulting in economic design of piled raft foundation.

- The vertical load in DPRF is tranferred partially by negative skin friction and some part by arching effect. Lateral loads is resisted mainly by raft soil interface frictional resistance and some part by passive pressure.
- In DPRF, a neutral plane exists in piles below the head of pile at which the maximum axial force and zero skin friction are associated. But in CPRF maximum axial force is generated at pile head under vertical loading.
- Due to disconnection less bending moment and shear force are generated at the pile head and at the pile-raft junction. This results in less stress concentration in both the raft and piles.
- The stiffness and thickness of interposed layer have major influence on the behavior of DPRF. More stiffer and thinner layer gives less settlement but more pile forces. Therefore, an optimum thickness and stiffness should be designed.
- The DPRF gives higher settlement and horizontal displacement in comparison of CPRF. But percentage increment in deformation is lesser than the percentage decrement in forces.
- To reduce the horizontal deformation of the piled raft system, geosynthectic layer can be used. For lateral confinement, geogrid mesh is more suitable geosynthectic because of its interlocking mechanism. Simultaneously, it reduces the vertical settlement also.
- Under harmonic loading, DPRF gives higher response but at the same time significant reduction in forces in both the piles and raft.
- In DPRF, the piles mainly reinforce the underlying soil layer and do not show beam action. Therefore a lesser factor of safety can be used against structural failures of the pile.

Future Scope

In this study only behavior under harmonic load has been investigated using embedded pile approach. Following future work in the field of disconnected piled raft system can be carried out:

- Future work should concentrate on the behavior of disconnected system under

seismic loading and also in liquefiable soil.

- Extensive research on the application of the geogrid in load distribution layer.
- Future investigation on use of embedded pile element in this type of foundation and also comparison with volume pile element.
- A parametric study should also be performed to investigate the influence of different parameters such as: stiffness pile and raft, pile spacing, length of pile, thickness of raft, etc.

Bibliography

http://kb.plaxis.com/tips-and-tricks/modelling-soil-structure-interaction-interfaces.

http://www.civil.ist.utl.pt/luisg/textos/interac

http://www.technicalcivils.co.uk/site-pages/geotechnical/geogrid.html.

Abdel-Fattah, T. T., A. A. Hemada, and M. T. Abdel-Fattah (2014, June). Modeling and safety assessment of a piled raft comprising defective piles. In A. . Hicks, R. B. . J. . Brinkgreve, and A. Rohe (Eds.), *Proceedings of the 8th European Conference on Numerical Methods in Geotechnical Engineering (NUMGE2014)*, Volume 1, pp. 639–644. London: Taylor & Francis group.

Ata, A., E. Badrawi, and M. Nabil (2015). Numerical analysis of unconnected piled raft with cushion. *Ain Shams Engineering Journal 6*, 421–428.

Benz, T. (2007). *Small-Strain Stiffness of Soils and its Numerical Consequences*. Ph. D. thesis, Institut für Geotechnik der Universität Stuttgart.

Benz, T., P. A. Vermeer, and R. Schwab (2009). A small-strain overlay model. *International journal for numerical and analytical methods in geomechanics 33*, 25–44.

Brinkgreve, R. B. J., E. Engin, and W. M. Swolfs (2013a). *PLAXIS 3D Material Model Manual*. Plaxis bv P.O. Box 572, 2600 AN DELFT, Netherlands.

Brinkgreve, R. B. J., E. Engin, and W. M. Swolfs (2013b). *PLAXIS 3D Reference Manual*. Plaxis bv P.O. Box 572, 2600 AN DELFT, Netherlands.

Brinkgreve, R. B. J., M. H. Kappert, and P. G. Bonnier (2007). Hysteretic damping in a small-strain stiffness model. In G. Pande and S. Pietrusczak (Eds.), *Proceedings of*

the Tenth International Symposium on Numerical Models in Geomechanics (NUMOG X), Rhodes, Greece, pp. 737–742. Taylor & Francis Group, London.

Brinkgreve, R. B. J., S. Kumarswamy, and W. M. Swolfs (2015a). *PLAXIS 3D Material Model Manual Anniversary Edition*. Plaxis bv P.O. Box 572, 2600 AN DELFT, Netherlands.

Brinkgreve, R. B. J., S. Kumarswamy, and W. M. Swolfs (2015b). *PLAXIS 3D Reference Manual Anniversary Edition*. Plaxis bv P.O. Box 572, 2600 AN DELFT, Netherlands.

Brinkgreve, R. B. J., S. Kumarswamy, and W. M. Swolfs (2015c). *PLAXIS 3D Scientific Manual Anniversary Edition*. Plaxis bv P.O. Box 572, 2600 AN DELFT, Netherlands: PLAXIS bv.

Burland, J., B. Broms, and V. de Mello (1977). Behavior of foundations and structures. *Proc.9 ICSMFE, Tokyo 2*, 495–546.

Cao, X. D., I. H. Wong, and M.-F. Chang (2004). Behavior of model rafts resting on pile-reinforced sand. *Journal of geotechnical and geoenvironmental engineering © ASCE 130*(2), 129–138.

Carroll, R. (1988). Specifying geogrids. *Geotechnical Fabrics Report 6*(2).

Chow, H. and J. Small (2008). Case histories for piled rafts. In *Proc. BGA Int. conf. on foundations*, Dundee, Scotland, pp. 451–462.

Dao, T. (2011). Validation of plaxis embedded piles for lateral loading. Master's thesis, Delft University of Technology.

Duncan, J. and C. Chang (1970). Nonlinear analysis of stress and strain in soils. *Journal of Soil Mechanics and Foundations Division, ASCE 96*(5), 1629–1653.

Ekici, A. and N. Huvaj (2014, June). Validation of 3d finite element solution for laterally loaded passive piles. In A. . Hicks, R. B. . J. . Brinkgreve, and A. Rohe (Eds.), *Proceedings of the 8th European Conference on Numerical Methods in Geotechnical Engineering*

(NUMGE2014), Volume 1, pp. 651–656. London: Taylor & Francis group: CRC Press 2014.

Engin, H. K., E. G. Septanika, and R. B. J. Brinkgreve (2007). Improved embedded beam elements for the modemodel of piles. In G. P. . S. Pietruszczak (Ed.), *Int. Symp. on Numerical Models in Geomechanics –NUMOG X*, pp. 475–480. London: Taylor & Francis group.

Eslami, A., M. Veiskarami, and M. M. Eslami (2012). Study on optimized piled-raft foundations (prf) performance with connected and non-connected piles- three case histories. *International Journal of Civil Engineering 10*(2), 100–111.

Faizi, K., A. S. A. Rashid, and R. Nazir (2013). Telescopic non-connected piled-raft foundation (tncprf). *Electronic journal of geotechnical engineering 18*, 6125–6134.

Fioravante, V. (2011). Load transfer from a raft to a pile with an interposed layer. *Géotechnique 61*(2), 121–132.

Fioravante, V. and D. Giretti (2010). Contact versus noncontact piled raft foundations. *Canadian Geotechnical Journal 47*, 1271–1287.

Floroiu, L. and H. F. Schweiger (2015). Parametric study of the seismic ground response of a linear visco-elastic soil layer improved by stone columns or pile-like elements. *Geotechnik 38*, 304–315.

Hardin, B. and V. Drnevich (1972). Shear modulus and damping in soils: Design equations and curves. *Soil Mechanics and Foundations Division, ASCE 98*(7), 667–692.

Horikoshi, K., T. Matsumoto, Y. Hashizume, T. Watanabe, and H. Fukuyama (2003a). Performance of piled raft foundations subjected to dynamic loading. *International Journal of Physical Modelling in Geotechnics 2*, 51–62.

Horikoshi, K., T. Matsumoto, Y. Hashizume, T. Watanabe, and H. Fukuyama (2003b). Performance of piled raft foundations subjected to static horizontal loads. *International Journal of Physical Modelling in Geotechnics 2*, 37–50.

Hudson, M., I. Idriss, and M. Beirkae (1994). *QUAD4M User's manual*.

Janbu, N. (1963). Soil compressibility as determined by oedometer and triaxial tests. In *Proc. ECSMFE Wiesbaden*, Volume 1, pp. 19–25.

Kumar, A., D. Choudhury, and R. Katzenbach (2016). Effect of earthquake on combined pile–raft foundation. *International Journal of Geomechanics © ASCE 04016013*.

Laera, A. and R. B. J. Brinkgreve (2015). *Ground response analysis in PLAXIS 2D*.

Liang, F.-Y., L.-Z. Chen, and X.-G. Shi (2003). Numerical analysis of composite piled raft with cushion subjected to vertical load. *Computers and Geotechnics © ELSEVIER 30*, 443–453.

Mandolinia, A., R. D. Laorab, and Y. Mascarucci (2013). Rational design of piled raft. In *11th International Conference on Modern Building Materials, Structures and Techniques*, Volume 57, pp. 45–52.

Mansour, M. H., A. Y. Akl, and H. K. Moustafa (2014, June). Behaviour of piled rafts with piles of different lengths and distributions under vertical loading. In A. . Hicks, R. B. . J. . Brinkgreve, and A. Rohe (Eds.), *Proceedings of the 8th European Conference on Numerical Methods in Geotechnical Engineering (NUMGE2014)*, Volume 1, pp. 687–692. London: Taylor & Francis group.

Mattsson, N., C. Simon, A. Menoret, and M. Ray (2013). Case study of a full-scale load test of a piled raft with an interposed layer for a nuclear storage facility. *Géotechnique 63*(11), 965–976.

McGown, A., I. Yogarajah, K. Andrawes, and M. Saad (1995). Strain behaviour of polymeric geogrids subjected to sustained and repeated loading in air and in soil. *Geosynthetics International 2*(1), 341–355.

Meymand, P. J. (1998). *Shaking table scale model tests of nonlinear soil-pile superstructure interaction in soft clay*. Ph. D. thesis, University. of California, Berkeley, CA.

Naesgaard, E., A. Azizian, D. Yang, M. Uthayakumar, A. Amini, and P. M. Byrne (2008). Golden ears bridge – geotechnical seismic design aspects. In *61st Canadian Geotechnical Conference, Canadian Geotechnical Society, Edmonton, Alberta*.

Nakai, S., H. Kato, R. Ishida, H. Mano, and M. Nagata (2004, March). Load bearing mechanism of piled raft foundation during earthquake. In I. O. B. M. Celebi (USGS), M.I. Todorovska (USC) and M. I. (NILIM) (Eds.), *Third UJNR Workshop on Soil-Structure Interaction*. U.S. Geological Survey, U.S. Department of the Interior, Building Research Institute of Japan, University of Southern California and National Institute for Land and Infrastructure Management, Japan Ministry of Land, Infrastructure and Transport.

Poulos, H. G. (2001). Piled raft foundations: design and applications. *Géotechnique 51*(2), 95–113.

Quick, H. (2005). Report on foundation design of high rise buildings. Technical report.

Richter, S., R. O. Cudmani, and C. Slominski (2011). The behavior of a spread footing over reinforced ground with gravel interface during a strong earthquake. *Geotechnik 34*(3), 193–204.

Santos, J. and A. Correia (2001). Reference threshold shear strain of soil. its application to obtain a unique strain-dependent shear modulus curve for soil. In *15th International Conference on Soil Mechanics and Geotechnical Engineering*, Volume 1, Istanbul, Turkey, pp. 267–270.

Sawwaf, M. E. (2010). Experimental study of eccentrically loaded raft with connected and unconnected short piles. *Journal of geotechnical and geoenvironmental engineering © ASCE 136*(10), 1394–1402.

Schanz, T. (1998). *Zur Modellierung des Mechanischen Verhaltens von Reibungsmaterialen*. Ph. D. thesis, Habilitation, Stuttgart Universität.

Schanz, T., P. A. Vermeer, and P. G. Bonnier (1999). The hardening-soil model: Formulation and verification. *In R.B.J. Brinkgreve, Beyond 2000 in Computational Geotechnics, Balkema, Rotterdam*, 281–290.

Septanika, E. G., H. K. Engin, and R. B. J. Brinkgreve (2008, 1-6 October, 2008). Estimation of pile group behavior using embedded piles. In *12th International Conference of International Association for Computer Methods and Advances in Geomechanics (IACMAG)*, Goa, India.

Sharma, V. J., S. A. Vasanvala, and C. H. Solanki (2011). Effect of cushion on composite piled raft foundation. *Journal of Engineering Research and Studies 2*(4), 132–135.

Sharma, V. J., S. A. Vasanvala, and C. H. Solanki (2015, January-March). Behaviour of cushioned composite piled raft foundation under lateral forces. *Indian Geotechnical Journal 45*(1), 89–97.

Taha, A. (2014). *Static and seismic performance of geosynthetics-strengthened pile foundations*. Ph. D. thesis, The school of graduate and postdoctoral studies, The university of western ontario, London.

Taha, A., M. E. Naggar, and A. Turan (2015a). Numerical modeling of the dynamic lateral behavior of geosynthetics-reinforced pile foundation system. *Soil Dynamics and Earthquake Engineering © ELSEVIER 77*, 254–266.

Taha, A., M. H. E. Naggar, and A. Turan (2014). Experimental and numerical study on lateral behaviour of geosynthetic-reinforced pile foundation system. *Geosynthetics International 21*(6), 352–363.

Taha, A., M. H. E. Naggar, and A. Turan (2015b). Experimental study on the seismic behaviour of geosynthetic-reinforced pile-foundation system. *Geosynthetics International 22*(2), 183–195.

Teguh, M., C. Duffield, P. Mendis, and G. Hutchinson (2006). Seismic performance of pile-to-pile cap connections: An investigation of design issues. *Electronic Journal of Structural Engineering 6*, 8–18.

Tradigo, F., F. Pisanò, and C. di Prisco (2016). On the use of embedded pile elements for the numerical analysis of disconnected piled rafts. *Computers and Geotechnics © ELSEVIER 72*, 89–99.

Tradigo, F., F. Pisanò, C. di Prisco, and A. Mussi (2015). Non-linear soil–structure interaction in disconnected piled raft foundations. *Computers and Geotechnics © ELSEVIER 63*, 121–134.

Tradigo, F., F. Pisanò, C. di Prisco, A. Mussi, and R. Persio (2014, June). Finite element analysis of soil-structure interaction in disconnected piled raft foundations. In A. . Hicks, R. B. . J. . Brinkgreve, and A. Rohe (Eds.), *Proceedings of the 8th European Conference on Numerical Methods in Geotechnical Engineering (NUMGE2014)*, Volume 1, Delft (Netherlands), pp. 705–710. London: Taylor & Francis group.

Tschuchnigg, F. (2013). *3D Finite element modelling deep foundation employing an embedded pile formulation*. Ph. D. thesis, Technische Universität Graz.

Tschuchnigg, F. and H. Schweiger (2015). The embedded pile concept – verification of an efficient tool for modelling complex deep foundations. *Computers and Geotechnics © ELSEVIER 63*, 244–254.

Turan, A., S. D.Hinchberger, and M. H. E. Naggar (2007). Dynamic properties of modified glyben as artificial clay for seismic applications. In K. D. Pitilakis (Ed.), *Proceeding of 4th International Conference on Earthquake Geotechnical Engineering*, Volume 135, Thessaloniki, Greece, pp. 280–290.

Turan, A., S. D.Hinchberger, and M. H. E. Naggar (2009). Mechanical characterization of an artificial clay. *Journal of Geotechnical and Geoenvironmental Engineering © ASCE 135*(2), 280–290.

Turan, A., S. D.Hinchberger, and M. H. E. Naggar (2011). Influence of pore fluid viscosity on the dynamic properties of an artificial clay. *Journal of Geotechnical and Geoenvironmental Engineering © ASCE 137*(12), 1190–1201.

von Soos, P. (1990). Properties of soil and rock (in german). *In In: Grundbautaschenbuch Part 4. Ernst & Sohn, Berlin.*.

Wong, I. H., M. F. Chang, and X. D. Cao (2000). *Design Applications of Raft Foundations*, Chapter Raft foundation with disconnected settlement-reducing piles, pp. 469–486. Thomas Telford.

Zienkiewicz, O. C. and R. L. Taylor (2000). *The Finite Element Method: The Basis* (5 ed.), Volume 1. Butterworth-Heinemann.

Appendix A

Dynamic properties of soil

The author used an artificial clay called Modified Glyben to represent the cohesive soil layer. The primary advantages of modified glyben for reduced scale model tests are: i) it consolidates at a very slow rate after application of confining pressure, and thus it can be used in 1-g and N-g tests without observing a consolidation stage; ii) it resists desiccation due to drying, and iii) its mechanical properties do not significantly change with time, which facilitates the multiple use in physical tests (*Turan et al. (2009)*). The modified glyben was prepared by mixing bentonite with glycerin and water. The fluid (mixture of glycerin) and water to mixture (gw/c) ratio was 46% and the water to fluid (w/gw)ratio was 33.33%. Figure A.1 illustrates the variation of maximum shear modulus (G_{max}) with different confining pressure and fluid content in mixture.

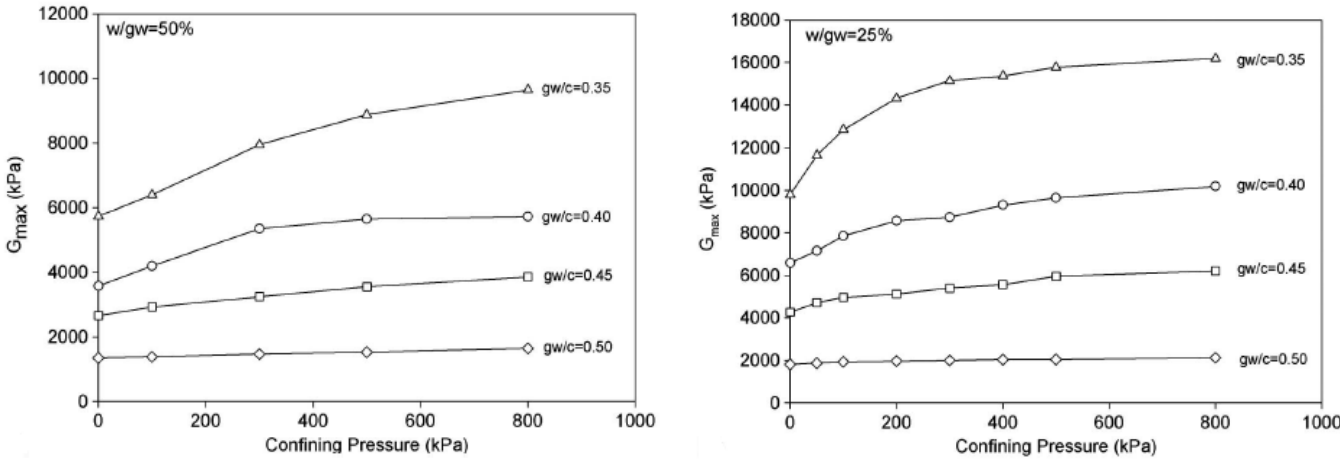

Figure A.1: Variation of G_{max} values with confining pressures for various (gw/c) ratios *Turan et al. (2007)*

⇒ Following Figures A.2, A.3, A.4 and A.5, derived from several laboratory tests which was performed by *Taha (2014)*, provides the dynamic properties of the soils:

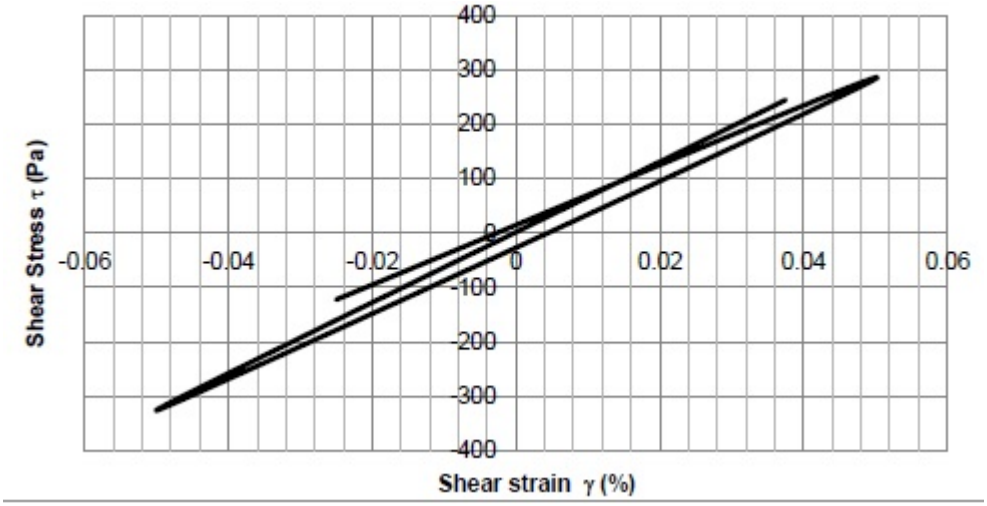

Figure A.2: Typical aggregate shear stress-strain loop *Taha (2014)*

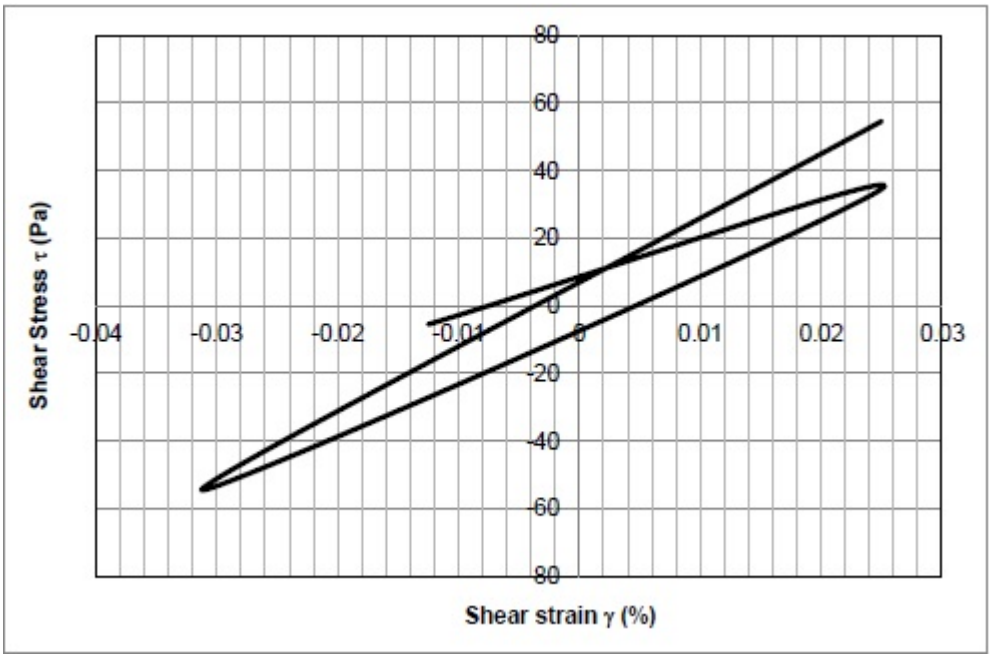

Figure A.3: Typical glyben shear stress-strain loop *Taha (2014)*

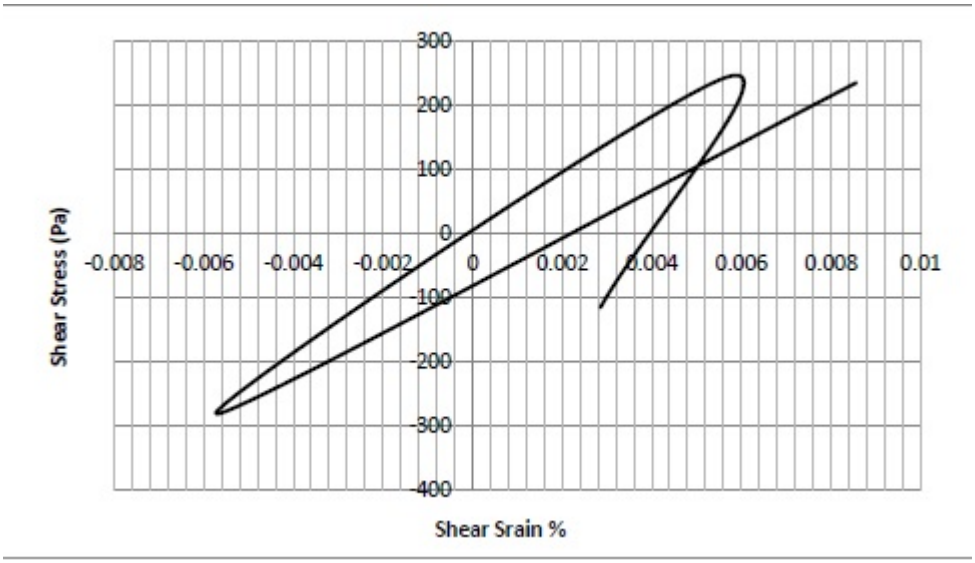

Figure A.4: Typical sand shear stress-strain loop *Taha (2014)*

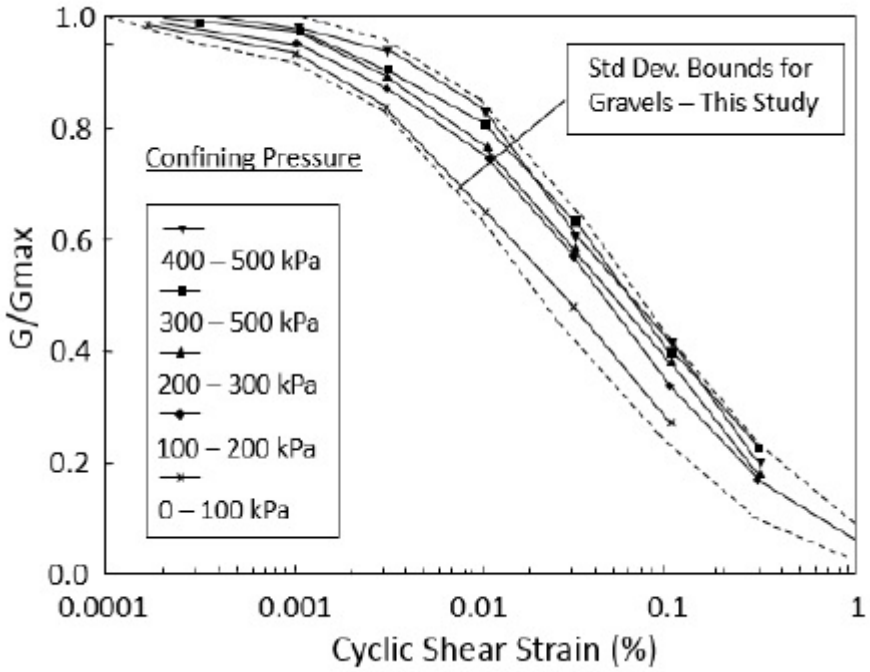

Figure A.5: Mean curves defining G/G_{max} versus shear strain (γ) relationships for gravelly soils at various confining pressures along with standard deviation boundaries for reduced data set, *Taha (2014)*

$\Rightarrow$ Since the author performed a reduced scale model test, therefore, a geometric scaling factor $\lambda = 20$ has been used. For modelling scaling relationship used according to *Meymand (1998)* as described in Table A.1.

Table A.1: Scaling relationships for primary system variables (*Meymand (1998)*)

Parameter	**Scaling factor**	**Parameter**	**Scaling factor**	**Parameter**	**Scaling factor**
Length	λ	Acceleration	1	Mass density	1
Force	λ^3	Shear wave velocity	$\lambda^{1/2}$	Stress	λ
Stiffness	λ^2	Time	$\lambda^{1/2}$	Strain	1
Modulus	λ	Frequency	$\lambda^{-1/2}$	EI	λ^5

λ = geometric factor scaling

$\Rightarrow$ The geogrid used in this study is a bi-axial knitted Microgrid manufactured by STRATAGRID. Following Table A.2 describes the engineering properties of geogrid:

Table A.2: Engineering properties of Geogrid mesh, *Taha (2014)*

Index Properties	**Value**
Ultimate strength	$29.2kN/m$
Creep limited strength	$16.8kN/m$
Strength at 2% strain	$2.2kN/m$
Strength at 5% strain	$7.3kN/m$
Aperture size	$2.54 \times 6.35mm$